Micromagnetism and Numerical Methods

Riccardo Hertel

CNRS and Université de Strasbourg
IPCMS Strasbourg, France

7th Italian School on Magnetism
Magnetic Nanomaterials
20–24 October 2025
Perugia, Italy



Outline

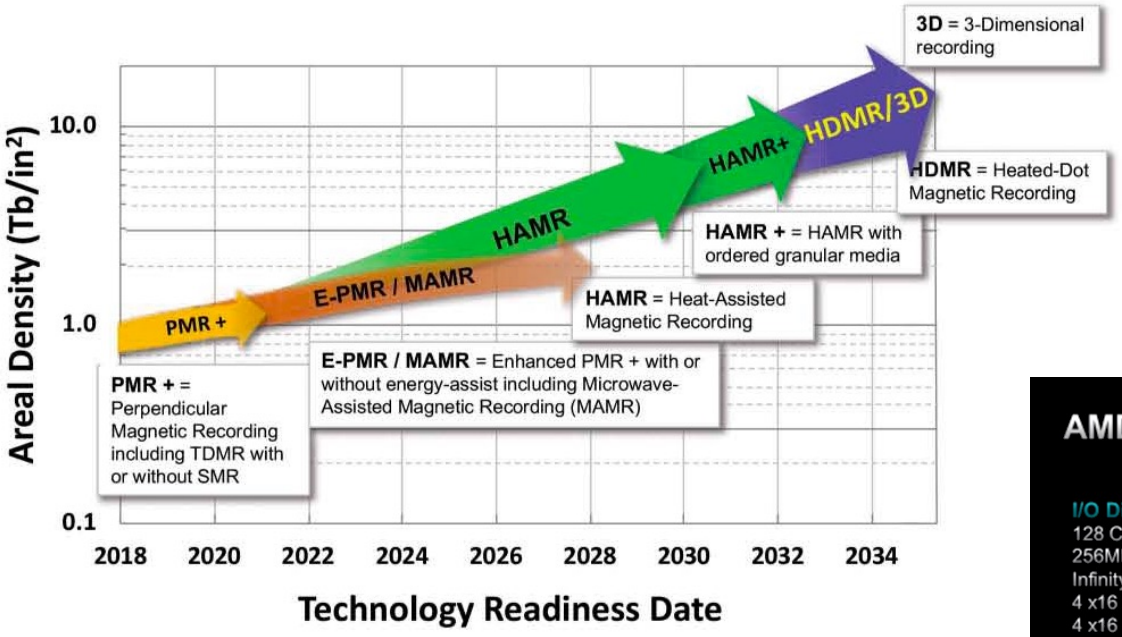
- Introduction and Motivation
  - 3D Nanomagnetism and nanotechnology

- Micromagnetic Theory
  - Energy terms
  - LLG equation
  - Effective fields

- Finite-element formulation and implementation in open-source software *tetmag*

- Simulation examples:
  - magnetic Hopfion
  - interconnected nanowire arrays
  - spin waves in nanoscale Möbius stripes

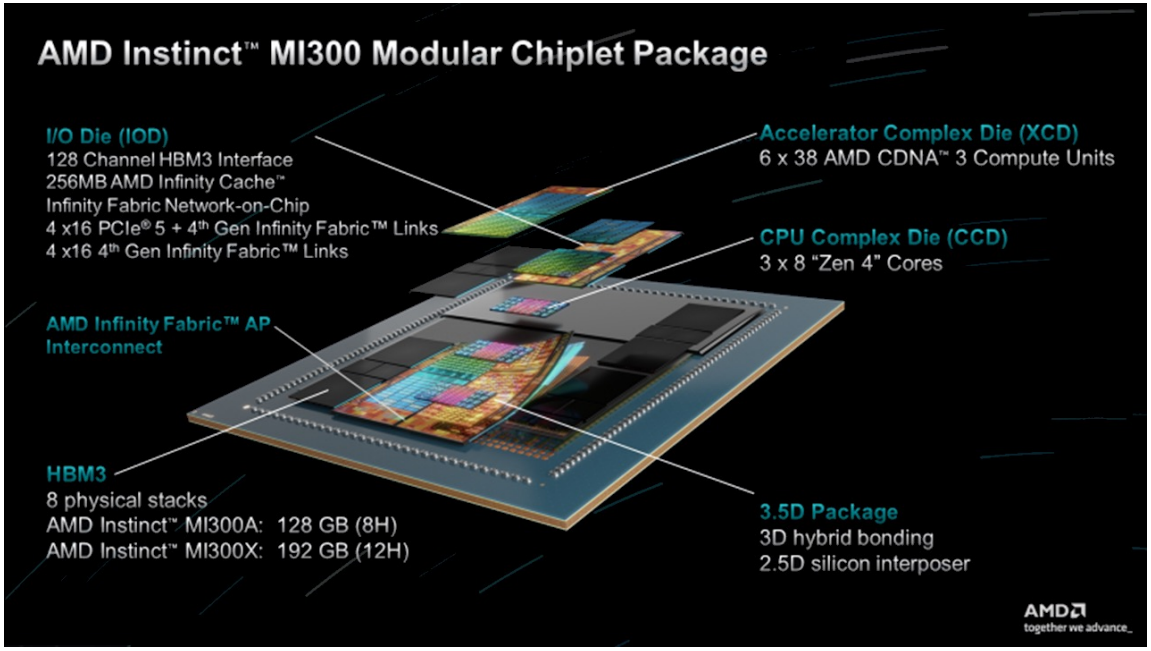
Trend Towards Three-Dimensional Nanotechnologies



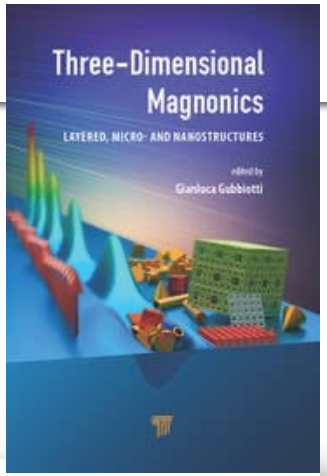
E. Roddick et al.,
A new Advanced Storage Research Consortium HDD Technology Roadmap
2022 IEEE 33rd Magnetic Recording Conference (TMRC)

3D integration in IT technology to enhance performance, density, and efficiency.

Issues: Thermal management, difficult fabrication



Three-dimensional magnetic nanostructures



Recent development in nanomagnetism:

Three-dimensional nanostructures with complex shapes

G. Gubbiotti (Ed.)

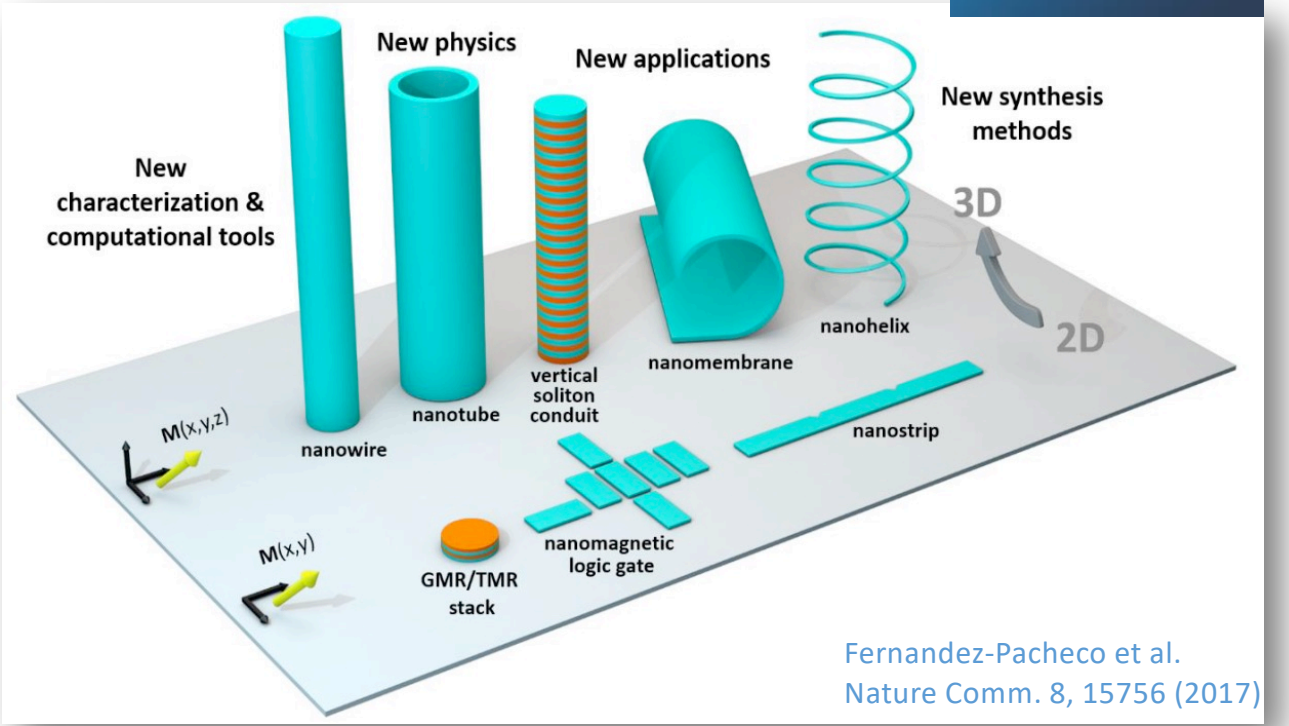
Functionality, physical properties may depend sensitively on the shape of the nanostructure

Large scale problems with nontrivial geometries

Typical situations in **3D nanomagnetism**

- Large samples of complex shape
- Arrays of interacting particles

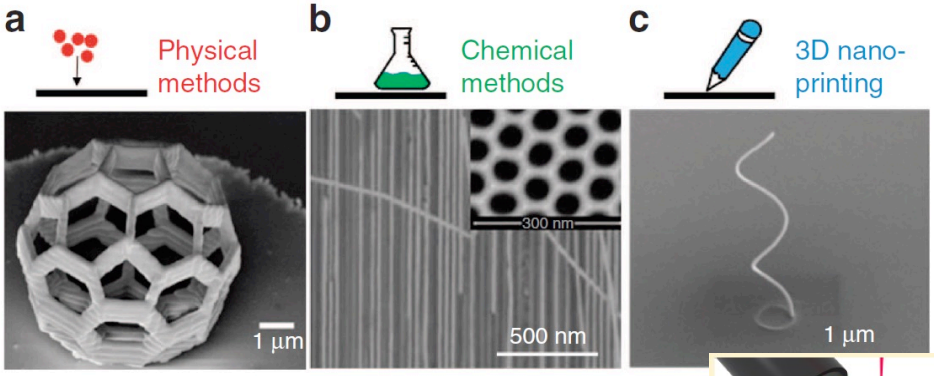
Challenges for both experiment and theory

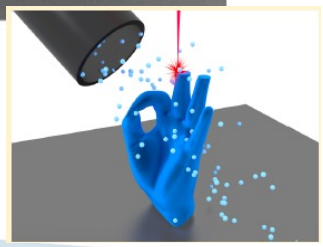


Fernandez-Pacheco et al.
Nature Comm. 8, 15756 (2017)

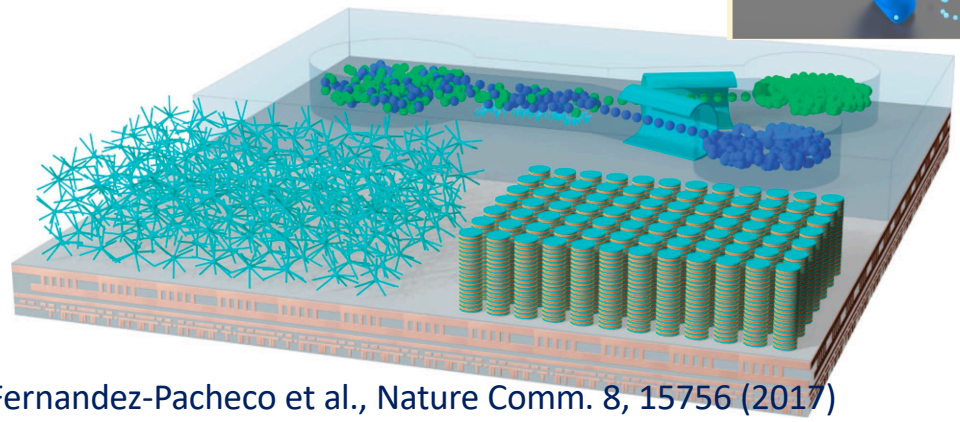
Three-dimensional nanomagnetism – recent developments

Advanced fabrication techniques





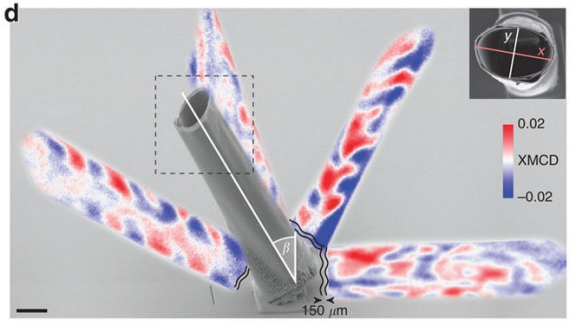
Futuristic vision of chip integrating 3D-magnetic nanostructures



Fernandez-Pacheco et al., Nature Comm. 8, 15756 (2017)
Skoric et al., Nano Lett. 20, 184 (2020)

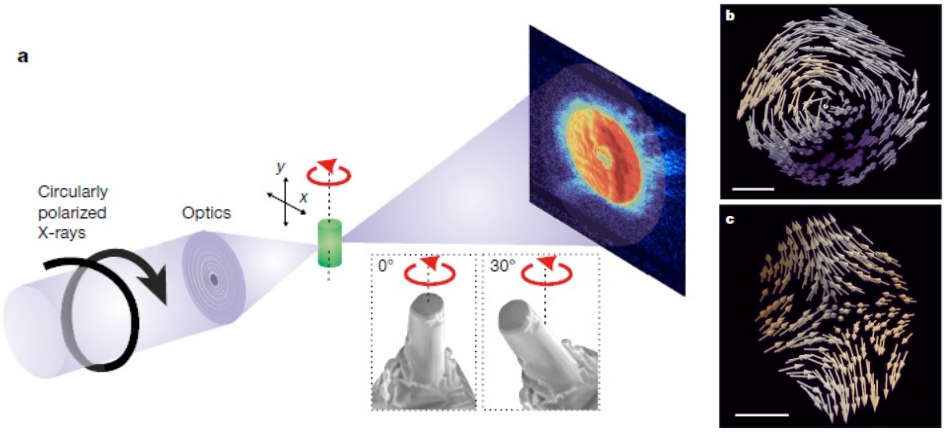
Three-dimensional imaging

XMCD shadow contrast analysis at different angles



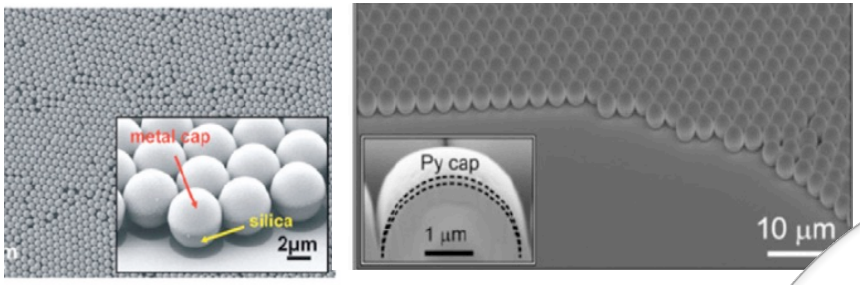
R. Streubel et al., Nature Comm. 6, 7612 (2015)

X-ray vector nanotomography

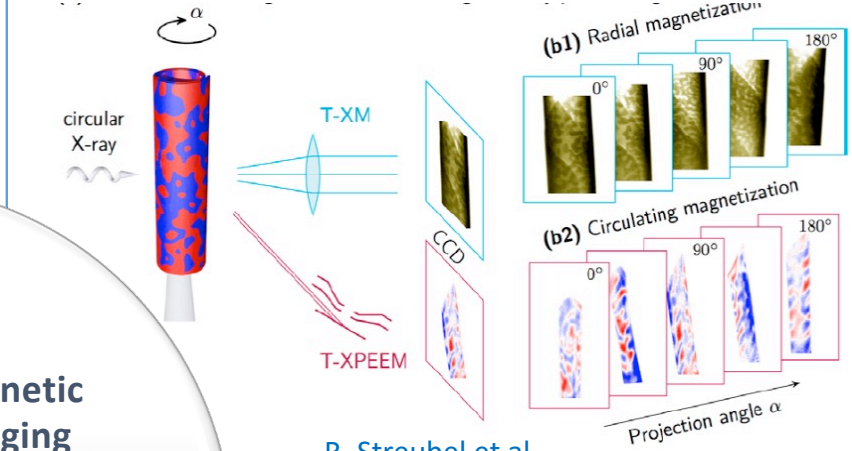


C. Donnelly et al., Nature 547, 328 (2017)

Challenges in Three-Dimensional Micromagnetism



L. Baraban et al., ACS Nano 6, 3383 (2012)



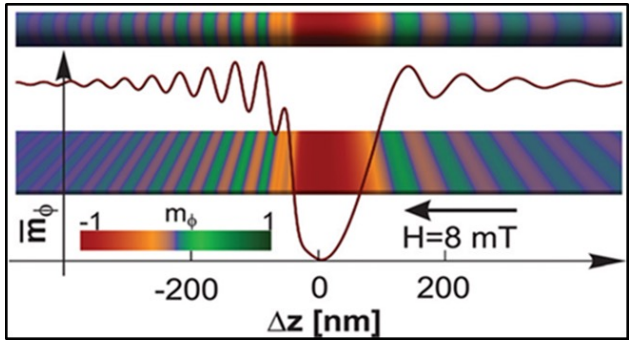
R. Streubel et al.
J. Phys. D: Appl. Phys. 49 363001 (2016)

Sample Fabrication

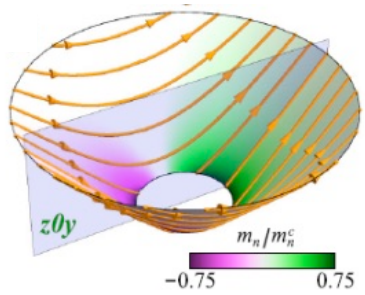
Magnetic Imaging

Micro-magnetic Simulations

Analytic Theory



M. Yan et al., Appl Phys. Lett. 99, 122505 (2011)

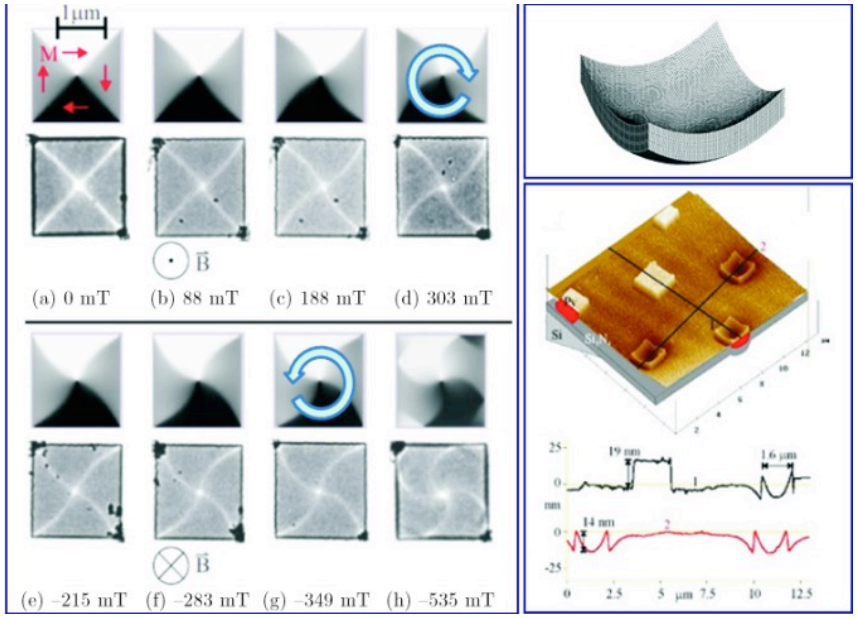


$$\mathcal{E}^{\mathrm{t}} = \mathbf{\Gamma}^2 + (\nabla\phi - \mathbf{\Omega})^2$$

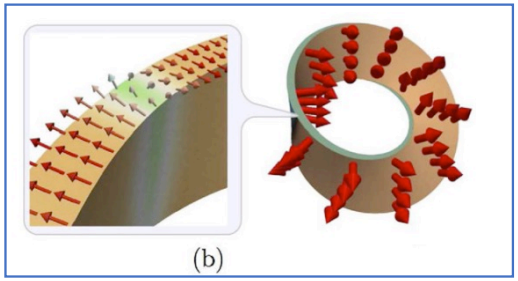
Y. Gaididei et al., Phys. Rev. Lett. 112 257203 (2014)

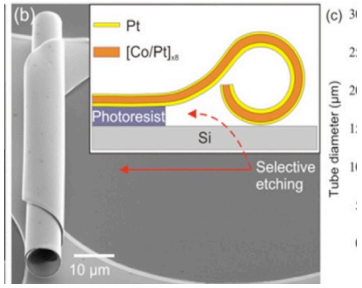
Micromagnetism on Curved Surfaces

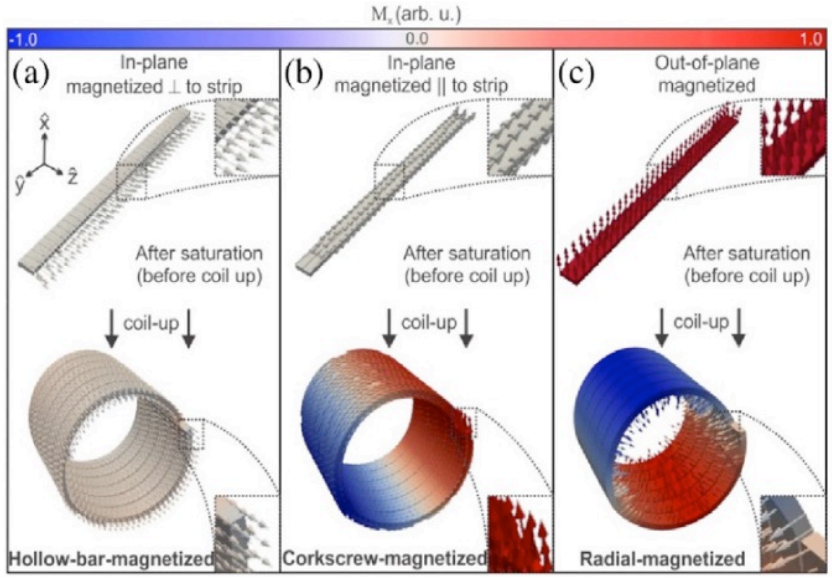
Intense activity, in particular since about 2013. Subtopic of Three-dimensional Nanomagnetism



C. Dietrich *et al.,* Phys. Rev. B 77, 174427 (2008).



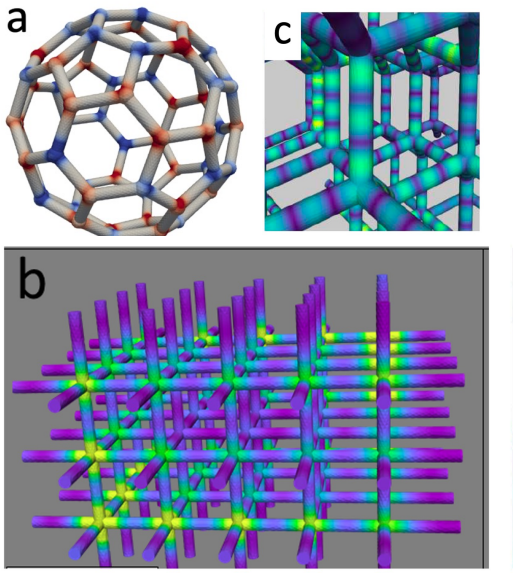




Review: Streubel *et al.,* J. Phys. D: Appl. Phys. 49 363001 (2016)

Simulation of magnetic nanostructures with complex 3D geometries

Interconnected nanowire arrays



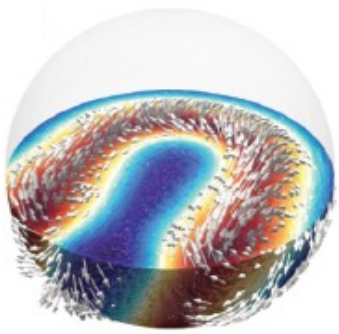
Magnetic structure and HF modes in 3D nanowire nanoarchitectures

2025 Roadmap on 3D Nanomagnetism
J. Phys.: Condens. Matter (2025)

The 2024 magnonics roadmap
J. Phys.: Condens. Matter 36 36350 (2024)

R. Cheenikundil and R. Hertel
Appl. Phys. Lett. 118, 212403 (2021)

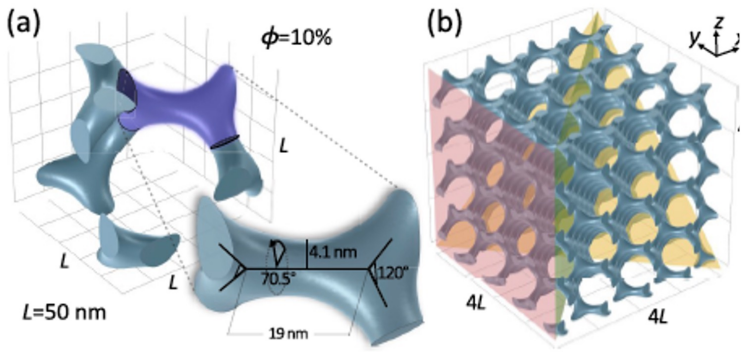
Nanospheres



Chiral spin texture in a FeGe nanospheres

S. Pathak and R. Hertel
Phy. Rev. B 103, 104414 (2021)

Gyroids

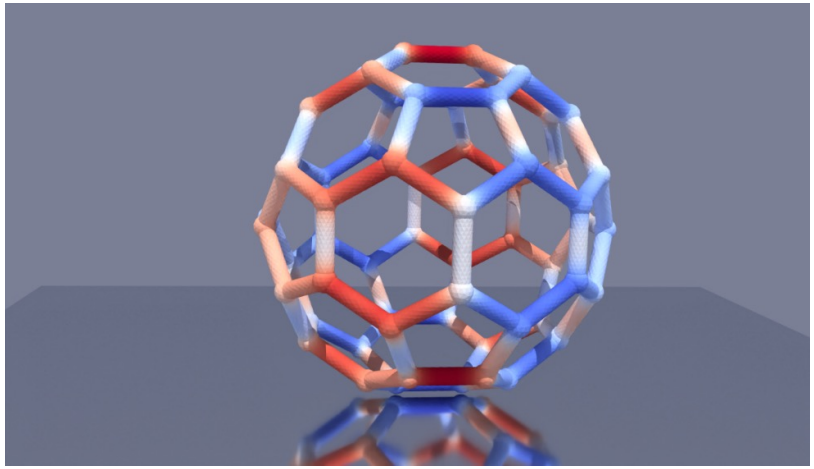


M. Gołębiewski et al.,
ACS Appl. Mater. Interfaces
16, 22177 (2024)

Efficient and flexible numerical simulation software required to investigate magnetization textures in complex 3D nanostructures with curved surfaces

Complex 3D magnetic nanostructures

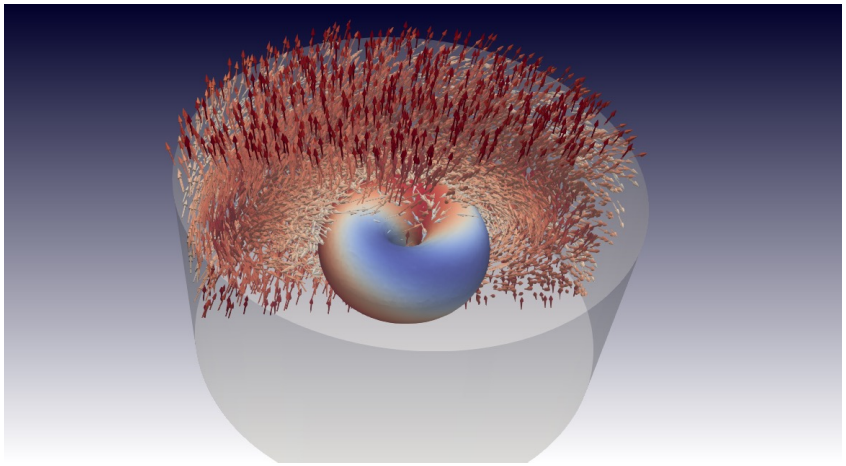
Geometrical 3D complexity



Artificial magnetic buckyball structure.
Nanoarchitecture of interconnected magnetic nanowires.

R. Cheenikundil and R. Hertel
Appl. Phys. Lett. 118, 212403 (2021)

Magnetic texture 3D complexity



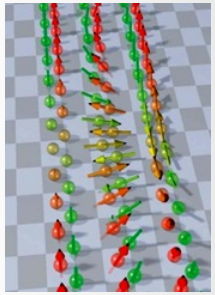
Magnetic Hopfion in a FeGe nanocylinder.
Simulation involving millions of finite elements.

L. Gallard, IPCMS Strasbourg (2024)
unpublished

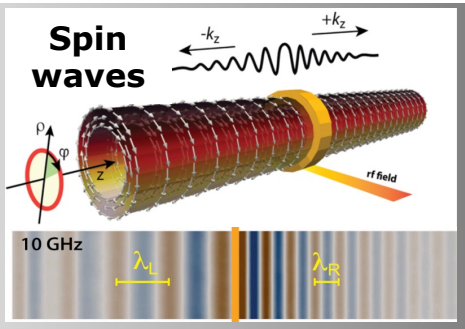
Simulating complex 3D nanostructures and magnetization textures requires versatile and efficient numerical methods

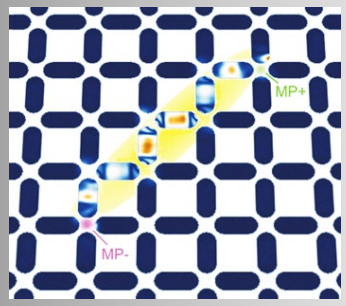
Length Scales in Magnetism

Atomic spin spirals



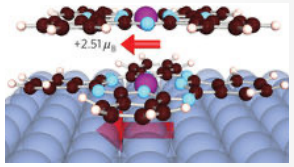
Spin waves

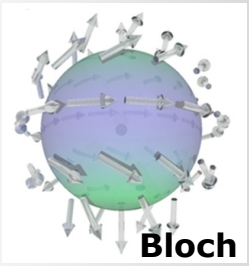




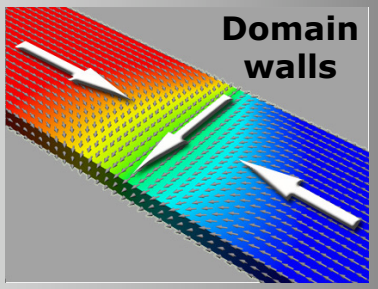
Artificial spin ice lattice

Molecular Magnetism

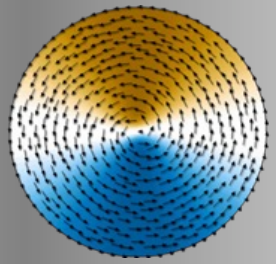




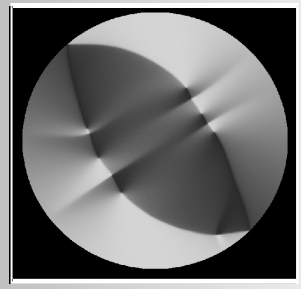
Bloch Point



Domain walls



Vortices



Domain structures

10^{-11} m | 10^{-9} m | 10^{-7} m | 10^{-6} m | 10^{-3} m

Electron theory
Quantum Physics

Heisenberg model
atomistic effects

Micromagnetism
vortices, spin waves
domain walls

Domain theory
Subdivision into domains;
domain walls as line defect

Theoretical Models in Ferromagnetism

Micromagnetism

- Continuum theory to calculate structure and dynamics of the magnetization
  Broad range of application (domain walls, spin waves, magnetostatic effects…)

Macrospin model

- Magnetization is modeled with a single, representative magnetic moment.
  Applicable for dynamic processes of very small, simple nanomagnets , up to 10 nm in size

Atomistic models

- Magnetism in low dimensions: atomic monolayers, atomic spin chains…
  Can describe cases at the limit of ferromagnetic order, when neighboring spins are strongly misaligned

Electron theory

- Fundamental magnetic order, intrinsic material properties
  Can provide input parameters for atomistic or continuum models

Main aspects of Micromagnetic Theory

Continuum theory to calculate the structure and dynamics of the magnetization $\boldsymbol{M} = \boldsymbol{M}(\boldsymbol{r}, t)$ in ferromagnets.

Repetitio est mater studiorum — Medieval Latin proverb

Fundamental assumptions

1. The magnetization $\boldsymbol{M}(\boldsymbol{r}, t)$ is a continuous vector field with constant magnitude $|\boldsymbol{M}(\boldsymbol{r}, t)| = M_s$
2. The vector field $\boldsymbol{M}$ is smooth on the atomic scale

General approach

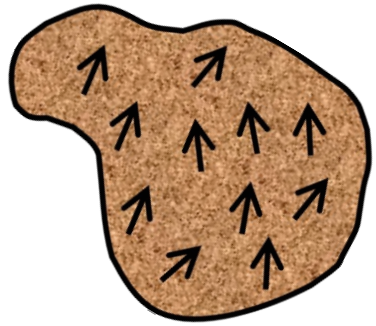
- **Static magnetic structures:**
  Calculate energy density $e(\boldsymbol{r})$ as a function of $\boldsymbol{M}(\boldsymbol{r})$
  Determine equilibrium magnetic structure by minimizing the total energy

- **Magnetization dynamics:**
  Calculate effective local field magnetic $\boldsymbol{H}_{\text{eff}}(\boldsymbol{r},t)$ of each energy contribution
  Solve the equation of motion of the magnetization $\boldsymbol{M}(\boldsymbol{r}, t)$ using the effective field (Landau-Lifshitz-Gilbert equation)

Magnetostatic field of a ferromagnet: From atomistic to continuum picture

Magnetostatic potential of a single point dipole: $$U_\mu(\boldsymbol{r}) = \frac{1}{4\pi}\,\boldsymbol{\mu}\cdot\frac{\boldsymbol{r}-\boldsymbol{r}_0}{|\boldsymbol{r}-\boldsymbol{r}_0|^3} = -\frac{1}{4\pi}\,\boldsymbol{\mu}\cdot\nabla\left(\frac{1}{|\boldsymbol{r}-\boldsymbol{r}_0|}\right)$$

A ferromagnet can be regarded as an ensemble of magnetic moments $\vec{\mu}_i$, each with the magnetic field of a point dipole:



Potential of a set $\{\mu_i\}$ of point dipoles: $$U = -\frac{1}{4\pi\mu_0}\sum_i \boldsymbol{\mu_i}\cdot\nabla\frac{1}{|\boldsymbol{r}-\boldsymbol{r_i}|}$$

Magnetostatic field: $$\vec{H}_d = -\nabla U$$

Introduce magnetization $\vec{M}(\vec{r})$ as the volume density of magnetic moments:

$$\mu_0\vec{M} = \lim_{\Delta V\to 0}\sum_i^{\Delta V}\frac{\vec{\mu}_i}{\Delta V}$$

The magnetization vector field $\vec{M}$ plays a central role in micromagnetic theory:

- primary goal in micromagnetism is to compute $\vec{M}(\vec{r}\,,t)$
- describes magnetic behavior on mesoscopic length

The magnetization is a directional field with $\left|\vec{M}\right| = M_s = const.$
The saturation magnetization M_s is a material-specific constant.

Magnetostatic potential of a continuous magnetic-moment distribution

Summation in the potential converts into a volume integral: $\sum_i \vec{\mu_i} \cdots \rightarrow \int dV' \vec{M}(\vec{r'}) \cdots$

Magnetostatic potential of magnetization distribution: $U(\vec{r}) = -\frac{1}{4\pi} \int_{V'} \vec{M}_i(\vec{r'}) \cdot \vec{\nabla}_r \frac{1}{|r - r_i|} dV'$

using $\nabla_r \frac{1}{\left|\vec{r} - \vec{r'}\right|} = -\nabla_{r'} \frac{1}{\left|\vec{r} - \vec{r'}\right|}$ and $\nabla \cdot \left[\vec{M} \cdot f\right] = \vec{M} \cdot \nabla f + f \cdot \nabla \cdot \vec{M}$

and by applying Gauss' Law, we obtain

$$U(\vec{r}) = \frac{1}{4\pi} \oint_{\partial V'} \frac{\vec{M}(\vec{r'}) \cdot \vec{n}}{\left|\vec{r} - \vec{r'}\right|} \mathrm{d}S' - \frac{1}{4\pi} \int_{V'} \frac{\nabla \cdot \vec{M}(\vec{r'})}{\left|\vec{r} - \vec{r'}\right|} \mathrm{d}V'$$

The potential results from a **surface integral** and a **volume integral**

Magnetostatic Charges and Poisson Equation

Introducing the

volume charge density

$$\rho = -\vec{\nabla} \cdot \vec{M}$$

and the

surface charge density

$$\sigma = \vec{M} \cdot \vec{n}$$

the potential can be written as

$$U(\vec{r}) = \frac{1}{4\pi} \oint_{\partial V'} \frac{\sigma(\vec{r}')}{\left|\vec{r} - \vec{r}'\right|} \, \mathrm{d}S' + \frac{1}{4\pi} \int_{V'} \frac{\rho(\vec{r}')}{\left|\vec{r} - \vec{r}'\right|} \, \mathrm{d}V'$$

This can be identified as the general solution of Poisson's equation

$$\Delta U(\vec{r}) = -\rho = \nabla \cdot \vec{M}(\vec{r})$$

Alternative derivation from continuum electrodynamics:
Starting from the constitutive relation:

$$\vec{B} = \mu_0 \vec{M} + \mu_0 \vec{H}$$

Take the divergence:

$$\vec{\nabla} \cdot \vec{B} = \mu_0 \vec{\nabla} \cdot \vec{M} + \mu_0 \vec{\nabla} \cdot \vec{H}$$

with Maxwell's second equation

$$\vec{\nabla} \cdot \vec{B} = 0$$

we obtain $\vec{\nabla} \cdot \vec{H} = -\vec{\nabla} \cdot \vec{M}$

and with $\vec{H} = -\vec{\nabla} U$

finally

$$\Delta U = \nabla \cdot \vec{M} = -\rho$$

Magnetic charges and domain formation

The **long-range** interaction given by the dipolar field $\boldsymbol{H_s}$ depends on the magnetic distribution and the **sample geometry.**

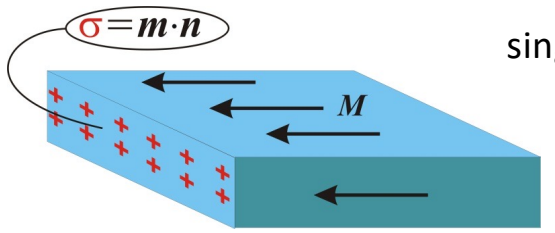
$$\vec{H}_s = \frac{1}{4\pi}\int_{\Omega} \rho(\vec{r'})\frac{(\vec{r}-\vec{r'})}{|\vec{r}-\vec{r'}|^3}\mathrm{d}V' + \frac{1}{4\pi}\oint_{\partial\Omega} \sigma(\vec{r'})\frac{(\vec{r}-\vec{r'})}{|\vec{r}-\vec{r'}|^3}\mathrm{d}S'$$

surface charges: $\sigma = \vec{M}\cdot\vec{n}$

volume charges: $\rho = -\vec{\nabla}\vec{M}$

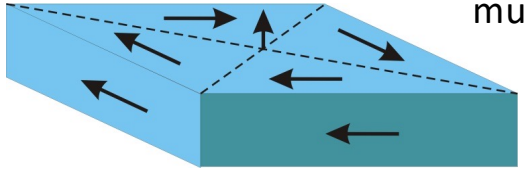
The integral extends over the **volume** and over the **surface** of the sample.

This gives rise to **finite-size effects** and the **formation of domains.**



single domain

magnetic surface charges (poles)



multi domain

flux closure, pole avoidance

In three-dimensional samples:
No cut-off radius allowed

Amount of charges increases geometrically at the same rate as their influence decays

Energy of the magnetostatic field

magnetostatic energy: $$E_m = -\frac{\mu_0}{2}\int \vec{M}\cdot\vec{H}_s \,\mathrm{d}V$$

Since $\vec{B}$ and $\vec{H}$ decay sufficiently fast with $|r| \to \infty$,

the relation $$\int_\infty \vec{H}\cdot\vec{B}\,\mathrm{d}V = 0$$

$$\nabla \times \boldsymbol{H} = 0$$

$$\nabla \boldsymbol{B} = 0$$

is fulfilled for the integral over the product of the solenoidal field $\vec{B}$ and the irrotational field $\vec{H}$.

With $\vec{B} = \mu_0\vec{H} + \mu_0\vec{M}$ one obtains:

$$\int_\infty \vec{H}(\mu_0\vec{H} + \mu_0\vec{M})dV = 0$$

$$\frac{\mu_0}{2}\int_\infty \vec{H}^2\mathrm{d}V' = -\frac{\mu_0}{2}\int_{(V)} \vec{H}\cdot\vec{M}\mathrm{d}V'$$

Energy stored in the field

Energy stored in the magnet

Brown's pole avoidance principle

Magnetostatic energy is non-negative:

$$E_{dem} = -\frac{\mu_0}{2}\int_{(V)} \vec{H}\cdot\vec{M}\,\mathrm{d}V' = \frac{\mu_0}{2}\int_{\infty} (\vec{H})^2\,\mathrm{d}V \geq 0$$

Minimum magnetostatic energy: $\vec{H}(\vec{x}) = 0$

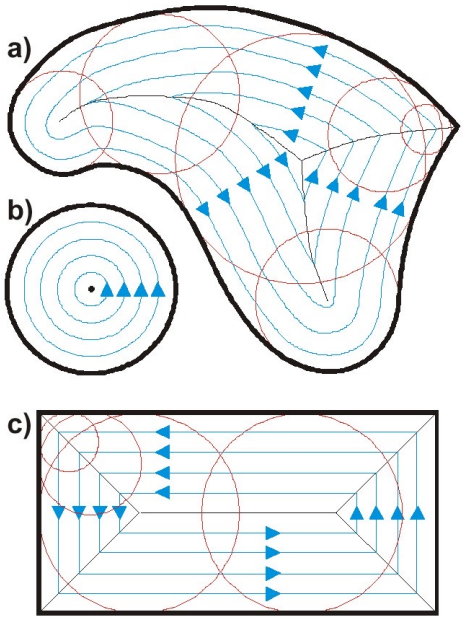
- Magnetostatic energy can be reduced by minimizing $|\vec{H}|$
- The sources (poles) of ***H*** are:

$$\rho = -\vec{\nabla}\cdot\vec{M} \qquad \sigma = \vec{M}\cdot\vec{n}$$

The ferromagnetic system tends to avoid these charges
In order to reduce the magnetostatic energy

Magnetic structures with $\rho = 0$ and $\sigma = 0$
minimize the magnetostatic energy

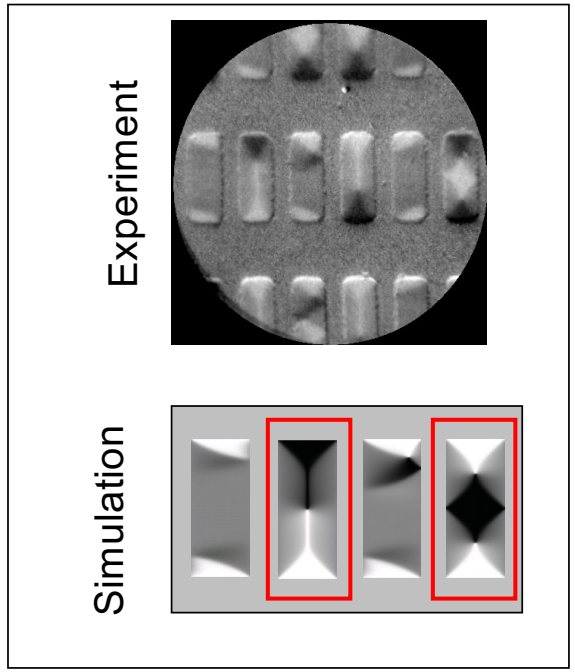
Divergenceless magnetic structures

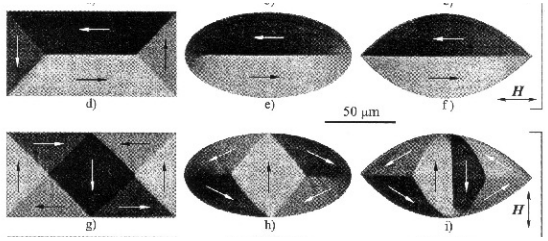


Van den Berg scheme

J. Appl. Phys. 57 (6) 2168 (1985)
J. Appl. Phys. 60 (3) 1104 (1986)
J. Appl. Phys. 62 (5) 1952 (1987)

Cherifi et al., J. Appl. Phys. 98, 043901 (2005)





Hubert, Schäfer "Magnetic Domains"

Ferromagnetic exchange interaction

Fundamental property of ferromagnetic materials:

Atomistic level: Tendency to align neighboring magnetic moments parallel to each other.
Heisenberg interaction:

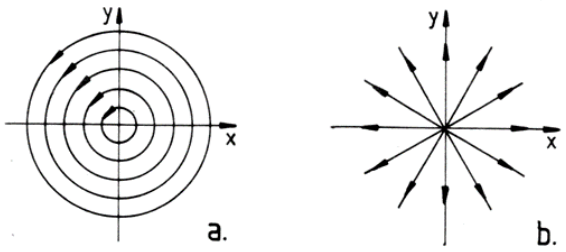
$$E_{\mathrm{Hei}} = -\sum_{i,j} J \cdot \boldsymbol{S_i} \cdot \boldsymbol{S_j} \qquad \text{with } J > 0 \text{ in ferromagnets.}$$

Continuum theory: Inhomogeneities of the magnetization lead to an increase of exchange energy

Phenomenological approach:

- Energy density must be a function of magnetization gradients $\partial M_i / \partial x_k$
- Any type of inhomogeneity must increase energy
- Symmetry considerations (time inversion, space inversion)

general form: $$e_{\mathrm{exc}} = \sum_{i,j,k} \frac{\alpha_{ij}}{2} \frac{\partial M_j}{\partial x_i} \frac{\partial M_j}{\partial x_k}$$



In practice, α_{ij} can be represented as a constant (no anisotropy in the exchange interaction), leading to

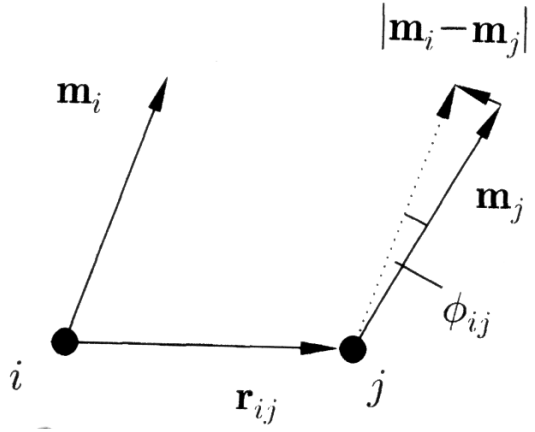
$$e_{\mathrm{exc}} = \frac{A}{M_s^2} \left[(\boldsymbol{\nabla} M_x)^2 + (\boldsymbol{\nabla} M_y)^2 + (\boldsymbol{\nabla} M_z)^2 \right]$$

Micromagnetic exchange derived from atomistic Heisenberg model

$$E_{\mathrm{Hei}} = -\sum_{i,j} J \cdot \boldsymbol{S_i} \cdot \boldsymbol{S_j}$$ ferromagnet: J>0

small angles between neighboring magnetic moments: $\cos\phi_{ij} \approx 1 - \phi_{ij}^2/2$

$$E = -JS^2 \sum_{<i,j>} \cos\phi_{ij} \approx const. + \frac{JS^2}{2} \sum_{<i,j>} \phi_{ij}^2$$



Small-angle expansion: $\left|\phi_{ij}\right| \approx \left|\vec{m}_i - \vec{m}_j\right| \approx \left|\left(\vec{r}_{ij} \cdot \vec{\nabla}\right)\vec{m}\right|$

Hence the energy is: $E \approx JS^2 \sum_{<i,j>} \left[(\vec{r}_{ij} \cdot \vec{\nabla})\vec{m}\right]^2$

Transition to continuum: $\sum_i \rightarrow \int \frac{dV}{a^3}, \qquad \boldsymbol{S}_i \rightarrow \boldsymbol{M}(\boldsymbol{r})$

yields:

$$E_{\mathrm{exc}} = \frac{A}{M_s^2} \int \left[(\nabla M_x)^2 + (\nabla M_y)^2 + (\nabla M_z)^2\right] \mathrm{d}V$$

where $A = 2JS^2 z/a$

a: distance to nearest neighbor

z: depends on crystal structure: z=1 (sc),2 (bcc), 4 (fcc)

Scaling property of micromagnetic exchange energy density

For a given magnetic structure ***M***, the exchange energy density scales with the size λ of the sample

$$e_{\mathrm{exc}} = \frac{A}{M_s^2}\left[(\nabla M_x)^2 + (\nabla M_y)^2 + (\nabla M_z)^2\right]$$

Scaling with parameter λ:

$$u = \lambda x$$

$$\left(\frac{\partial}{\partial u}\right)^2 = \frac{1}{\lambda^2}\left(\frac{\partial}{\partial x}\right)^2$$

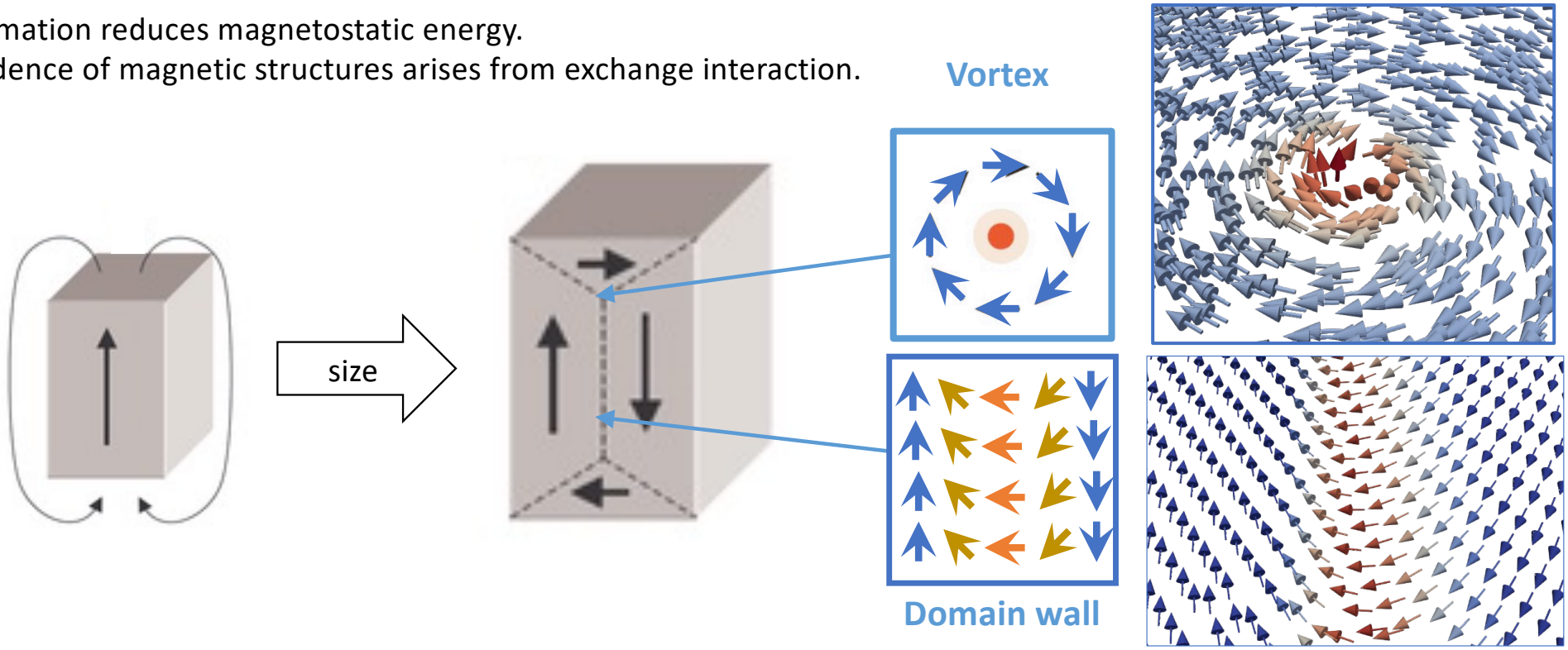
The exchange energy density decreases with increasing sample size. It scales with a factor of $1/\lambda^2$.

Other terms in micromagnetic energy densities (magnetostatics, anisotropy, Zeeman term) are invariant with respect to scaling

Exceptions: Surface anisotropy and Dzyaloshinskii-Moriya interaction. These terms are size-dependent and scale with $1/\lambda$.

Magnetostatics drives the Formation of Magnetic Domains

Domain formation reduces magnetostatic energy.
Size-dependence of magnetic structures arises from exchange interaction.

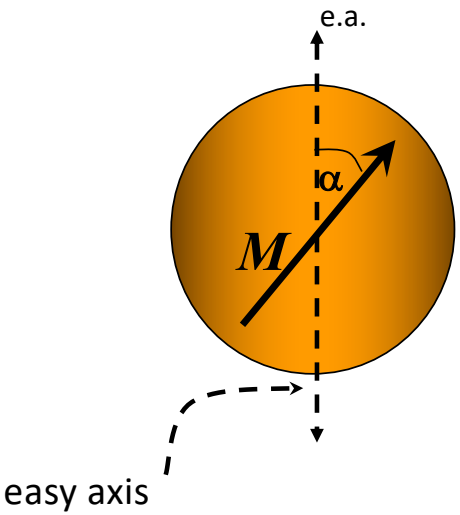


- Subdivision into domains minimizes magnetic charges (pole avoidance principle)
- Domains are separated by domain walls, vortices
- Magnetic structures develop on multiple length scales
- At short length scales, the exchange interaction dominates

Magnetocrystalline anisotropy

Crystalline magnetic materials display preferential (“easy”) axes along which the magnetization tends to align.

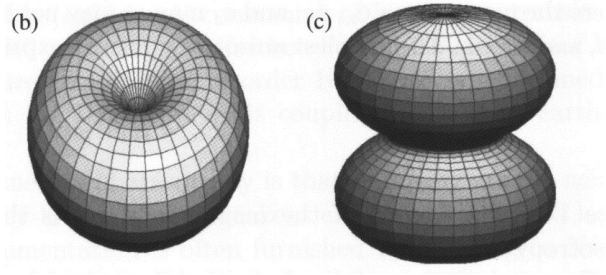
The symmetry of the crystal has a direct impact on the magnetic energy.



uniaxial anisotropy

Deviations from the easy axis direction increase the magnetocrystalline anisotropy energy:

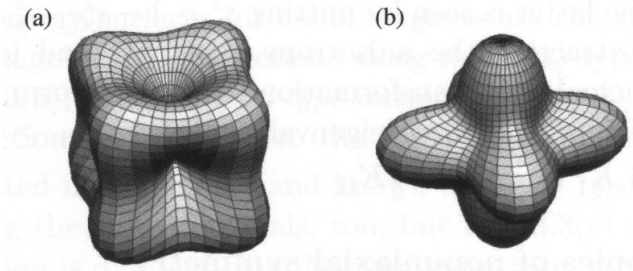
$$e_{\mathrm{K_u}} = K_{\mathrm{u1}} \sin^2 \alpha + K_{\mathrm{u2}} \sin^4 \alpha$$



R. Skomski "Simple Models of Magnetism"
Oxford University Press 2008

cubic anisotropy

$$e_{\mathrm{K_c}} = K_{\mathrm{c1}} \left(m_x^2 m_y^2 + m_x^2 m_z^2 + m_y^2 m_z^2 \right) + K_{\mathrm{c2}} m_x^2 m_y^2 m_z^2$$



Three orthogonal easy (or hard) axes

Dzyaloshinky-Moryia interacition

Antisymmetric exchange interaction in non-centrosymmetric ferromagnetic materials. On an atomistic scale, it favors a chiral configuration with an orthogonal alignment of neighboring magnetic moments

$$E_{\mathrm{DMI}} = \sum_{\langle i,j \rangle} \mathbf{D}_{ij} \cdot (\mathbf{S}_i \times \mathbf{S}_j)$$

where D_{ij} is the DMI vector. For a chiral lattice, we can assume $\boldsymbol{D}_{ij} = \frac{\vec{r_i} - \vec{r_j}}{|\vec{r_i} - \vec{r_j}|}$, $\mathbf{r}_j = \mathbf{r}_i + a\hat{k}$, $\mathbf{D}_{ij} = D_0 \hat{k}$

Using a small-angle approximation as we did in the Heisenberg model (assuming ferromagnetic exchange dominates):

$$\mathbf{S}_j \approx \mathbf{S}_i + a(\hat{k} \cdot \boldsymbol{\nabla})\mathbf{S}_i \qquad \mathbf{S}_i \times \mathbf{S}_j \approx a\mathbf{S}_i \times (\partial_k \mathbf{S}_i)$$

The DMI energy can be approximated as

$$E_i \approx \sum_k 2D_0 a\hat{k} \cdot (\mathbf{S}_i \times (\partial_k \mathbf{S}_i))$$

Taking the continuum limit:

$$E_{\mathrm{DMI}} = \frac{1}{M_s^2} \int D\mathbf{M} \cdot (\nabla \times \mathbf{M})\, dV \qquad \text{where} \qquad D = \frac{2D_0 a^4}{(g\mu_B S)^2}$$

Micromagnetic energy terms: Competing interactions

- Ferromagnetic exchange

$$e_{\mathrm{exc}} = {}^{A}/_{M_s^2}\left[(\nabla M_x)^2 + \left(\nabla M_y\right)^2 + (\nabla M_z)^2\right]$$

⟹ minimal if $\vec{\boldsymbol{M}}$ is homogeneous

- Magnetocrystalline anisotropy

$$e_{\mathrm{uni}} = K_{u1}\sin^2\alpha$$

⟹ minimal if $\vec{\boldsymbol{M}}$ is aligned along easy axis

- Magnetostatic energy due to demagnetizing field

$$e_{stray} = -\frac{\mu_0}{2}\boldsymbol{H}_s \cdot \boldsymbol{M}$$

⟹ minimal when $\nabla \cdot \vec{\boldsymbol{M}} = 0$

- Zeeman energy in external field

$$e_{\mathrm{Zeeman}} = -\mu_0 \vec{\boldsymbol{M}} \cdot \vec{\boldsymbol{H}}_{\mathrm{ext}}$$

⟹ minimal when $\vec{\boldsymbol{M}}$ is parallel to $\vec{\boldsymbol{H}}_{\mathrm{ext}}$

- Dzyaloshinsky-Moriya Interaction (antisymmetric exchange)

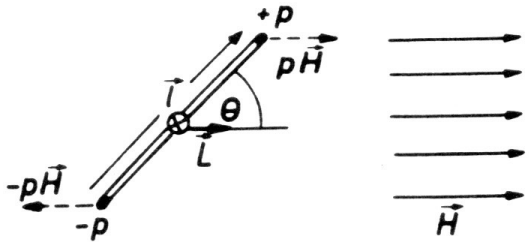
$$e_{\mathrm{DMI}} = \frac{D}{M_s^2}\vec{\boldsymbol{M}} \cdot \left(\nabla \times \vec{\boldsymbol{M}}\right)$$

⟹ minimal when $\vec{\boldsymbol{M}}$ develops a helical state

Magnetization dynamics

A homogeneous magnetic field exerts a torque on a magnetic dipole according to

$$\vec{T} = \vec{l} \times p\vec{H} = \vec{\mu} \times \vec{H} = \mu H \sin\theta$$



The torque defines a change in the angular momentum

$$\vec{T} = \frac{d\vec{L}}{dt}$$

Angular momentum and magnetic moment (magnetization) are related via the gyromagnetic ratio γ_0:

$$\vec{M} = \gamma_0 \vec{L} \qquad \text{with} \qquad \gamma_0 = \frac{ge\mu_0}{2m_e}$$

Precessional motion of the magnetization $\vec{M}$ in a field $\vec{H}$:

$$\frac{d\vec{M}}{dt} = \gamma_0 \left[\vec{M} \times \vec{H}\right]$$

Note: Changes of the magnetization are perpendicular to $\vec{M}$, preserving $|\vec{M}| = M_s$

Phenomenological damping term according to Landau & Lifshitz

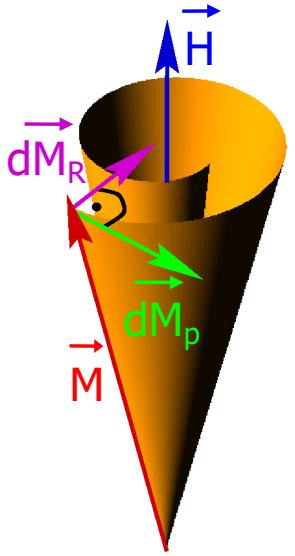
Precessional motion $$\frac{d\vec{M}}{dt} = \gamma_0 \left[\vec{M} \times \vec{H}\right]$$

Equilibrium condition: $\vec{M} \times \vec{H} = 0$, i.e., magnetization parallel to the field $\vec{H}$.

After a certain time, the static equilibrium will be reached through dissipation processes.
The precessing magnetization is gradually aligned along $\vec{H}$.

Addition of phenomenological damping term leads to the Landau-Lifshitz equation:

$$\frac{\mathrm{d}\boldsymbol{M}}{\mathrm{d}t} = \gamma_{\mathrm{L}} \left[\boldsymbol{M} \times \boldsymbol{H}\right] - \frac{\alpha_{\mathrm{L}}}{M_{\mathrm{s}}} \left[\boldsymbol{M} \times (\boldsymbol{M} \times \boldsymbol{H})\right]$$



Relaxation term preserves the norm of $\vec{M}$ and leads to an asymptotic alignment towards $\vec{M} \times \vec{H} = 0$

Gilbert equation vs. Landau & Lifshitz equation

$$\frac{\mathrm{d}\boldsymbol{M}}{\mathrm{d}t} = \gamma_\mathrm{L}\left[\boldsymbol{M}\times\boldsymbol{H}\right] - \frac{\alpha_\mathrm{L}}{M_\mathrm{s}}\left[\boldsymbol{M}\times\left(\boldsymbol{M}\times\boldsymbol{H}\right)\right]$$

Landau-Lifshitz equation

In this phenomenology, the damping parameter α_L only acts on relaxation, not on precession.

Gilbert equation:

$$\frac{\mathrm{d}\boldsymbol{M}}{\mathrm{d}t} = \gamma_\mathrm{G}\left[\boldsymbol{M}\times\boldsymbol{H}\right] - \frac{\alpha_\mathrm{G}}{M_\mathrm{s}}\left[\boldsymbol{M}\times\frac{\mathrm{d}\boldsymbol{M}}{\mathrm{d}t}\right]$$

In the Gilbert equation, the entire motion of ***M*** is damped.

Gilbert equation and Landau-Lifshitz equation are mathematically equivalent.

The Gilbert equation can be written in the Landau-Lifshitz form:

$$\frac{\mathrm{d}\boldsymbol{M}}{\mathrm{d}t} = \frac{\gamma_\mathrm{G}}{1+\alpha_\mathrm{G}^2}\left[\boldsymbol{M}\times\boldsymbol{H}\right] - \frac{\alpha_\mathrm{G}\gamma_\mathrm{G}}{\left(1+\alpha_\mathrm{G}^2\right)M_\mathrm{s}}\left[\boldsymbol{M}\times\left(\boldsymbol{M}\times\boldsymbol{H}\right)\right]$$

$$\gamma_\mathrm{L} = \frac{\gamma_\mathrm{G}}{1+\alpha_\mathrm{G}^2} \qquad \alpha_\mathrm{L} = \frac{\alpha_\mathrm{G}\gamma_\mathrm{G}}{\left(1+\alpha_\mathrm{G}^2\right)M_\mathrm{s}}$$

Usually, only the Gilbert damping parameter α_G is used.

Because of their formal equivalence, the Landau-Lifshitz equation and the Gilbert equation are commonly described as the **Landau-Lifshitz-Gilbert equation (LLG)**

Effective field

The effective magnetic field $\vec{H}_{\text{eff}}$ is the negative functional derivative of the total energy with respect to the magnetization:

$$\mathbf{H}_{\text{eff}} = -\frac{1}{\mu_0}\frac{\delta E}{\delta \mathbf{M}}$$

It accounts for the influence of the various energy terms on the magnetization dynamics, treating each energy term as a field contribution acting on the magnetization.

$$\boldsymbol{H}_{\text{eff}} = \boldsymbol{H}_{\text{ext}} - \frac{2A}{M_s^2\mu_0}\Delta \boldsymbol{M} - \nabla u - \frac{2D}{M_s^2\mu_0}\boldsymbol{M}\left(\boldsymbol{\nabla} \times \boldsymbol{M}\right) - \frac{1}{\mu_0}\frac{\delta e_{\text{ani}}}{\delta \boldsymbol{M}}$$

The effective field accounts for the influence of the various energy terms on the magnetization dynamics, treating each energy term as a field contribution acting on the magnetization.

Boundary conditions of the magnetization

Conditions for the magnetization at the boundary can be obtained by considering an equilibrium configuration, where the variation of the total energy vanishes.

$$\delta E(\boldsymbol{M}) = 0$$

The energy variation with respect to fluctuations of the magnetization $\vec{M} \to \vec{M} + \delta\vec{M}$, with the constraint $\vec{M} \cdot \delta\vec{M} = 0$ leads to the condition

$$\boldsymbol{H}_{\text{eff}} \times \boldsymbol{M} = 0$$

in the **volume** and

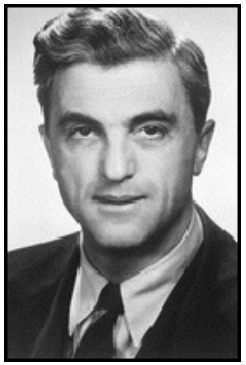
$$\frac{\partial \boldsymbol{M}}{\partial \boldsymbol{n}} = -\frac{D}{2A}(\boldsymbol{M} \times \boldsymbol{n}) + \frac{K_s}{A}\left[(\boldsymbol{M} \cdot \boldsymbol{n})\boldsymbol{M} - M_s^2 \boldsymbol{n}\right] \qquad \text{with} \qquad \frac{\partial \boldsymbol{M}}{\partial n} = \boldsymbol{\nabla} \boldsymbol{M} \cdot \boldsymbol{n}$$

at the **surface** ($\boldsymbol{n}$ is the outward oriented surface normal vector) in the case of a non-zero (bulk) DMI, and a **surface anisotropy** energy term of the form

$$E_{\text{surface}} = \int_{\partial V} K_s \left(1 - (\boldsymbol{m} \cdot \boldsymbol{n})^2\right) dS$$

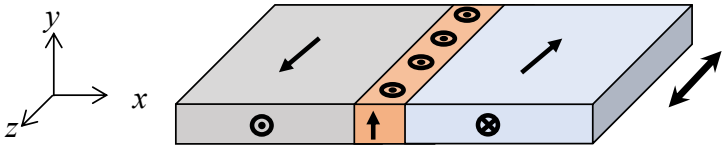
In ordinary ferromagnets, we have Brown's boundary condition $\dfrac{\partial \boldsymbol{M}}{\partial \boldsymbol{n}} = 0$

Size dependence: Domain wall width as intrinsic length scale



Felix Bloch (1905-1983)

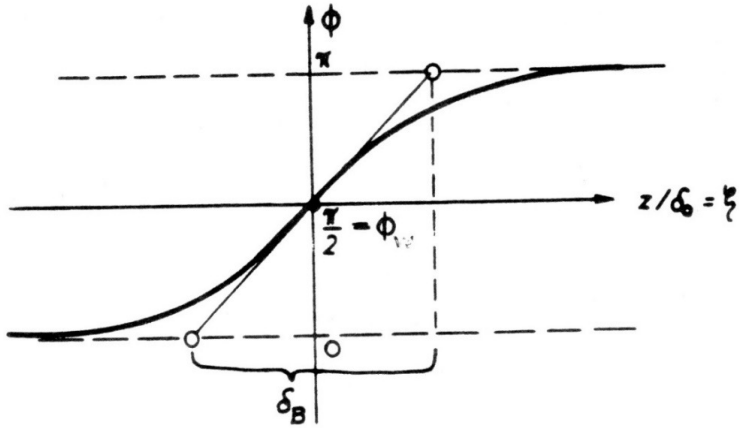
1952 Physics Nobel prize



$$m_z = \cos\vartheta(x)$$
$$m_y = \sin\vartheta(x)$$
$$m_x = 0$$

Magnetization rotation by 180° in a uniaxial ferromagnet

- **One-dimensional energy minimization problem**
- **Domain wall profile $\vartheta(x)$:** $\cos\vartheta(x) = \tanh(x/l_k)$



- **Exchange length:** $l_k = \sqrt{A/K}$

A: Exchange constant
K: Uniaxial anisotropy constant

Exchange length: Typical extension of magnetic inhomogeneities

Domain wall width results in a material-specific length scale.

The exchange length provides an estimate for the typical size of magnetic inhomogenities.

Soft-magnetic materials:
(low anisotropy)

hard-magnetic materials:
(strong anisotropy)

$$l_s = \sqrt{A/K_d} = \sqrt{2A/(\mu_0 M_s^2)}$$

$$l_k = \sqrt{A/K}$$

Exchange lengths

The exchange lengths are of the order of **several nm.**
This justifies *a posteriori* the continuum model (no atomistic treatment needed).

Table 3.1. *Exchange lengths of transition metals and intermetallic compounds using the material parameters of Tables 2.1–2.3. All lengths in units of nm = 10 Å (H_{ext} = 1000 Oe = $10^6/(4\pi)$ A/m; σ_H = 10 MN/m²).*

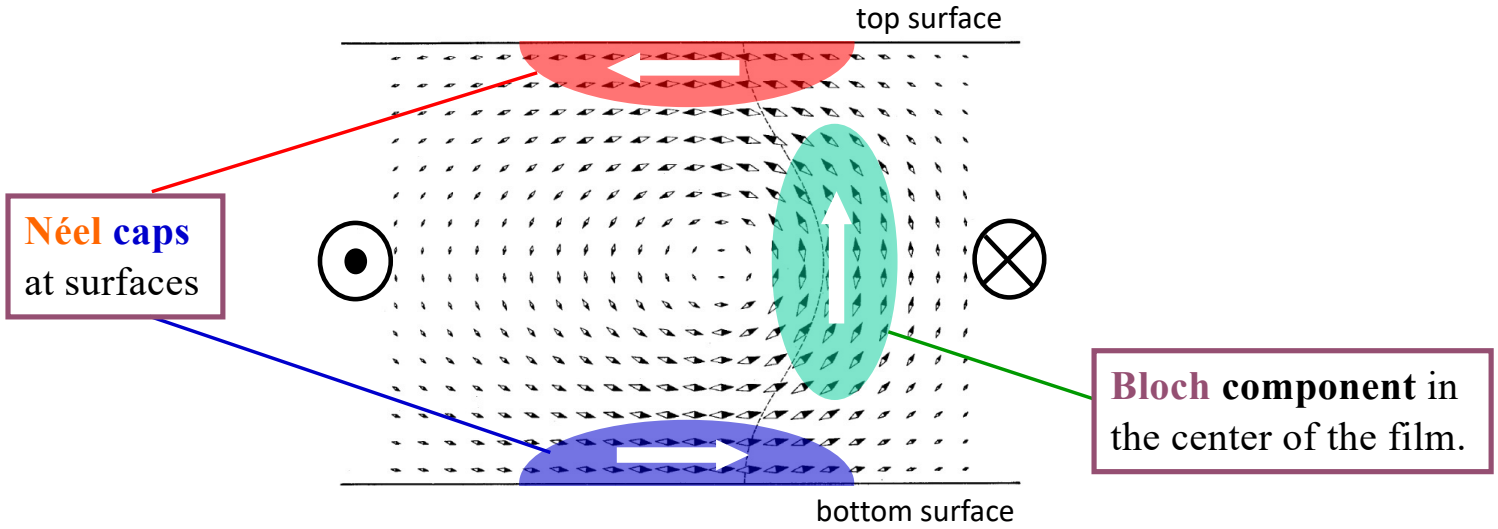
Material	l_K	l_s	l_H	l_σ
α-Fe	21	3.3	15.6	80
Co	8.3	4.9	20.4	56
Ni	42	8.7	16.1	31
Ni_3Fe	57	3.7	12.7	51
$Nd_2Fe_{14}B$	1.4	2.8	11.2	
$Pr_2Fe_{14}B$	1.4	3.1	14.0	
$SmCo_5$	0.84	5.3	17.1	
Sm_2Co_{17}	1.83	4.6	16.6	
$Sm_2Fe_{17}N_3$	1.18	4.4	14.0	
$BaFe_{12}O_{19}$	4.45	8.3	18.2	

Table 4.1. *Wall width and specific wall energy of some uniaxial crystals ($J/m^2 = 10^3$ erg/cm²). δ_B has been determined according to* $\delta_B = \pi(A/(K_1 + K_2))^{1/2}$.

Ferromagnet	δ_B [nm]	γ_B [10^{-2} J/m²]
Co	22.3	1.49
$SmCo_5$	2.64	5.71
Sm_2Co_{17}	5.74	3.07
$Nd_2Fe_{14}B$	3.82	2.24
$Sm_2Fe_{17}N_3$	3.36	4.06
$BaFe_{12}O_{19}$	13.94	0.57

from
H. Kronmüller, M. Fähnle
"Micromagnetism and the Microstructure of Ferromagnetic Solids"

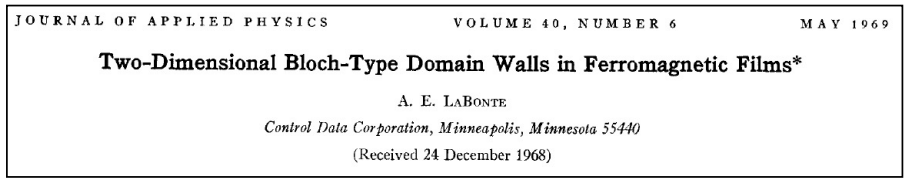
Mixed domain wall type: Asymmetric domain wall



Asymmetric Bloch walls:

- occur in thick, soft-magnetic films
- reduce the magnetostatic energy by combinin the fundamental wall types
  - Néel caps at der surface (no surface charges)
  - Bloch wall in the central part (no volume charges)
- were predicted by the first micromagnetic simulations in 1969 (LaBonte, Hubert)

J. Appl. Phys. 40 (6) 2450 (1969) A. E. LaBonte
phys. stat. sol. 32 (2) 519 (1969) A. Hubert


JOURNAL OF APPLIED PHYSICS VOLUME 40, NUMBER 6 MAY 1969

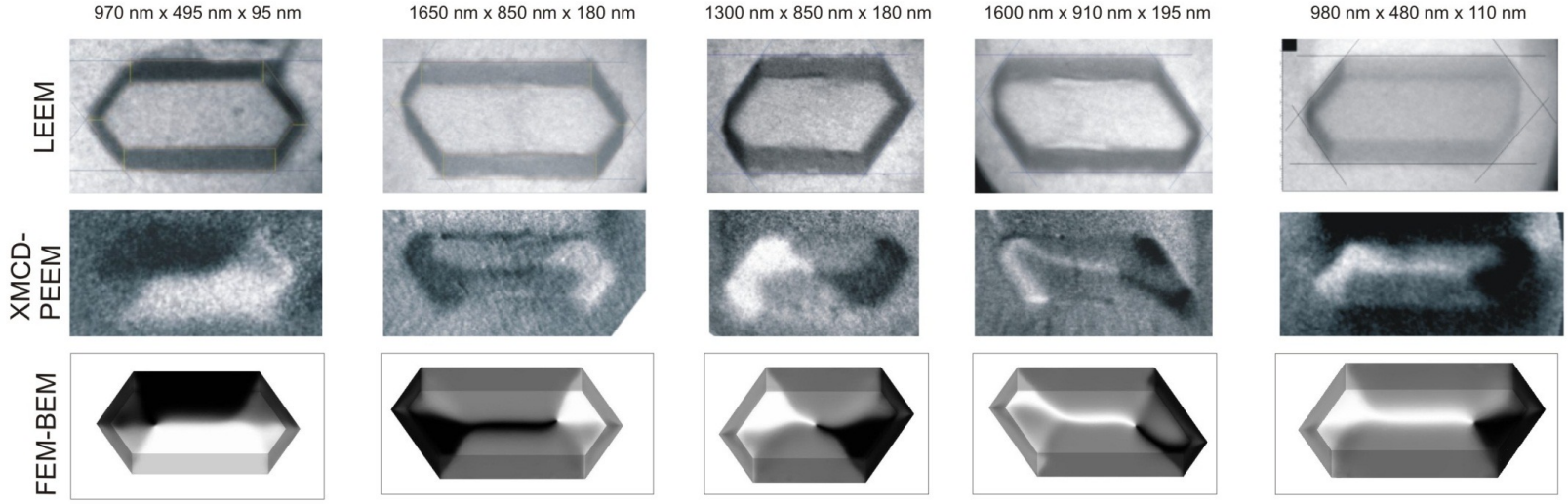
Two-Dimensional Bloch-Type Domain Walls in Ferromagnetic Films*

A. E. LaBonte

Control Data Corporation, Minneapolis, Minnesota 55440

(Received 24 December 1968)

Thick Fe/Mo (110) islands: experiment and simulation



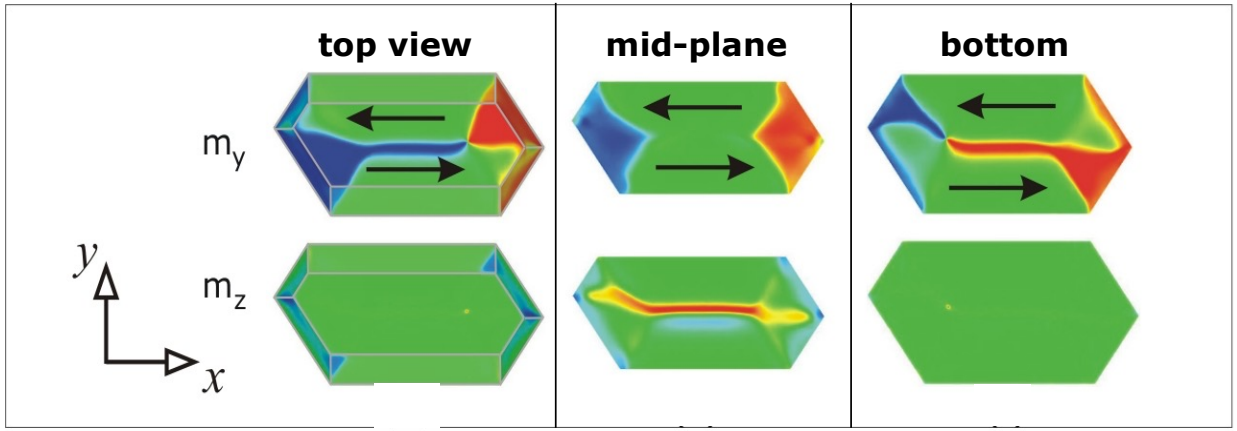
Excellent agreement between observed and simulated magnetic structures.

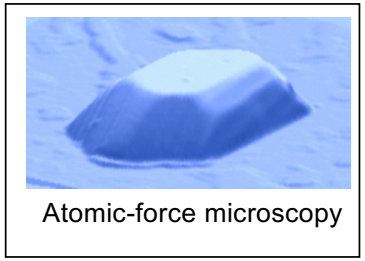
→ Simulated magnetic structures correspond to the real magnetization structures.

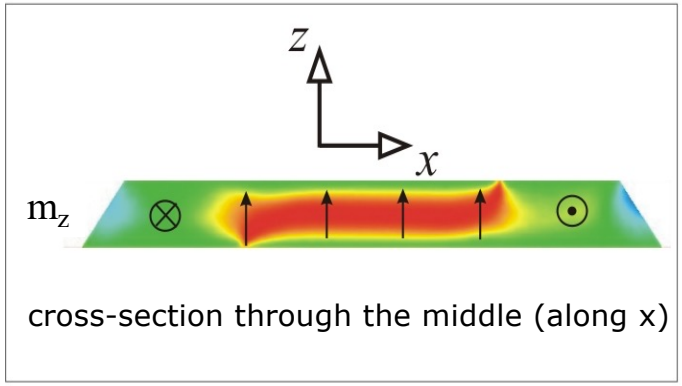
→ Simulations can be used to study the internal, three-dimensional magnetic structure inside the sample, which is not accessible in the experiment.

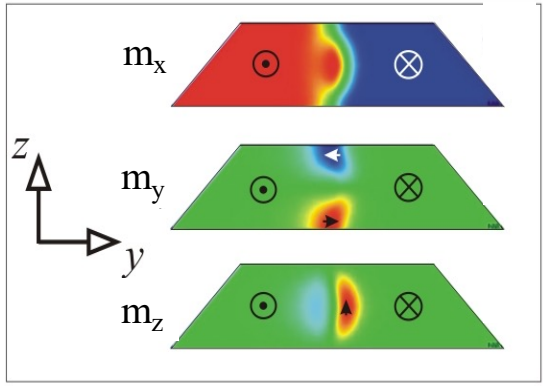
Phys. Rev. B 72, 214409 (2005)

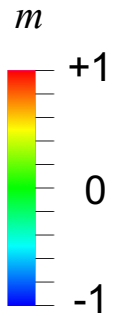
Insight provided by simulations











Different **cross-sections** through the sample show the **three-dimensional magnetic structure**:

-**Different asymmetry** on the top and on the bottom surface.

-**Asymmetric Bloch wall**: Néel wall at the surface, Bloch wall in the middle of the sample.

-Magnetic flux is carried through the Bloch wall from one vortex to the other, on the opposite side.

R. Hertel et al., Phys. Rev. B 72, 214409 (2005)

Micromagnetic modeling with tetmag

An open-source finite-element software with GPU acceleration



https://github.com/R-Hertel/tetmag

Motivation for a new micromagnetic software: 3D nanomagnetism

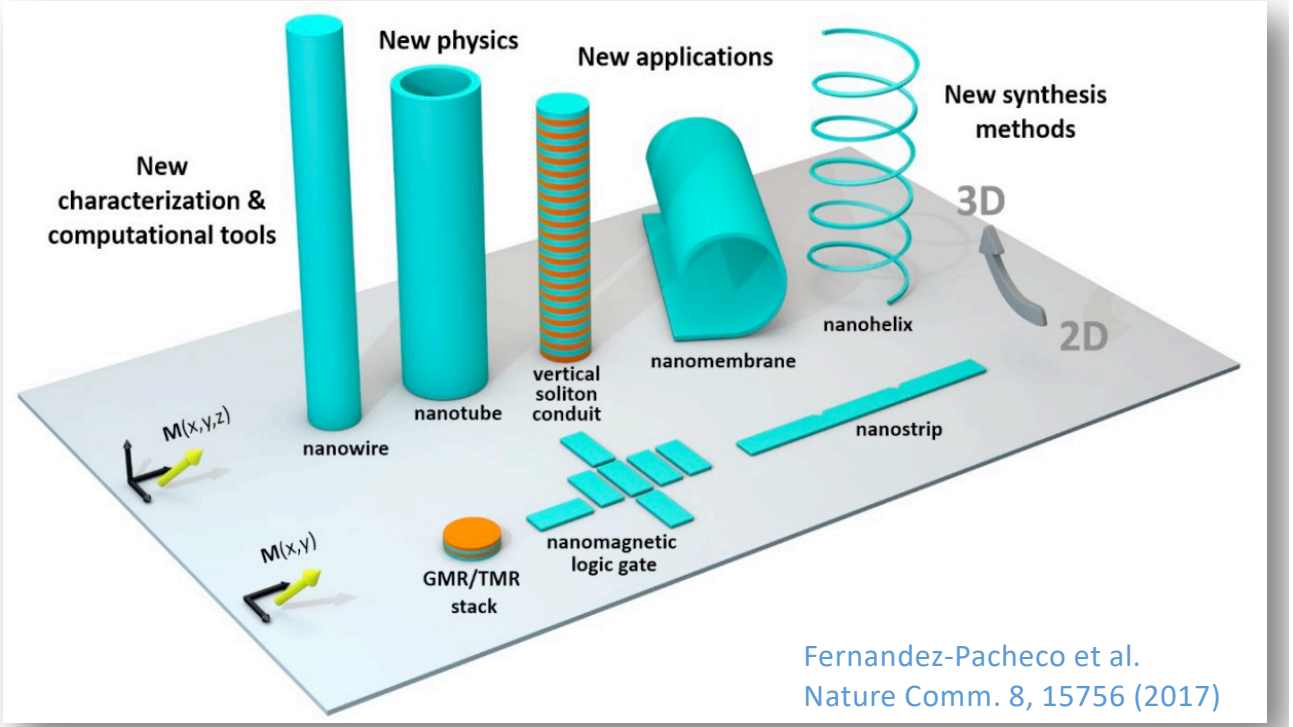
3D magnetic nanostructures with complex shapes

Functionality, physical properties may depend sensitively on the 3D shape of the nanostructure

Typical situations in **3D nanomagnetism:**

- Relatively large structures
- Complex geometries
- Smooth, curved surfaces
- Low volume occupancy
- Arrays of interacting particles

Theoretical studies require versatile and fast simulations



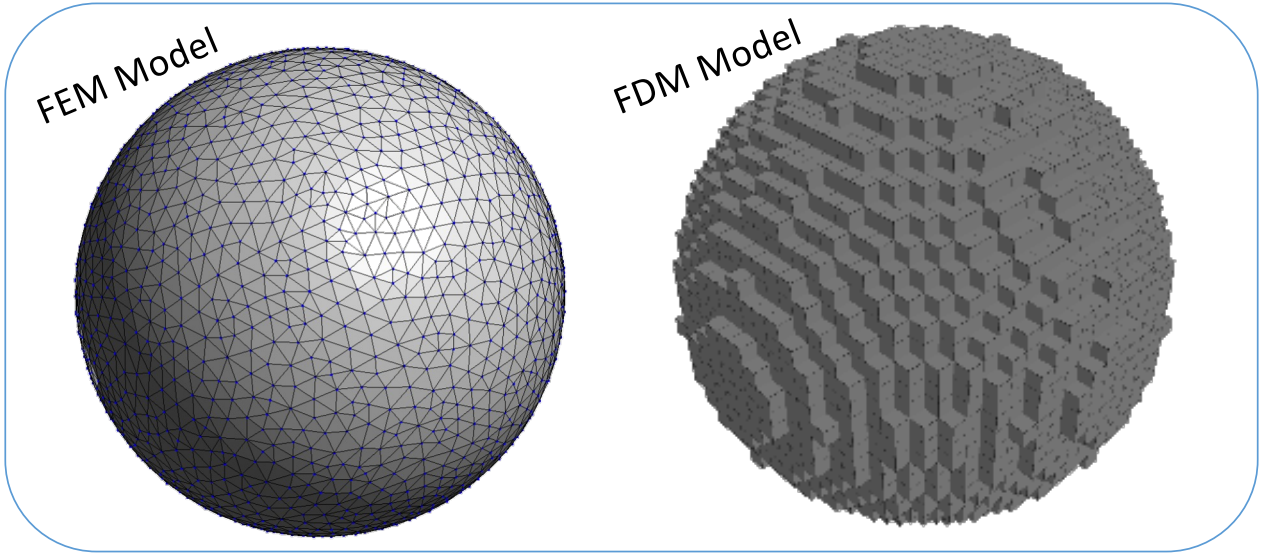
Fernandez-Pacheco et al. Nature Comm. 8, 15756 (2017)

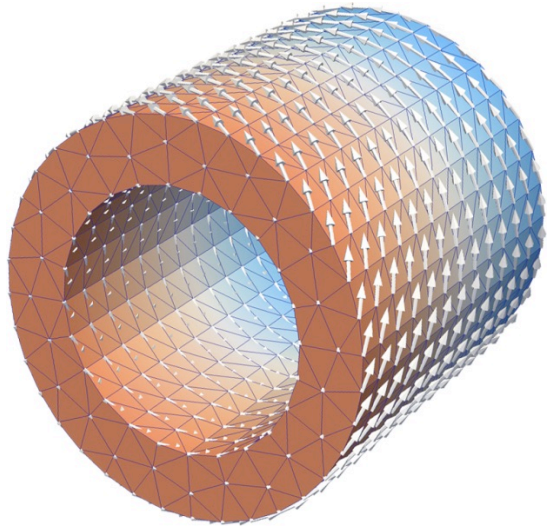
Curved 3D geometries are difficult to handle with commonly used finite-difference based software

Finite Elements for Geometric Flexibility

Advantages of Finite Difference Method	Advantages of Finite Element Method
Relatively easy to implement	Accurate approximation of non-trivial geometries
Low memory requirements per DOF	Adaptive mesh refinement
fast and easy to parallelize	Well suited for three-dimensional nanostructures

Details of the sample shape can have a decisive impact on the magnetic properties.
Subtle geometric effects, like curvature-induced asymmetries, require precise geometric models.





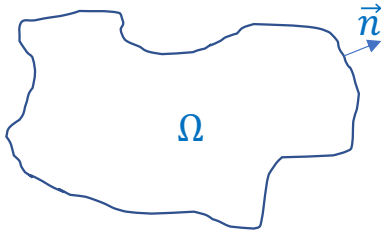
Exchange field implementation in FEM: Weak form

Problem

Find H_i such that

$$H_i = -c\Delta m_i \text{ in } \Omega$$

with $i = x, y, z$ $c = \frac{2A}{M_s \mu_0}$, $\frac{\partial m_i}{\partial n} = g_N$ on $\partial\Omega_N$.



Weak form

1. The exchange field H_i satisfies $\int_\Omega (c\nabla^2 m + H_i) \cdot v \, dV = 0$ for arbitrary test functions v.
2. Integration by part yields

$$\int_\Omega v \cdot H_i \, dV = \int_\Omega c\nabla m_i \cdot \nabla v \, dV - \oint_{\partial\Omega} cv \cdot \frac{\partial m_i}{\partial n} \, dS$$

With **Brown's boundary condition** $\frac{\partial m}{\partial n} = g_n = 0$

$$\int_\Omega v \cdot H_{exc,i} \, dxdy = \int_\Omega c\nabla m_i \cdot \nabla v \, dxdy$$

Straightforward implementation, use element shape functions as test functions, matrix-vector product of stiffness matrix and discretized magnetization.

Dzyaloshinskii-Moriya Interaction: Effective field and boundary conditions

Energy density

$$e_{DMI} = D\boldsymbol{m} \cdot (\boldsymbol{\nabla}\times\boldsymbol{m})$$

Effective field

$$\boldsymbol{H}_{DMI} = -\frac{1}{\mu_0 M_s}\frac{\delta \int e_{DMI} dV}{\delta \boldsymbol{m}} = -\frac{2D}{\mu_0 M_s}(\nabla\times\boldsymbol{m})$$

The effective DMI field can be calculated directly with linear elements.
But the **DMI changes the boundary conditions used in the ferromagnetic exchange field calculation**.

Boundary conditions with DMI:

$$\frac{\partial \boldsymbol{m}}{\partial \boldsymbol{n}} = \frac{D}{2A}(\boldsymbol{m}\times\boldsymbol{n})$$

Rohart & Thiaville, PRB 88, 184422 (2013)

$$\int_\Omega v \cdot H_{\mathrm{exc},i}\, dV = \int_\Omega c\nabla m_i \cdot \nabla v\, dV - \oint_{\partial\Omega} cv \cdot \frac{\partial m_i}{\partial n} dS = \int_\Omega v H_{\mathrm{exc},i}{}^{(bulk)}\, dV - \int_{\partial\Omega} v \cdot \frac{D}{\mu_0}(m\times n)_i dS$$

Boundary conditions of ferromagnetic exchange field are modified if DMI is non-zero

Additional surface contribution in the case of nonzero DMI

Exchange energy calculation via effective field

Each partial energy term is monitored during the simulation.

The effective fields are computed at each time step.
To efficiently calculate the exchange energy, the effective field of the exchange term can be used:

Exchange energy density: $e_{xc} = A \sum_{i=x,y,z} (\boldsymbol{\nabla} m_i)^2$

Effective exchange field: $\boldsymbol{H}_{exc} = -\frac{1}{\mu_0}\frac{\delta e}{\delta \boldsymbol{m}} = -\frac{2A}{\mu_0}\Delta \boldsymbol{m}$

$$\boxed{\frac{\mu_0}{2}\boldsymbol{m} \cdot \boldsymbol{H}_{\mathrm{exc}}} = -A\boldsymbol{m} \cdot \Delta \boldsymbol{m} = -A\nabla(\boldsymbol{m} \cdot \nabla \boldsymbol{m}) + A(\nabla \boldsymbol{m})^2 \boxed{= e_{xc}}$$

since $\boldsymbol{m} \cdot \nabla \boldsymbol{m} = \frac{1}{2}\nabla(\boldsymbol{m}^2) = 0$, because of $|\boldsymbol{m}| = \mathrm{const.}$

Reusing available data ($\vec{H}_{exc}$) reduces computational costs.

Magnetostatic field calculation - Basic Equations

Non-local long-range interaction, computationally expensive.
Irregular FEM mesh incompatible with commonly used FFT method.
Numerical calculation of magnetostatic potential in real space:

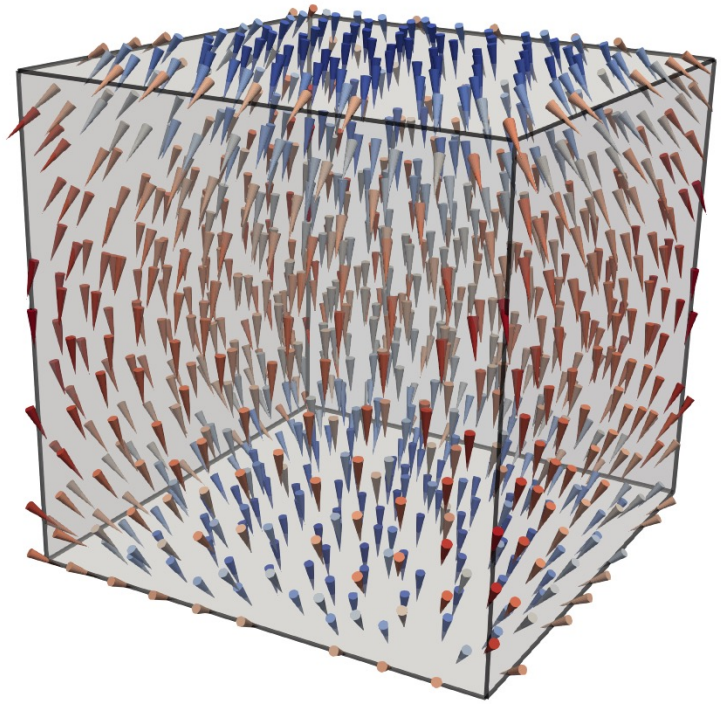
Gradient field $\boldsymbol{H} = -\boldsymbol{\nabla} u$

Poisson Equation $\Delta u = -\rho$

Volume charges $\rho = -\boldsymbol{\nabla} \cdot \boldsymbol{M}$

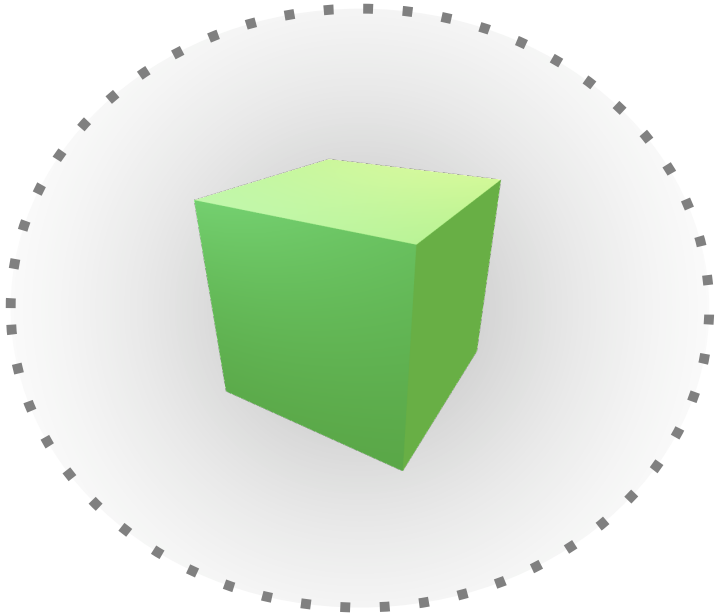
Jump condition at the surface: $\dfrac{\partial u^i}{\partial \boldsymbol{n}} - \dfrac{\partial u^o}{\partial \boldsymbol{n}} = \boldsymbol{M} \cdot \boldsymbol{n}$

boundary conditions of u at surface?



Demagnetizing field of a homogeneously magnetized cube

Open Boundary Problem – Hybrid FEM/BEM



Boundary conditions of Poisson equation defined at infinite distance from the sources.

Magnetostatic potential only required in magnetic region

FEM-BEM solution

Split potential in two parts; $u = u_1 + u_2$
Solve u_1 and u_2 only in magnetic region Ω
u_1 is zero outside magnetic region Ω

D.R. Fredkin and T.R. Koehler, IEEE Trans. Mag. 26, 415 (1990)

Boundary conditions for u_1 and u_2 defined at the surface

Poisson Problem with Neumann B.C.

$$\Delta u_1 = \nabla \cdot M$$

$$\frac{\partial u_1}{\partial n} = M \cdot n$$

$$\Delta u_2 = 0$$

u_2 at surface $\partial\Omega$
not immediately known

Laplace Problem with Dirichlet B.C.

In *tetmag*: Fast solution of PDEs by using algebraic multigrid method with GPU acceleration (AMGCL library)

FEM-BEM Boundary Integral

Dirichlet Boundary conditions of u_2 are related to boundary values of solution u_1.

$$u_2(\boldsymbol{x}) = \oint u_1(\boldsymbol{x}') \frac{\partial G}{\partial \boldsymbol{n}'} \mathrm{d}S' + \left(\frac{\Psi}{4\pi} - 1 \right) u_1(\boldsymbol{x}) \qquad \text{with} \qquad G(\boldsymbol{x}, \boldsymbol{x}') = -\frac{1}{4\pi} \frac{1}{|\boldsymbol{x} - \boldsymbol{x}'|}$$

D.R. Fredkin and T.R. Koehler,
IEEE Trans. Mag. 26, 415 (1990)

Numerical Form
Matrix-Vector Product

$$\underline{u_2} = \underline{\underline{M}} \cdot \underline{u_1}$$

Where $\underline{\underline{M}}$ is a dense *N* x *N* matrix

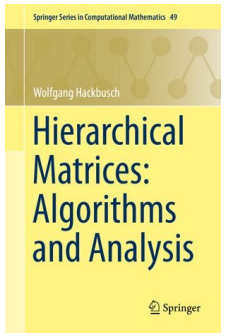
- **Huge memory requirements O(N²)**
- **Large number of operations in MVP**
- **Slow calculation of matrix elements**

Large-scale computations are impossible with this method in its original form

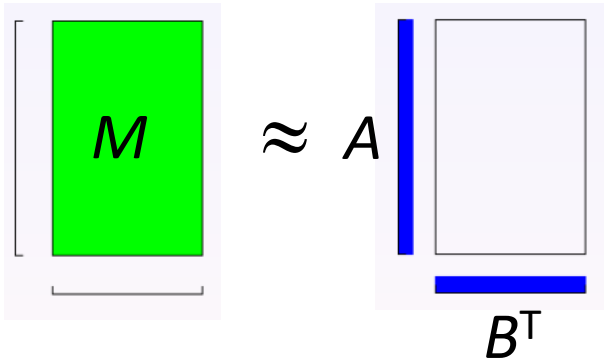
Hierarchical Matrix Compression (H-Matrix)

- Data-sparse approximation of non-sparse matrix
- Submatrices approximated by product of low-rank matrices

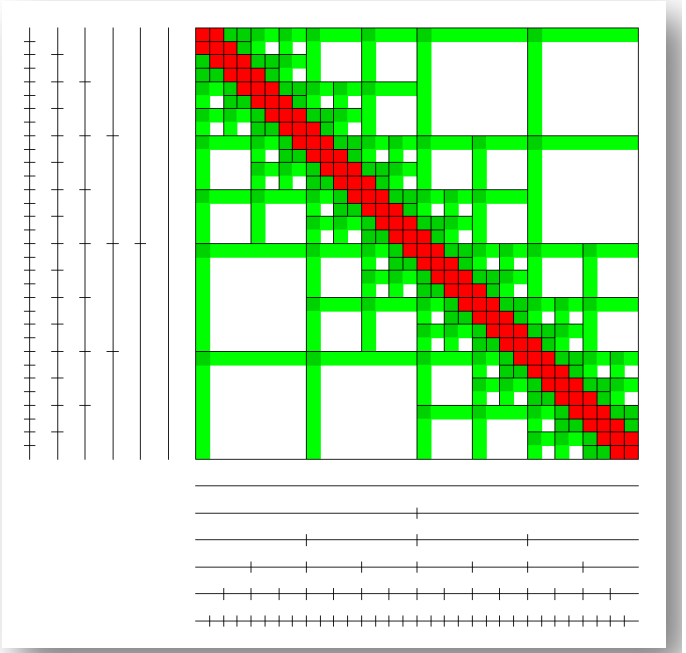
W. Hackbusch



$$\underline{\underline{M}}|_{t\times s} \approx \underline{\underline{A}}\,\underline{\underline{B}}^T$$



$$\underline{\underline{A}} \in \mathbb{R}^{t\times k}, \underline{\underline{B}} \in \mathbb{R}^{s\times k}$$



- Proven to be efficient in FEM micromagnetics

H. Forster et al., IEEE Trans. Mag. 39, 2513 (2003)
A. Knittel et al., J. Appl. Phys. 105, 07D542 (2009)
A. Kakay et al. IEEE Trans. Mag 46, 2301 (2010)

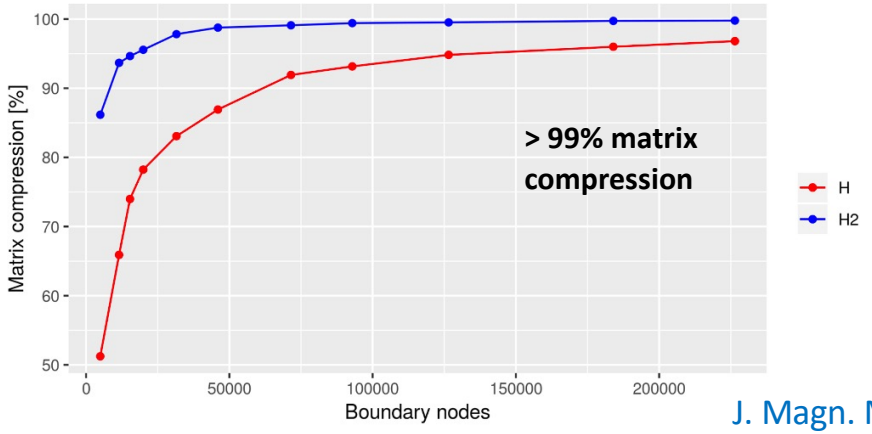
Scaling of total memory requirements reduced from $O(N^2)$ to $O(N \log N)$

Memory efficiency and linear scaling

Accurate magnetostatic field calculation with
Fredkin-Koehler type hybrid FEM-BEM algorithm

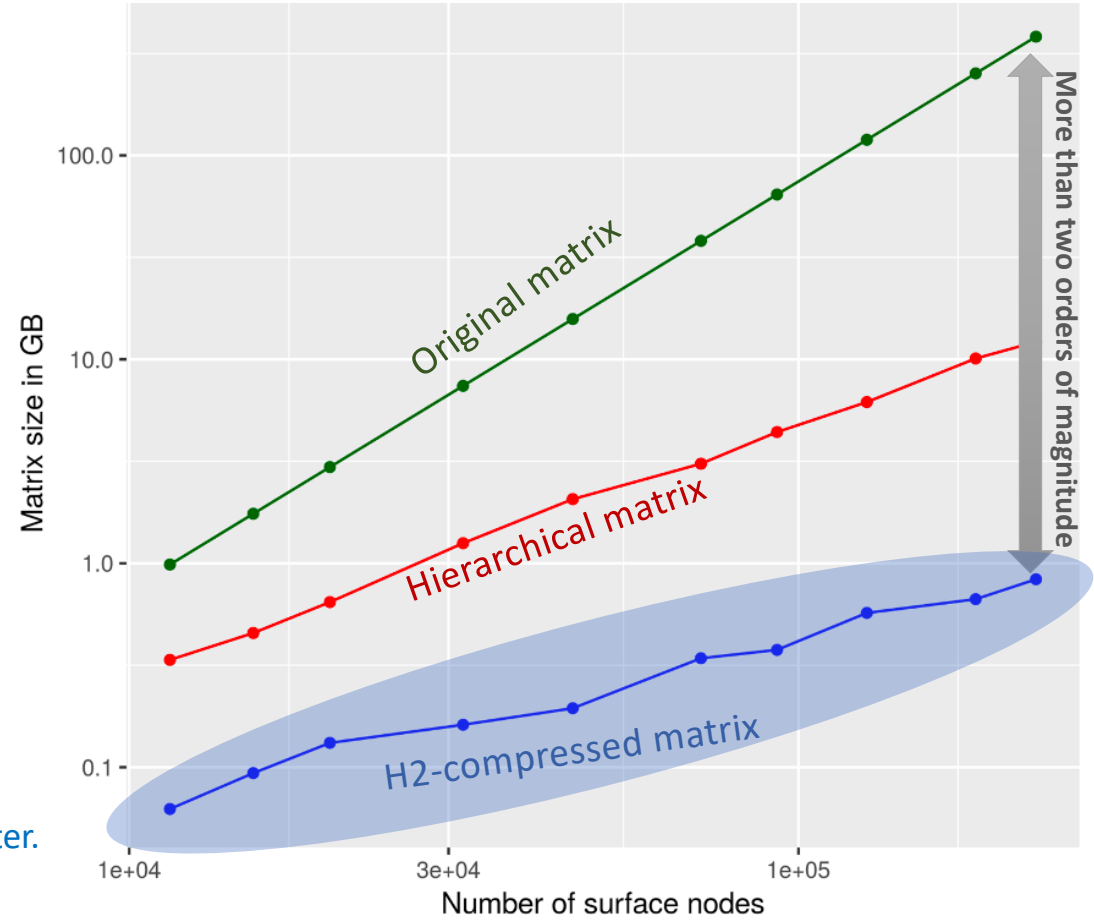
D.R. Fredkin and T.R. Koehler,
IEEE Trans. Mag. 26, 415 (1990)

Massive reduction of numerical costs
by using H2-type hierarchical matrices



Conversion of a problem of complexity $\mathcal{O}(N^2)$ to $\mathcal{O}(N)$

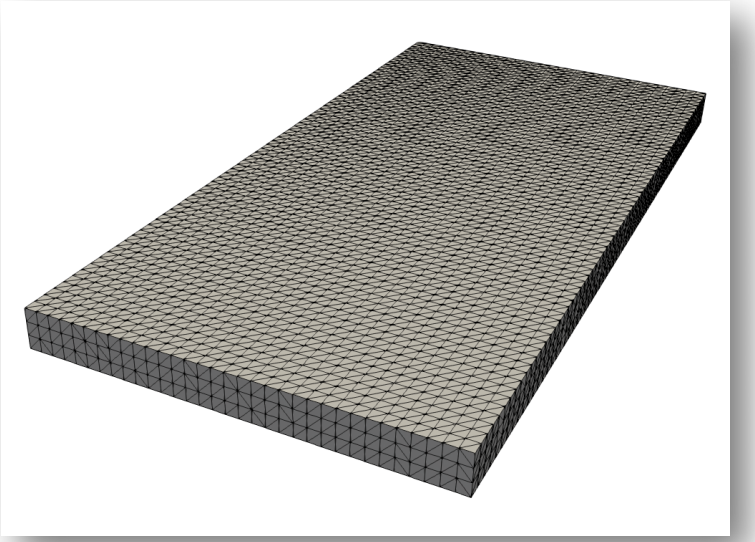
J. Magn. Magn. Mater. 477, 118 (2019)



Efficient mathematical algorithms and numerical implementations can save large amounts of hardware resources and countless hours of calculation time

Test Cases of H2 Implementation in Micromagnetic Code

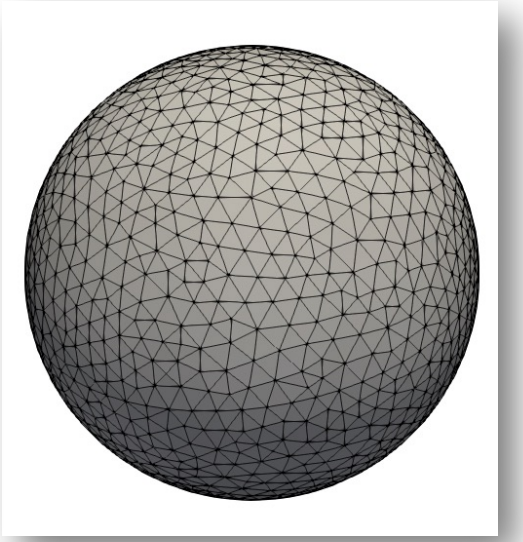
Simple geometries with analytic solutions of the demagnetizing field and energy (for specific magnetic structure)



Rectangular prism

Demagnetizing factors

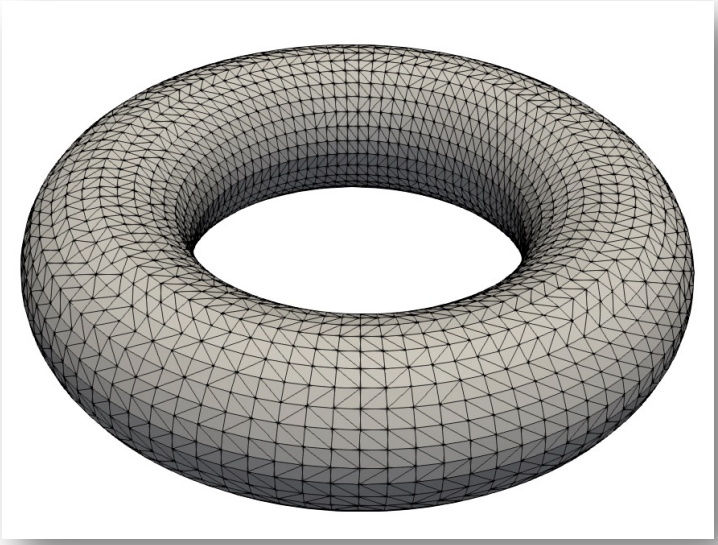
A. Aharoni, J. Appl. Phys 83, 3432 (1997)



Ellipsoid

Demagnetizing factors

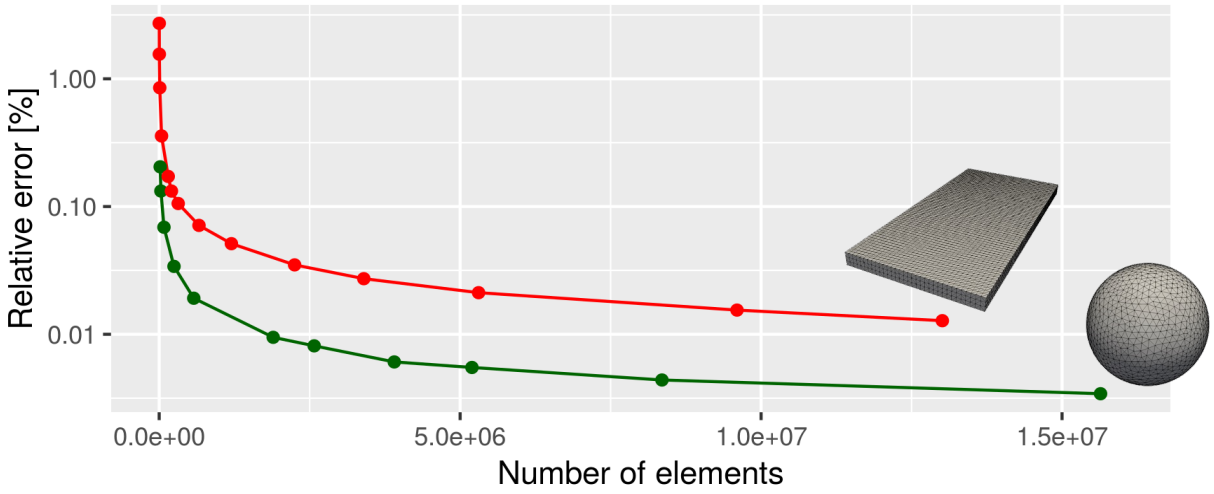
J.A. Osborn Phys. Rev. 67, 351 (1945)

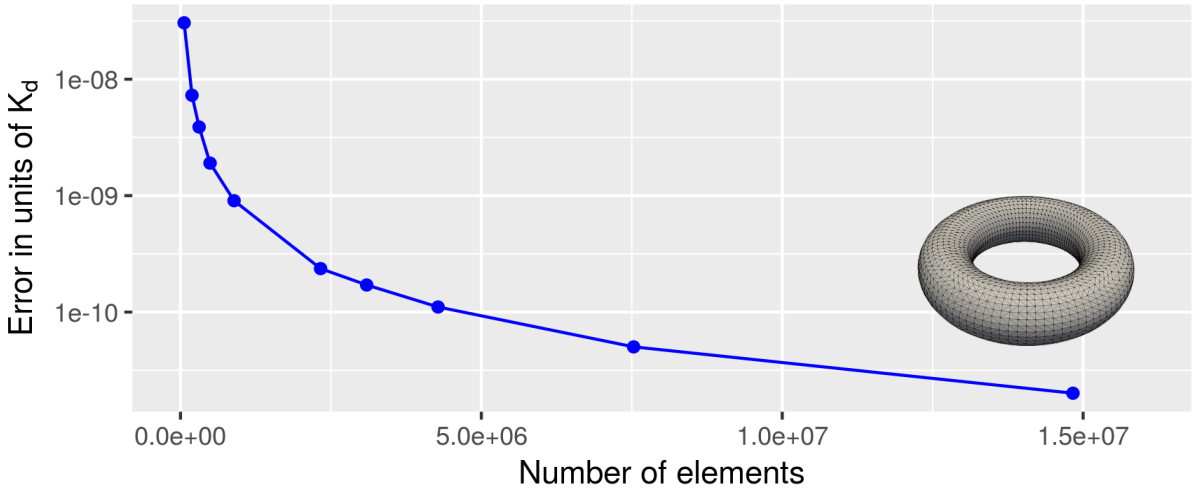


Torus

Trivial solution for azimuthal magnetic structure
(no sources of *H* field)

Tests of H2 Implementation in Micromagnetic Code

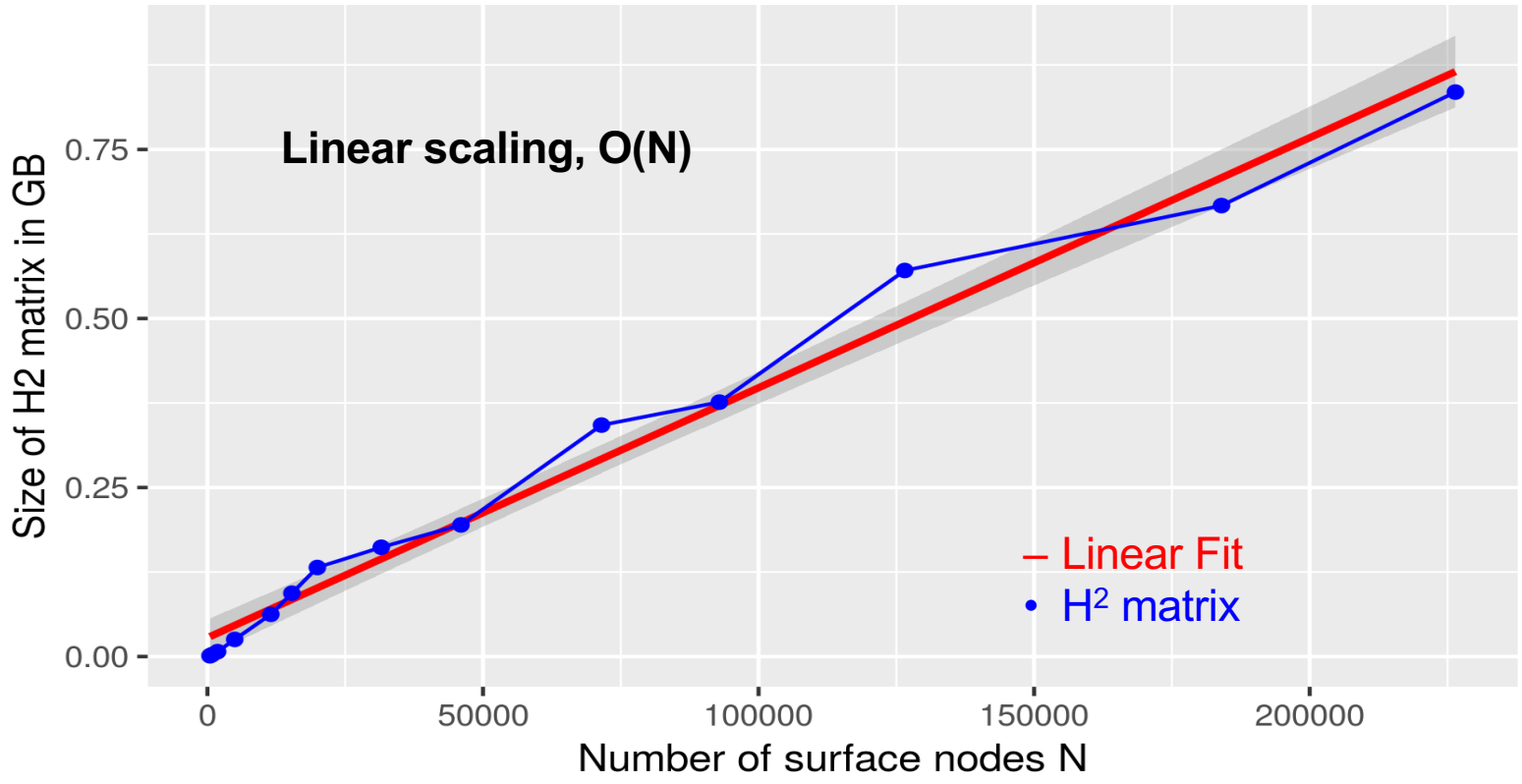




- **Small global error, decreases with increasing discretization density.**
- **Lower convergence rate in case of prism due to logarithmic divergence at corner and edges.**

  A. Thiaville et al. phys. stat. sol. (a) 170, 125 (1998)
- **Errors are not determined by H^2 approximation, but by FEM discretization**

Linear scaling with H2 matrix compression



R. Hertel, S. Christophersen and S. Börm,
J. Magn. Mag. Mater 477, 118 (2019)

Main features of tetmag

tetmag

Open-source software for finite-element micromagnetic simulations

https://github.com/R-Hertel/tetmag

Features

- General-purpose micromagnetic simulations with LLG + STT
- FEM for geometric flexibility
- Object-oriented C++
- Hybrid FEM-BEM calculation of magnetostatic field calculation
- H2-type matrix compression for efficient BEM integration
- GPU acceleration with CUDA
- Thread-parallelization of CPU version with OpenMP
- Suitable for large-scale simulations
- Platform-independent - tested on Linux and MacOS

Software to treat common micromagnetic simulation tasks:

- Static magnetization structures
- Field-driven magnetization dynamics
- Current-driven dynamics
- Hysteresis loops
- Interacting particles
- Implements bulk DMI, cubic & uniaxial, and surface anisotropy

Powered by several efficient libraries and numerical tools

















Micromagnetic simulation workflow

input

simulation parameters, material parameters

FEM mesh generation



Gmsh

Geometry design



Initial configuration

Calculate effective fields

Calculate energy

LLG integration

Check Termination criterion

Update effective fields during time steps

Main loop

Write output

tetmag

https://github.com/R-Hertel/tetmag

Repeated evaluation of effective fields in the main loop

Typical parameters:

- LLG integration time step < 1ps,
- Simulation time ~ 10 ns
- Approx. 10^5 of DOF

Millions of effective-field evaluations

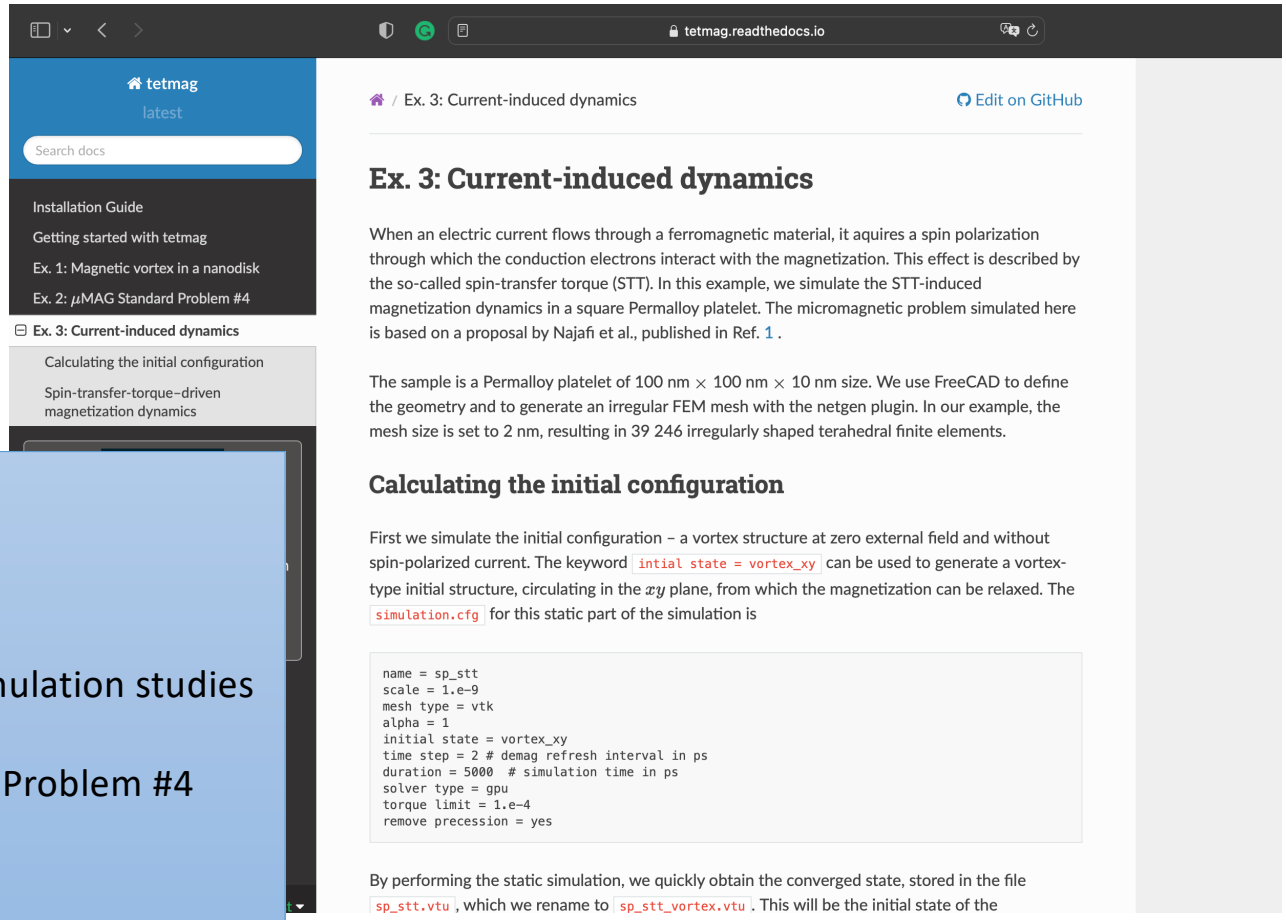
GPU-accelerated efficient algorithms allow for large-scale simulations

Visualization and data analysis

ParaView

tetmag documentation

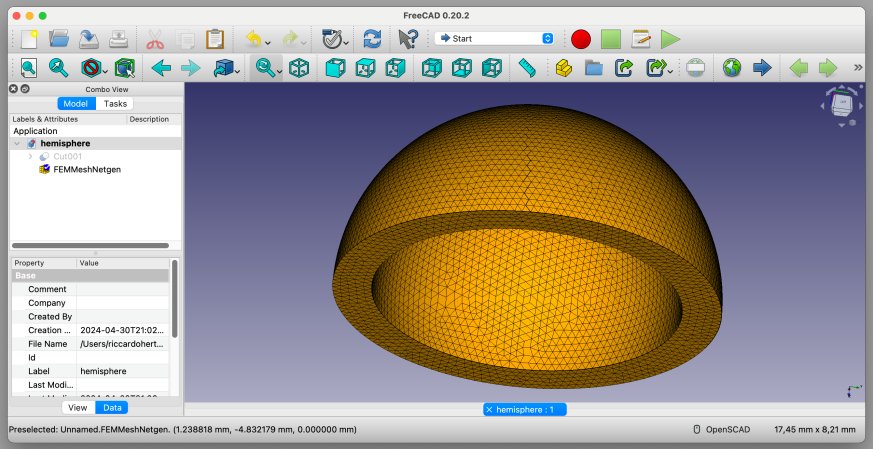
https://tetmag.readthedocs.io



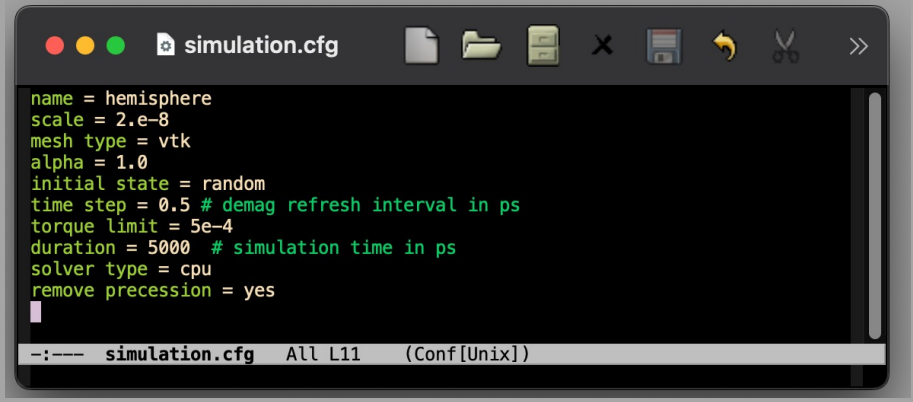
- Installation guide
- Introduction describing basic usage
- Step-by-step description of example simulation studies
- Field-driven switching: µMAG Standard Problem #4
- Current-driven magnetization dynamics
- Continuously updated with new features and examples

tetmag in action

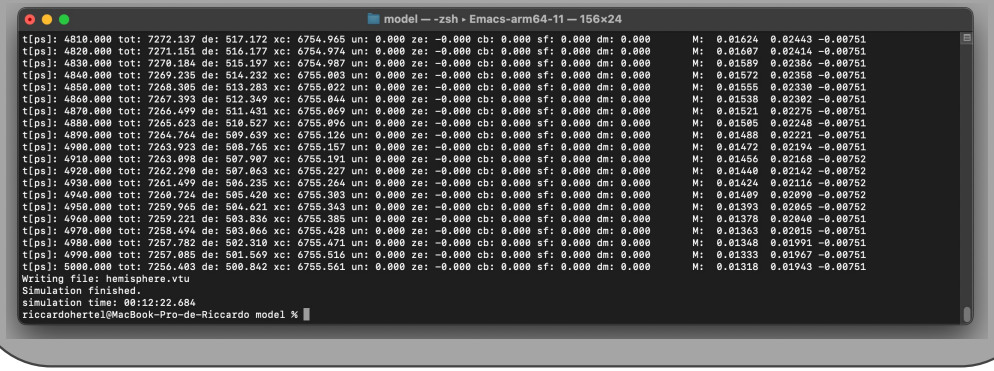
1. Define geometry and FEM mesh (FreeCAD)



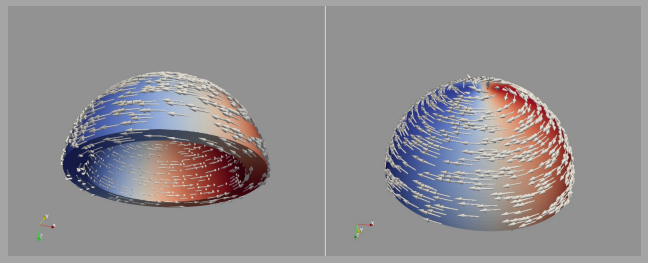
2. Supply input data (ASCII file)

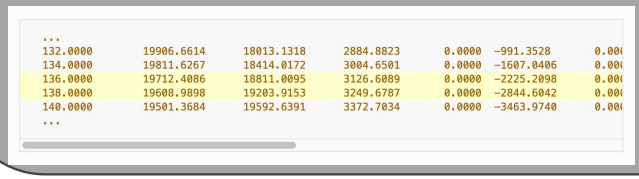


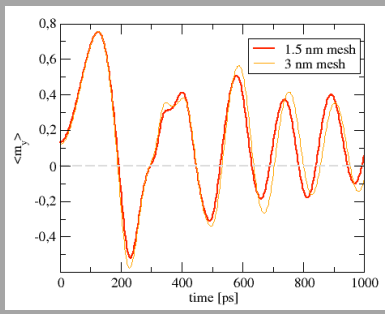
3. Run the simulation



4. Analyze the results

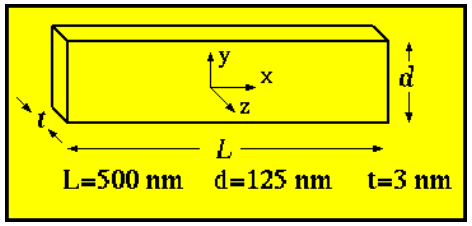




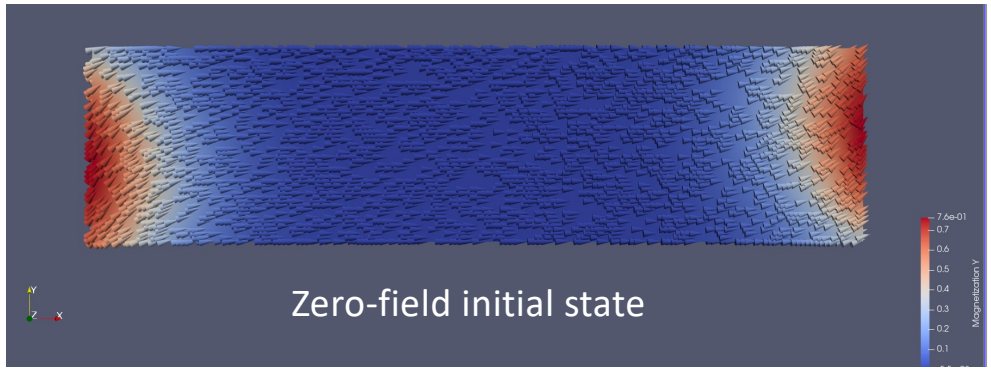


Magnetic switching: Standard Problem #4

Example/comparison: Field-induced magnetic switching of a Permalloy nanoplatelet



https://www.ctcms.nist.gov/~rdm/std4/spec4.html

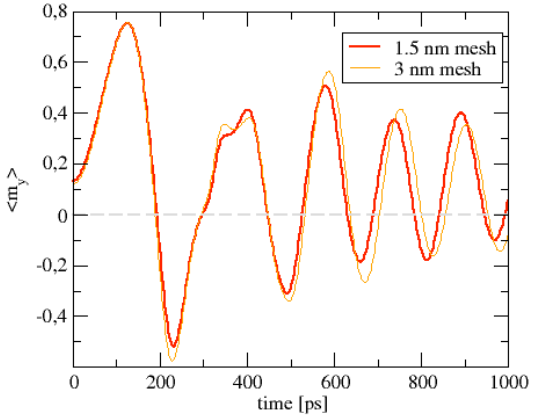


tetmag input file

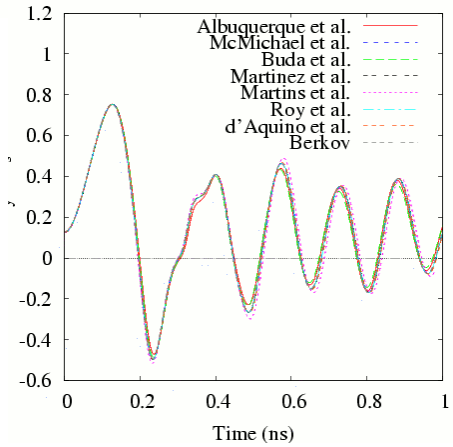
```
name = sp4_
scale = 1.e-9
mesh type = vtk
alpha = 0.02
initial state = fromfile_sp4_s-state.vtu
time step = 0.1 # demag refresh interval in ps
duration = 1000  # simulation time in ps
solver type = gpu

external field = 25.0 #  Hext in mT
    theta_H = 90 # polar angle of the field direction in degree
    phi_H = 170 # azimuthal angle
```

https://tetmag.readthedocs.io



tetmag result



Results reported by other teams

Current-induced dynamics: Vortex driven by DC current

Spin-Transfer Torque driven magnetization dynamics

$$\frac{d\vec{M}}{dt} = -\gamma' \vec{M} \times \vec{H}_{\text{eff}} - \frac{\alpha\gamma'}{M_s}\vec{M} \times (\vec{M} \times \vec{H}_{\text{eff}})$$

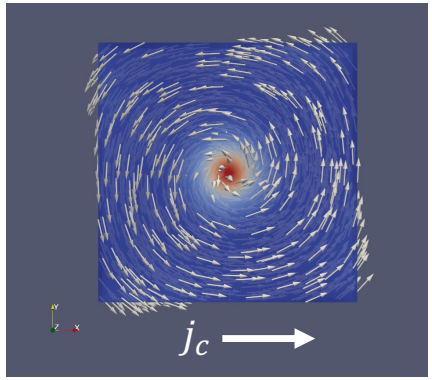
$$- \frac{b_j'}{M_s^2}(1 + \alpha\xi)\vec{M} \times (\vec{M} \times (\vec{j} \cdot \vec{\nabla})\vec{M})$$

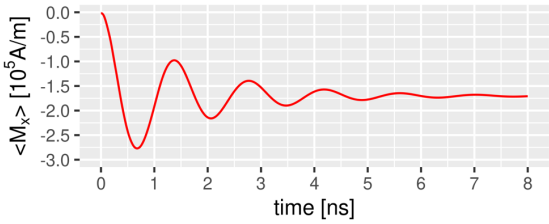
$$- \frac{b_j'}{M_s}(\xi - \alpha)\vec{M} \times (\vec{j} \cdot \vec{\nabla})\vec{M}$$

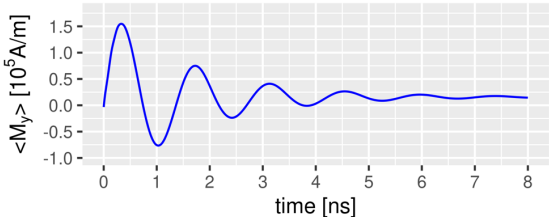
tetmag input file

```
name = sp_stt
scale = 1.e-9
mesh type = vtk
alpha = 0.1
initial state = fromfile_sp_stt_vortex.vtu
time step = 0.1
duration = 14000
solver type = gpu

current type = dc
     spin polarization = 1.0 # degree of spin polarization in stt dynamics
     current density =  1.0 # current density for STT dynamics [in 10^12 A/m^2]
     beta = 0.05 # non-adiabaticity parameter in STT term (also known as xi)
     current theta = 90 # polar angle of electric current flow [in degrees]
     current phi = 0 # azimuthal angle of electric current flow [in degrees]
```





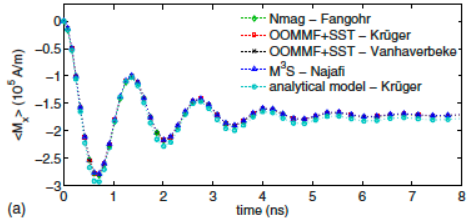


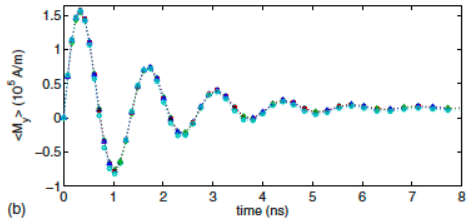
tetmag result

https://tetmag.readthedocs.io

Instantaneous application of an in-plane DC current.

Vortex oscillates towards new equilibrium position.





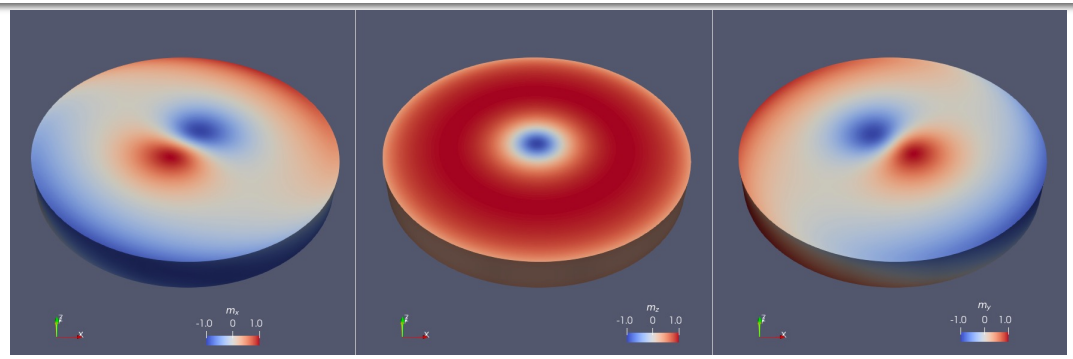
Results reported by other teams

M. Najafi et al., J. Appl. Phys. 105, 113914 (2009)

Skyrmion in a FeGe disk

Example with “bulk”-type Dzyaloshinskii-Moriya interaction:

$$e_{DMI} = D\boldsymbol{m} \cdot (\boldsymbol{\nabla} \times \boldsymbol{m})$$



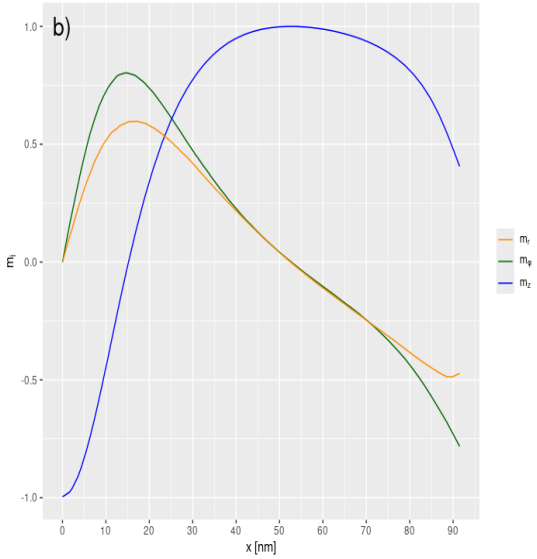
Static magnetization structure in a FeGe disk,
d = 180 nm, t = 20 nm, $H_{\text{ext}} = 400\ \text{mT}$

```
A = 8.78e-12
Ms = 0.384e6
D = 1.58e-3
```

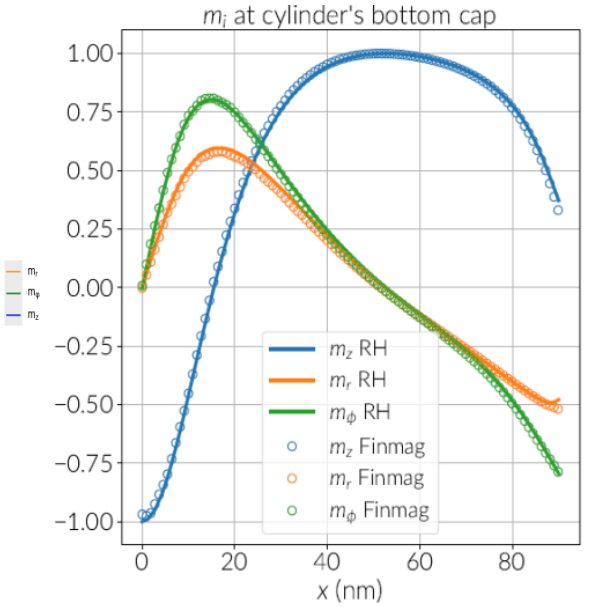
tetmag input file for material parameters

Perfect agreement between results from tetmag and the FDM code of the Southampton group (fidimag)

Comparison of results: magnetization profiles (radial line scans)



tetmag result



D. Cortés-Ortuño et al.,
New J. Phys. 20, 113015 (2018)

Interacting magnetic particles

Software allows for simulation of an **ensemble of magnetostatically coupled particles.**
No need to discretize the non-magnetic area between the objects.

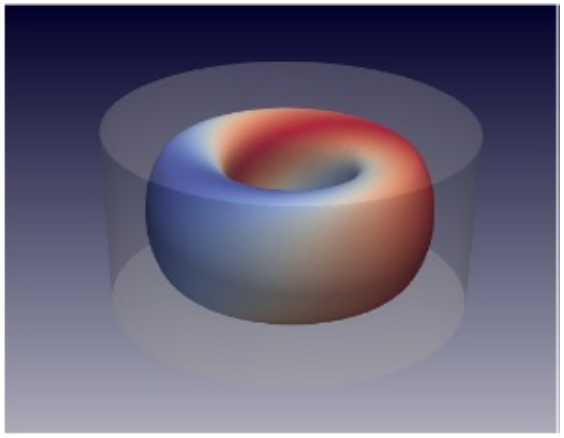
Example: The tetmag logo



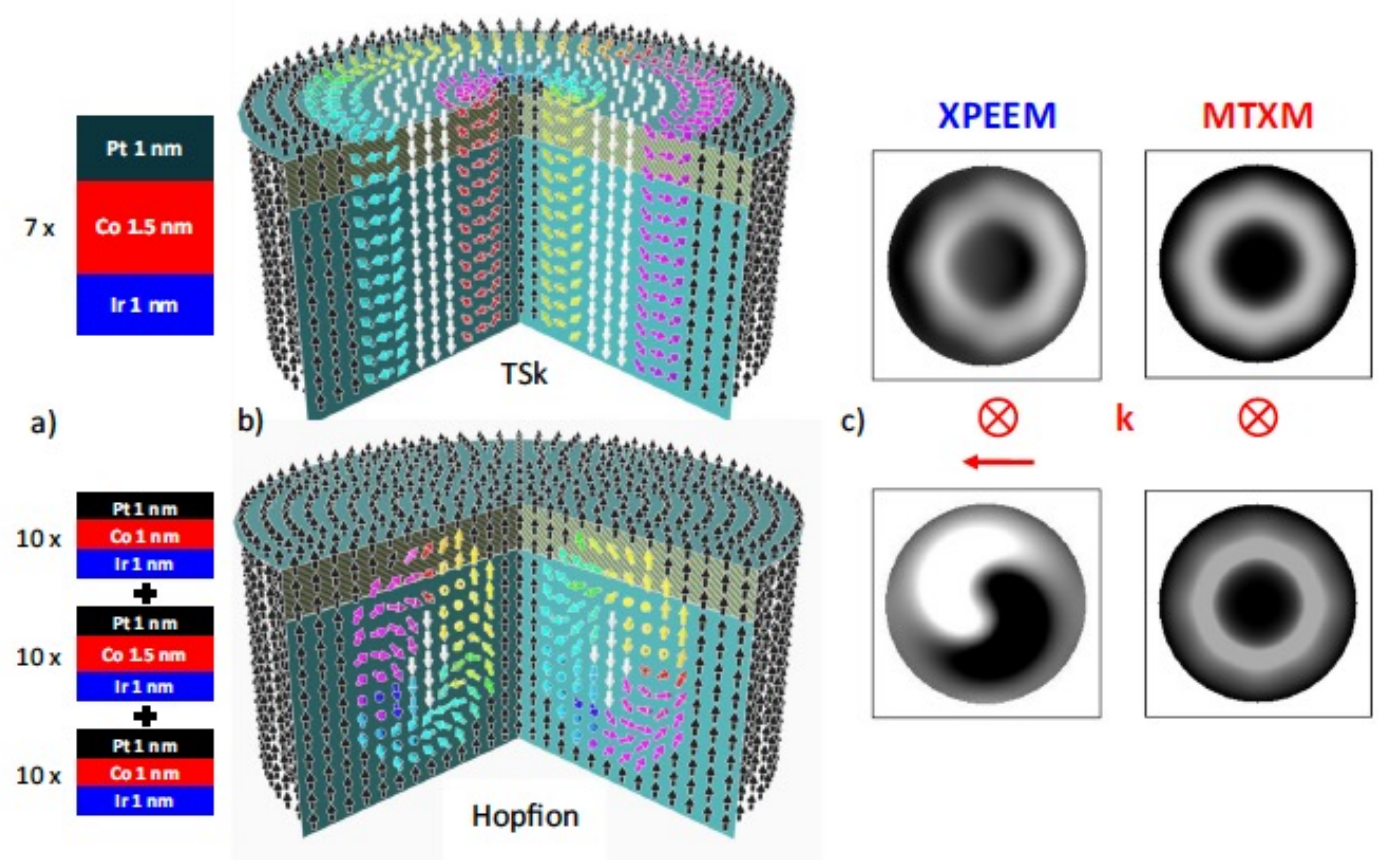


- In this example, each letter is a 3D magnetic object.
- The magnetostatic interaction between the objects is fully considered.
- The colors represent a magnetization component of the zero-field state.

Magnetic Hopfions



First experimental observation of a Hopfion

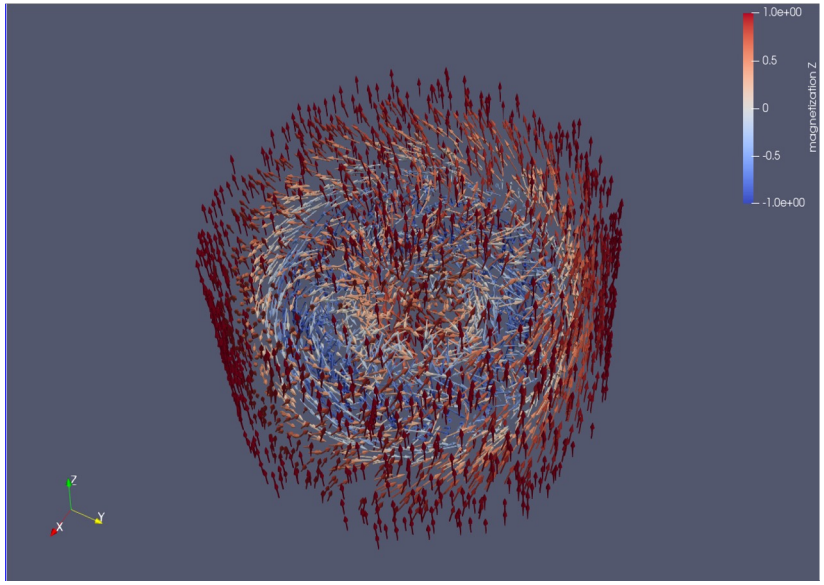


N. Kent et al., Nat. Commun. 12, 1562 (2021)

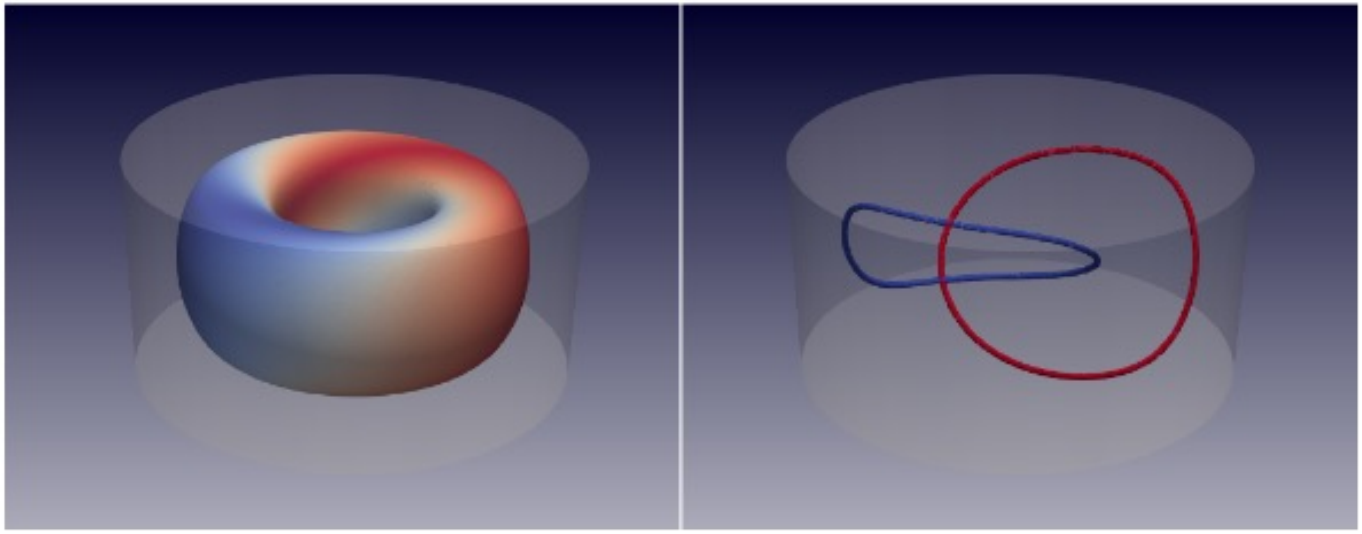
Thick magnetic nanodisk / nanocylinder with complex multilayer structure.
Interpretation of XPEEM and MTXM contrast by comparison with simulation.

Visualizing a Hopfion: Isosurface and Preimage representation

Direct vector field representation is usually not helpful in the case of Hopfions



Visualizing a Hopfion: Isosurface and Preimage representation



Isosurface $m_z = 0$
characteristic toroidal shape

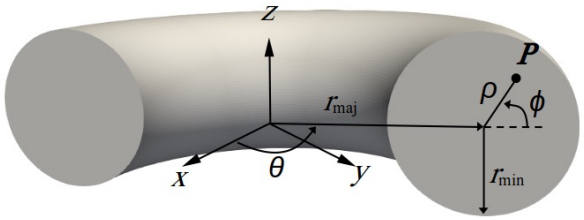
Preimages $m_x = 1$, $m_x = -1$
linked, closed loops

Intertwined (linked) rings in preimages are a signature of the Hopfion topology

Analytic form of a Hopfion texture

Vector field distribution in a cylinder or torus:

$$m_x = \sin\left(\pi\frac{\rho}{r_{\min}}\right)\cos\left(v\theta - u\phi + \alpha\right)$$
$$m_y = \sin\left(\pi\frac{\rho}{r_{\min}}\right)\sin\left(v\theta - u\phi + \alpha\right)$$
$$m_z = m_0\cos\left(\pi\frac{\rho}{r_{\min}}\right)$$

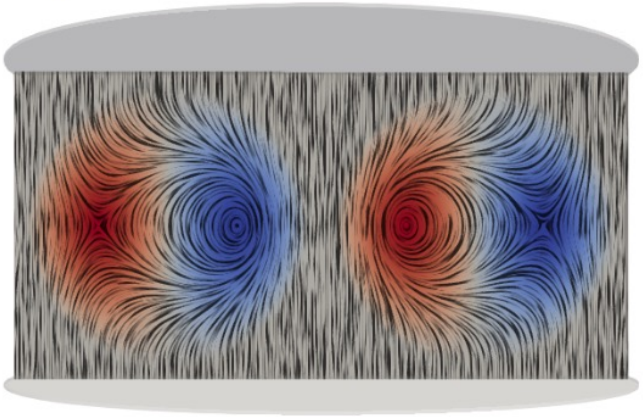


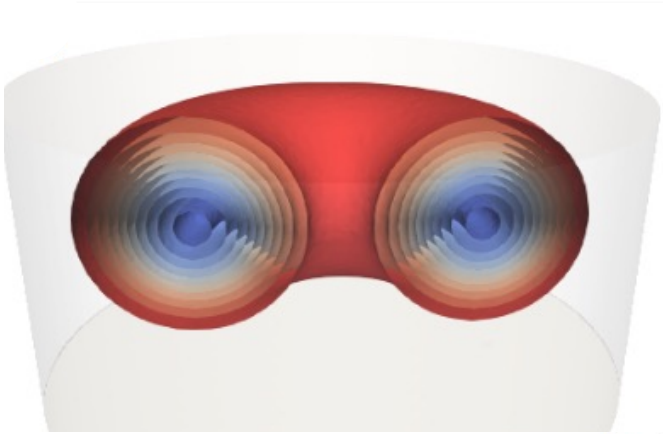
This ansatz generates a toroidal bimeron tube with a toroidal twist v and a poloidal twist u.

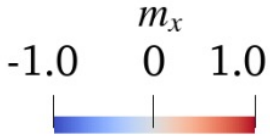
The knotted (linked) texture has a topological charge $N_H = vu$

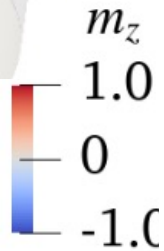
with

$$\rho = \sqrt{z^2 + (\sqrt{x^2+y^2} - r_{\mathrm{maj}})^2}$$
$$\theta = \arctan(y/x)$$
$$\phi = \arctan\left(\frac{z}{\sqrt{x^2+y^2} - r_{\mathrm{maj}}}\right)$$









L. Gallard and R. Hertel,
J. Appl. Phys. 138, 043907 (2025)

Hopfion - Topological Characterization

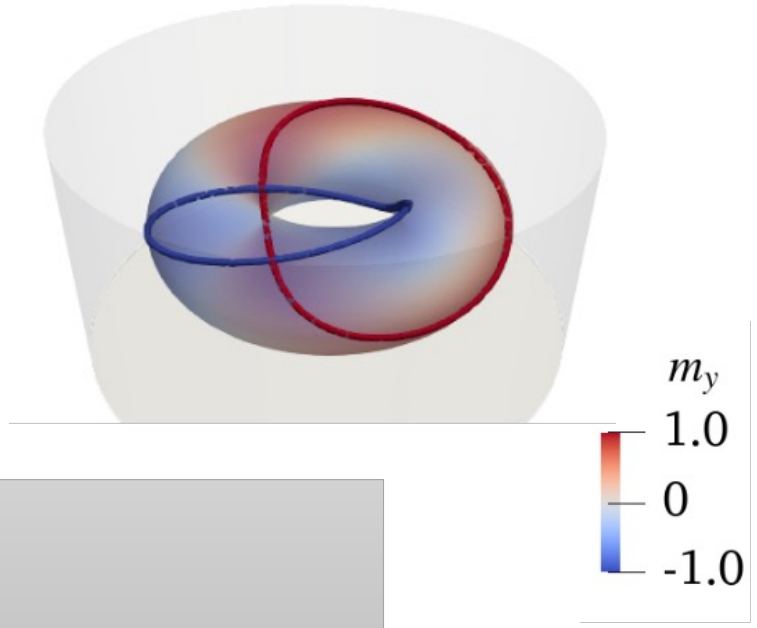
Hopf index $$N_H = -\int \boldsymbol{J} \cdot \boldsymbol{A}\, \mathrm{d}V$$

Vector potential: $$\nabla \times \boldsymbol{A} = \boldsymbol{J}$$

Topological current: $$J_i = \frac{1}{8\pi}\epsilon_{ijk}\boldsymbol{m} \cdot \left(\frac{\partial \boldsymbol{m}}{\partial x_j} \times \frac{\partial \boldsymbol{m}}{\partial x_k}\right)$$

J. H. C. Whitehead, Proceedings of the National Academy of Sciences 33, 117 (1947)

L. Gallard and R. Hertel, J. Appl. Phys. 138, 043907 (2025)



Note: The topological current is divergence-free, $\nabla \cdot \boldsymbol{J} = 0$, yielding closed flux lines, if $\boldsymbol{m}$ is smooth.

The Hopf index N_H is a topological invariant that

- characterizes the topology of a Hopfion
- counts the linking number of preimages under the magnetization field
- serves as the 3D analogue of the Skyrmion number that classifies 2D magnetic textures

Hopf Index – Vector potential calculation via Biot-Savart law

$$\boldsymbol{A}(\boldsymbol{r}) = \nabla \times \frac{1}{4\pi} \int \frac{\boldsymbol{J}(\boldsymbol{r'})}{|\boldsymbol{r} - \boldsymbol{r'}|} \mathrm{d}V'$$

Two-fold volume integration is computationally too time-consuming. Instead, solve equivalent PDE:

Use Coulomb gauge: $\boldsymbol{\nabla} \cdot \boldsymbol{A} = 0$

Poisson equation: $\Delta \boldsymbol{A} = -\nabla \times \boldsymbol{J}$

Jump condition at surface: $(\boldsymbol{n} \cdot \nabla)\boldsymbol{A}_{\mathrm{in}} - (\boldsymbol{n} \cdot \nabla)\boldsymbol{A}_{\mathrm{out}} = \boldsymbol{J} \times \boldsymbol{n}$

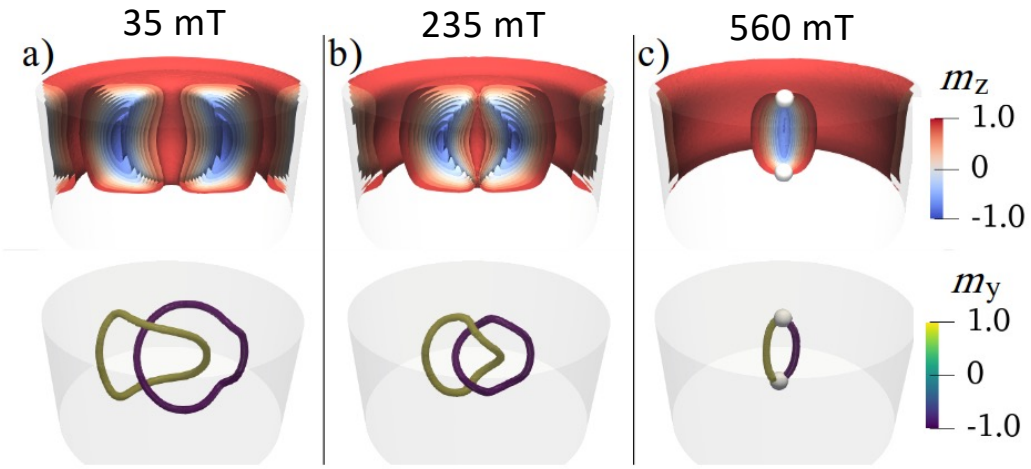
Decay at infinity: $\lim_{|\boldsymbol{x}| \to \infty} \boldsymbol{A}(\boldsymbol{x}) = \boldsymbol{0}$

The problem **formally analogous to the Oersted field calculation** for a current-carrying conductor.

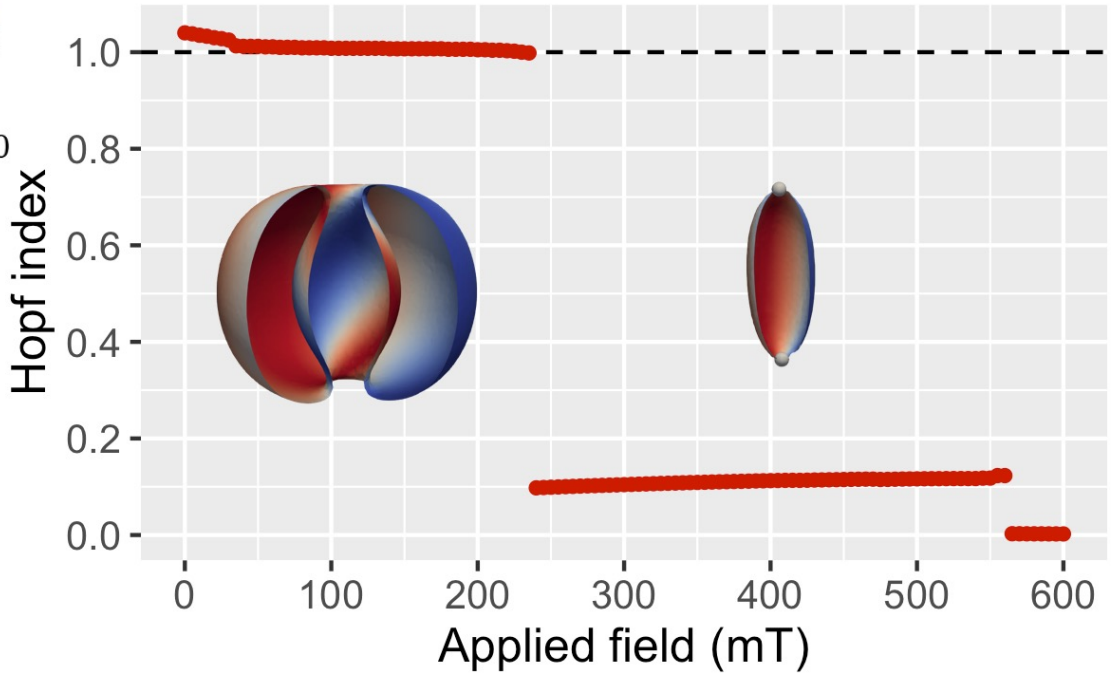
R. Hertel and A. Kákay, JMMM 369, 189 (2014)

Can be solved numerically using a FEM/BEM algorithm (Fredkin & Koehler), similar to the magnetostatic field calculation.

Micromagnetic simulation: Topological transition from Hopfion to Toron



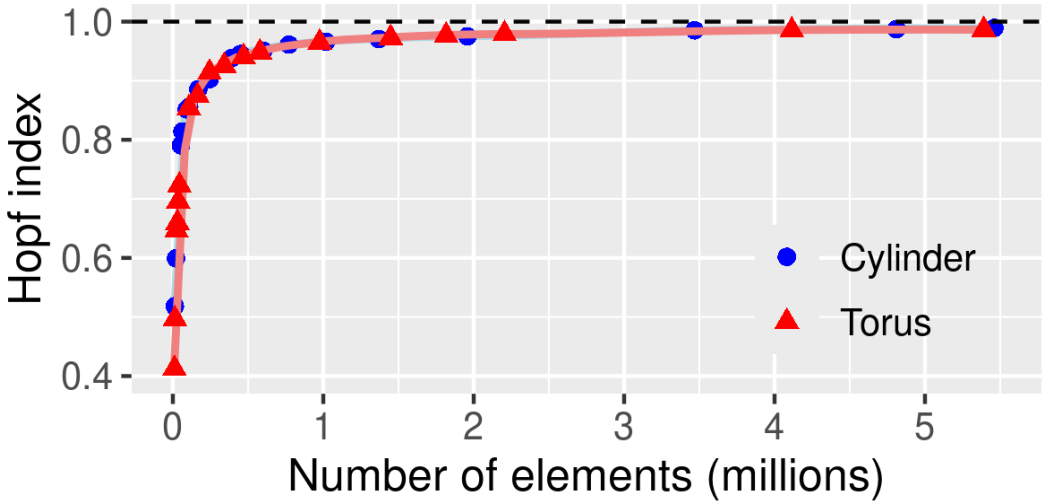
FeGe nanocylinder with surface anisotropy to pin $m_z = 1$ at top and bottom surfaces.
Field-dependent evolution of the structure and the Hopf index



- Constant Hopf index $\simeq 1$ prior to topological transition
  No topological changes despite distortion of preimages.
- Sudden drop to significantly lower value
  as the Hopfion converts into a toron (two Bloch points)
- In a second jump, N_H decreases to zero as
  the magnetic field destroys the toron

L. Gallard and R. Hertel,
J. Appl. Phys. 138, 043907 (2025)

Hopf Index – Numerical accuracy

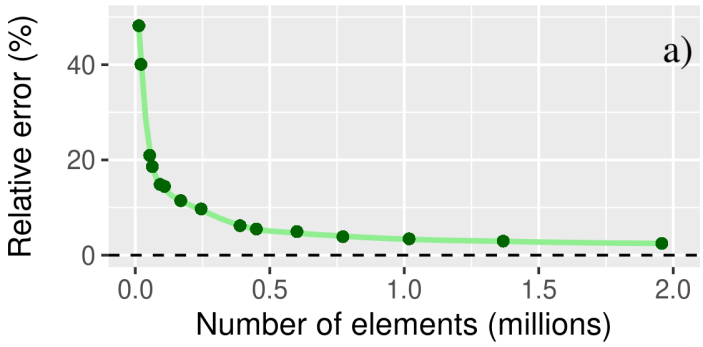


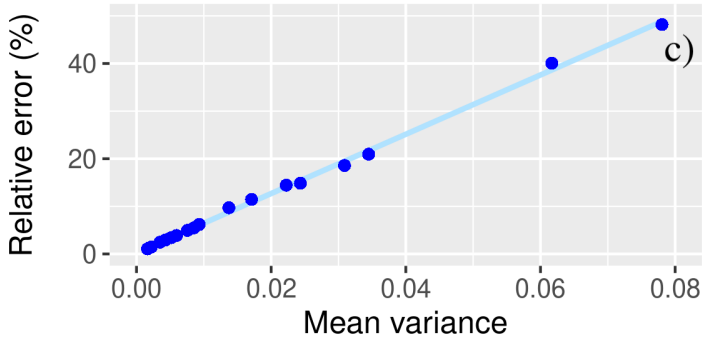
- Slow convergence towards exact value.
- Hopf index value is significantly underestimated at low discretization
- Error is mainly due to the calculation of the topological current
- Loss of accuracy due to product of numerically computed derivatives of m

$$J_i = \frac{1}{8\pi}\epsilon_{ijk}\boldsymbol{m}\cdot\left(\frac{\partial \boldsymbol{m}}{\partial x_j}\times\frac{\partial \boldsymbol{m}}{\partial x_k}\right)$$

Observations:

- Numerical error systematically underestimates the value of N_H
- Size of error correlates with variance (inhomogeneity in finite elements)





L. Gallard and R. Hertel, J. Appl. Phys. 138, 043907 (2025)

A posteriori phenomenological correction

Phenomenological correction:

- Use local variance of the magnetization as error indicator:

$$\sigma_n^2 = \sum_{j=x,y,z} \langle m_j^2 \rangle - \langle m_j \rangle^2$$

$$= 1 - \sum_{j=x,y,z} \left[\left(\sum_{i=1}^{4} \frac{m_{i,j}}{4} \right)^2 \right]$$

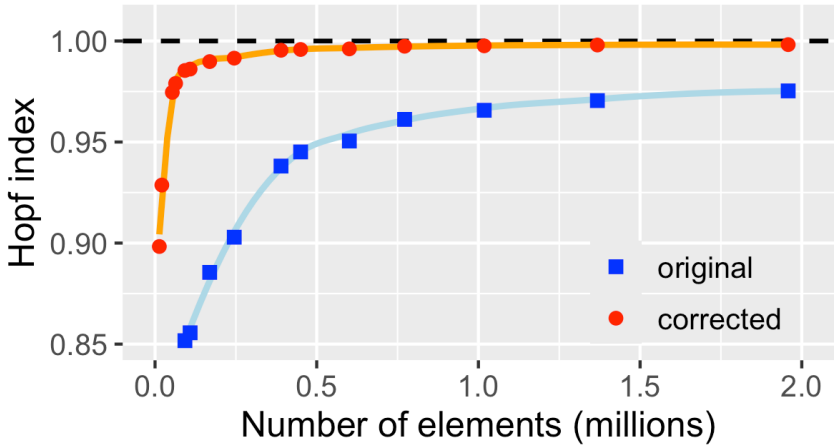
- Augment calculated Hopf density according to

$$\varrho_i \rightarrow \varrho_i \cdot \exp\left(\alpha \sigma_i^2\right)$$

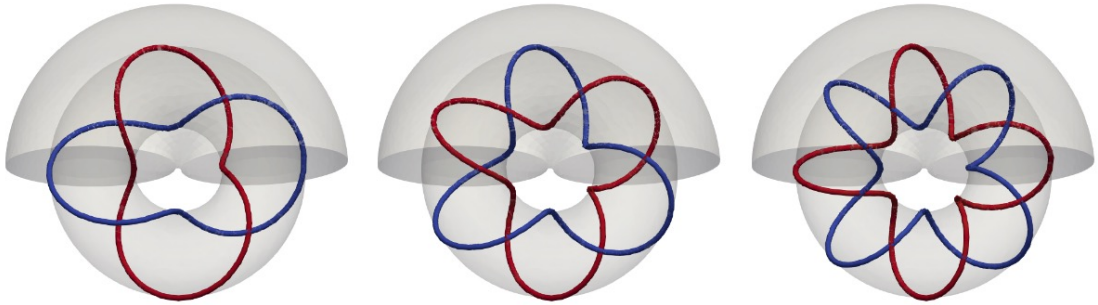
Where $\rho_i = \vec{A}_i \cdot \vec{J}_i$ at each node i and $\alpha =$ const.

L. Gallard and R. Hertel, J. Appl. Phys. 138, 043907 (2025)

Correction leads to significant accuracy improvement:



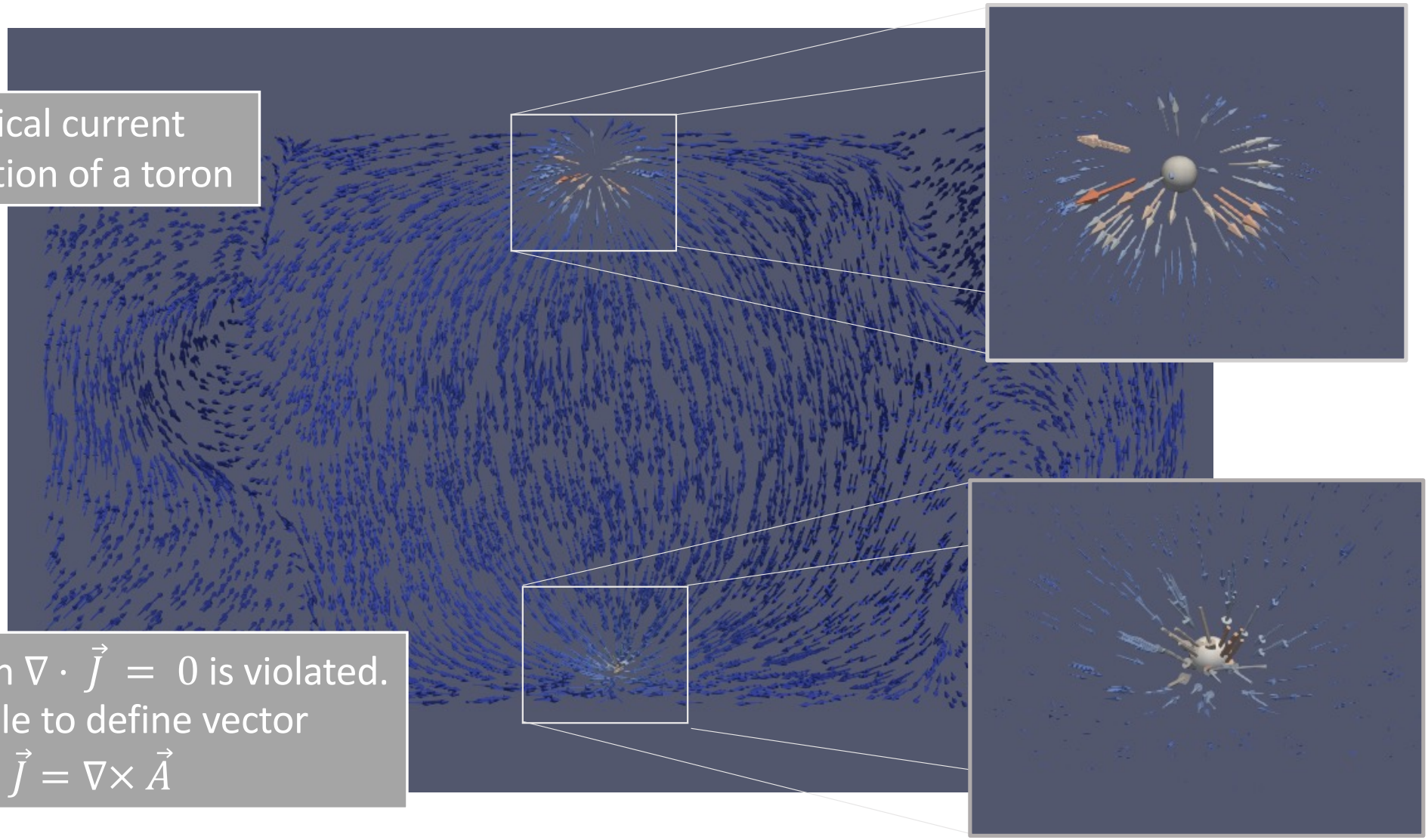
Correction method tested for several scenarios and textures:



$N_H = 1.995$ $N_H = 2.998$ $N_H = 3.999$

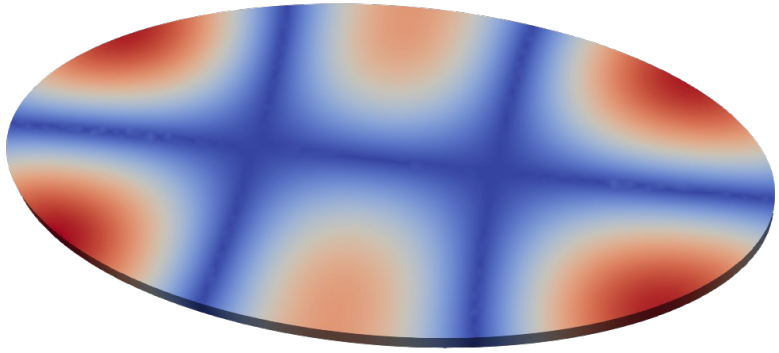
Bloch points: Sources and sinks of the topological current

Topological current distribution of a toron



Condition $\nabla \cdot \vec{J} = 0$ is violated. Impossible to define vector potential $\vec{J} = \nabla \times \vec{A}$

Linearized oscillatory dynamics



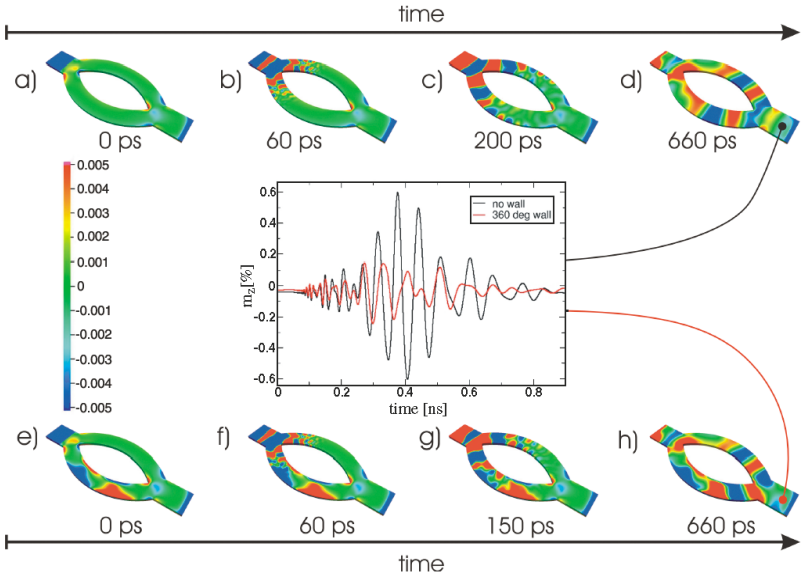
Magnonics - Importance of Micromagnetic Simulations

Role of micromagnetic simulations

- Prediction of new effects
- High reliability -> virtual experiments
- Interpretation of experimental data
- Design of magnonic devices

Spin wave logics: The beginning…

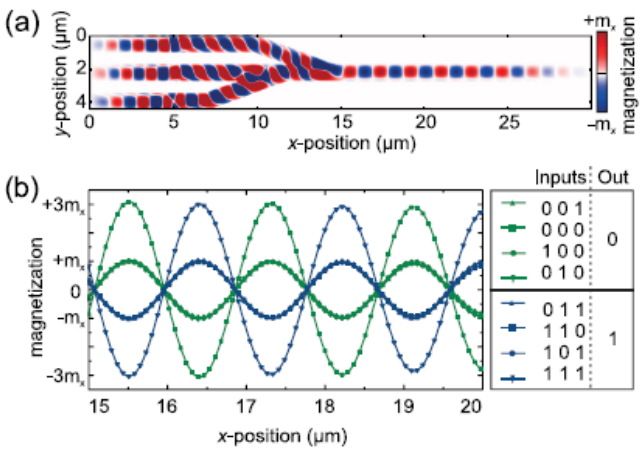
First concept of a spin-wave based logical device.
Mach-Zehnder type spin-wave interferometer.
Domain walls as phase-shifters. Logical XOR gate



Hertel, Wulfhekel, Kirschner
PRL 93, 257202 (2004)

Evolution and improvement…

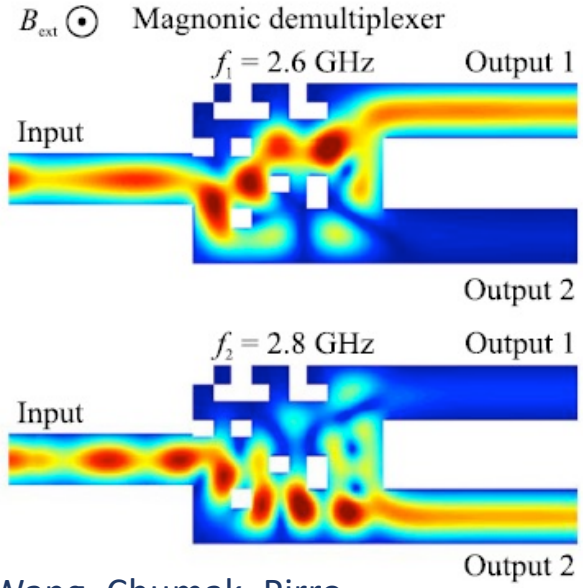
Majority gate for spin-wave logics



Klingler et al.,
Appl. Phys. Lett. 106, 212406 (2015)

The future…?

Algorithm-based device design



Wang, Chumak, Pirro
Nat. Comm. 12:2636 (2021)

Simulation Methods for Magnonic Problems

Typical problem: Calculation of **spin waves and magnetic high-frequency oscillations**.
Small-angle, low-amplitude oscillations around magnetic equilibrium state.

Two alternative approaches

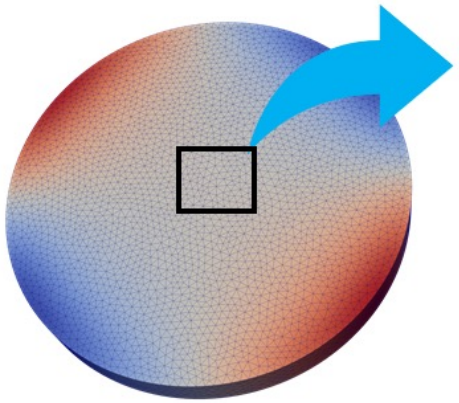
Full-scale micromagnetic simulations – time domain

- Simulation of static equilibrium state
- Perturbation by, e.g., pulse excitation of the system, or continuous excitation with harmonic field
- Simulation of LLG dynamics in the time domain
- Extraction of the dynamic magnetization via FFT

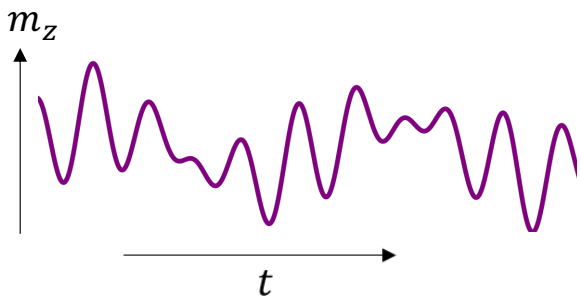
Linearized dynamics – Frequency domain

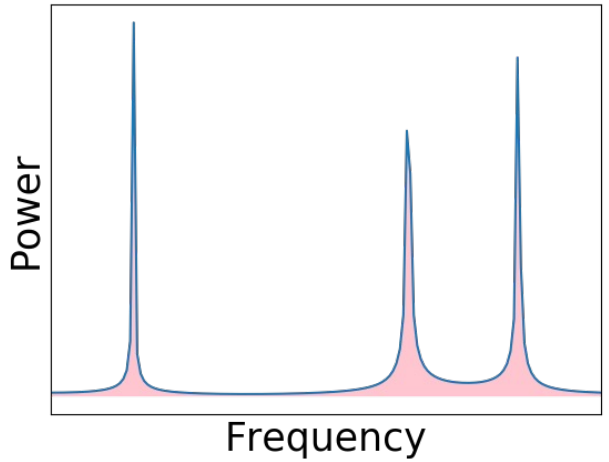
- Decompose magnetization into static and dynamic part:
  $$\boldsymbol{M}(\boldsymbol{x}, t) = \boldsymbol{M}_0(\boldsymbol{x}) + \delta\boldsymbol{M}(\boldsymbol{x}) \cdot \exp(i\omega t)$$
- Static simulations to calculate equilibrium state $\boldsymbol{M}_0(\boldsymbol{x})$
- Linearization of LLG equation
- Calculation of $\delta\boldsymbol{M}(\boldsymbol{x})$ in the frequency domain

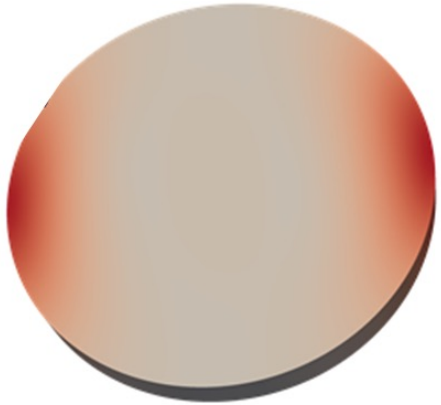
Ringdown method: Analysis of oscillatory magnetization dynamics

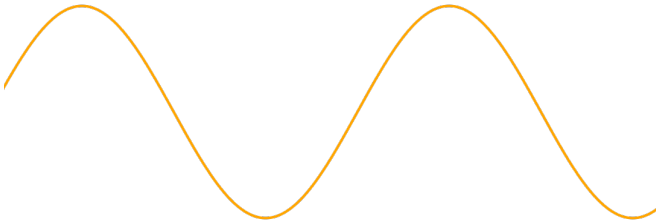


Oscillation at nodes









Windowed inverse Fourier transform to isolate specific modes

Principle:

- Shift system out of equilibrium (e.g.: short pulse, sudden field change)
- Record the magnetization dynamics during relaxation
- Identify modes through Fourier analysis

Established and reliable method. Analysis can be tedious and often requires long computation times

McMichael and Stiles,
J. Appl. Phys. 97, 10J901 (2005)

Yan et al.,
Phys. Rev. B 76, 094407 (2007)

Alternative approach: Linearized Magnetization Dynamics

Linearized LLG equation

- Assume small-angle variations of the magnetization around equilibrium $\boldsymbol{m}_0$
- Expand magnetization into static and oscillating part

$$\vec{m}(\vec{x},t) = \vec{m}_0(\vec{x}) + \delta\vec{m}(\vec{x}) \cdot \exp(i\omega t) \qquad \text{with} \quad |\delta\vec{m}| \ll |\vec{m}_0|$$

- Small variations in $\delta\,\vec{m}$ lead to small variations of the effective field:

$$h^{\text{eff}}(\vec{x},t) = \vec{h}_0^{\text{eff}}(\vec{x}) + \delta\vec{h}_{\text{eff}}(\vec{x}) \cdot \exp(i\omega t)$$

- Linearize LLG equation retaining only first-order terms

M. d'Aquino et al.,
J. Comp. Phys. 228, 6130 (2009)

Advantages of linearized method compared to full LLG dynamics:

- **Faster and more accurate** calculation of the high-frequency dynamics
- Optimal approximation for usual situation in **magnonics** (spin waves, high-frequency modes)
- Direct calculation of $\delta\vec{m}$ in the **frequency domain** (no time integration, no Fourier analysis)
- Access to magnetic **eigenmodes**

Linearized Magnetization Dynamics – Three variants

i) Calculation of eigenmodes and eigenfrequencies

$$i\omega\delta\hat{\boldsymbol{m}} = -\boldsymbol{m}_0 \times \left(\delta\hat{\boldsymbol{h}}_{\text{eff}} - h_0\delta\hat{\boldsymbol{m}}\right)$$

Generalized eigenvalue problem

ii) Forced dynamics I: driven by external, time-harmonic field

$$-i\omega\left(\alpha\delta\hat{\boldsymbol{m}} + \boldsymbol{m}_0 \times \delta\hat{\boldsymbol{m}}\right) = \mathcal{P}\cdot\left(h_0\delta\hat{\boldsymbol{m}} - \delta\hat{\boldsymbol{h}}_{\text{eff}} - \delta\hat{\boldsymbol{h}}_{\text{ext}}\right)$$

Linear problem for a given frequency ω

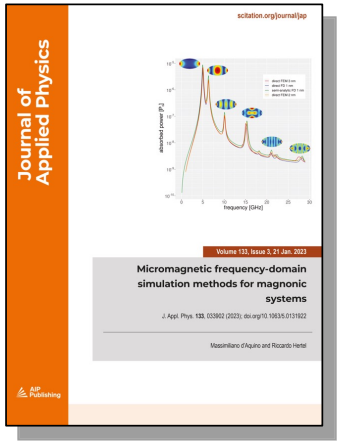
iii) Forced dynamics II: Eigenmodes as basis set

$$\underline{\delta\hat{m}} \approx \sum_{k=1}^{n} \frac{\omega_k}{\omega_k' - \omega}\,\underline{\varphi}_k \cdot \underline{\varphi}_k^H \cdot R^T \cdot P_{m_0} \cdot \underline{\delta\hat{h}}_{\text{ac}}$$

Frequency- and field-dependent dynamic magnetization represented as a superposition of eigenmodes

In all cases:

- Matrix-free implementation, suitable for large-scale computations (no “dynamic matrix”)
- Effective-field calculation with existing modules and classes, reused from micromagnetic code



M. d’Aquino, R. Hertel
J. Appl. Phys. 133, 3, 033902 (2023)

Linearized Oscillatory Magnetization Dynamics – Basic Equations

Equilibrium configuration m_0:

$$\boldsymbol{m}_0(\boldsymbol{x}) \times \boldsymbol{h}_{\mathrm{eff}0}(\boldsymbol{x}) = \boldsymbol{0} \quad \forall \boldsymbol{x} \qquad \boldsymbol{h}_{\mathrm{eff}0} = -\frac{1}{\mu_0 M_s} \frac{\delta E[\boldsymbol{M}_0(\boldsymbol{x})]}{\delta \boldsymbol{M}}$$

Consider small fluctuations $\delta\boldsymbol{m}$:

$$\boldsymbol{m}(\boldsymbol{x},t) = \boldsymbol{m}_0(\boldsymbol{x}) + \delta\boldsymbol{m}(\boldsymbol{x},t) \quad \text{with} \quad |\delta\boldsymbol{m}| \ll |\boldsymbol{m}_0|$$

Condition due to $|\boldsymbol{m}| = 1$:

$$\boldsymbol{m}_0 \cdot \delta\boldsymbol{m} = 0$$

Fluctuations of effective field induced by $\delta\boldsymbol{m}$:

$$\boldsymbol{h}_{\mathrm{eff}}(\boldsymbol{x},t) = \boldsymbol{h}_{\mathrm{eff}0}(\boldsymbol{x}) + \delta\boldsymbol{h}_{\mathrm{eff}}(\boldsymbol{x},t) \quad \text{with} \quad |\delta\boldsymbol{h}_{\mathrm{eff}}| \ll |\boldsymbol{h}_{\mathrm{eff}0}| \,.$$

$$\delta\boldsymbol{h}_{\mathrm{eff}}[\delta\boldsymbol{m}] = -\mathcal{C}\delta\boldsymbol{m} \,.$$

Time-harmonic variations of $\delta\boldsymbol{m}$ and $\delta\boldsymbol{h}_{\mathrm{eff}}$:

$$\delta\boldsymbol{m}(\boldsymbol{x},t) = \mathrm{Re}\left\{\delta\hat{\boldsymbol{m}}(\boldsymbol{x})\exp(i\omega t)\right\}$$

$$\delta\boldsymbol{h}_{\mathrm{eff}}(\boldsymbol{x},t) = \mathrm{Re}\left\{\delta\hat{\boldsymbol{h}}_{\mathrm{eff}}(\boldsymbol{x})\exp(i\omega t)\right\}$$

Linearized Oscillatory Magnetization Dynamics - Eigenmodes

Time-harmonic variations of $\delta\boldsymbol{m}$ and $\delta\boldsymbol{h}_{\text{eff}}$:

$$\delta\boldsymbol{m}(\boldsymbol{x},t) = \text{Re}\left\{\delta\hat{\boldsymbol{m}}(\boldsymbol{x})\exp(i\omega t)\right\}$$
$$\delta\boldsymbol{h}_{\text{eff}}(\boldsymbol{x},t) = \text{Re}\left\{\delta\hat{\boldsymbol{h}}_{\text{eff}}(\boldsymbol{x})\exp(i\omega t)\right\}$$

Insert into Landau-Lifshitz Gilbert equation:

$$\frac{\partial\boldsymbol{m}}{\partial\tau} = -\boldsymbol{m}\times\boldsymbol{h}_{\text{eff}} + \alpha\boldsymbol{m}\times\frac{\partial\boldsymbol{m}}{\partial\tau}$$

$$\frac{\partial\delta\boldsymbol{m}}{\partial\tau} = -\delta\boldsymbol{m}\times\boldsymbol{h}_{\text{eff0}} - \boldsymbol{m}_0\times\delta\boldsymbol{h}_{\text{eff}}$$

M. d'Aquino et al.,
J. Comp. Phys. 228, 6130 (2009)

Transition to frequency domain

$$i\omega\delta\hat{\boldsymbol{m}} = -\boldsymbol{m}_0\times\left(\delta\hat{\boldsymbol{h}}_{\text{eff}} - h_0\delta\hat{\boldsymbol{m}}\right) = \boldsymbol{m}_0\times\mathcal{A}_0\delta\hat{\boldsymbol{m}}$$

$$\mathcal{A}_0 = \mathcal{C} + h_0(\boldsymbol{x})\mathcal{I}$$
$$\mathcal{B}_0 = -i\Lambda(\boldsymbol{m}_0(\boldsymbol{x}))$$

Generalized eigenvalue problem:

$$\mathcal{A}_{0\perp}\boldsymbol{\varphi} = \omega\mathcal{B}_0\boldsymbol{\varphi}$$

Linearized Magnetization Dynamics: Magnetic Eigenmodes

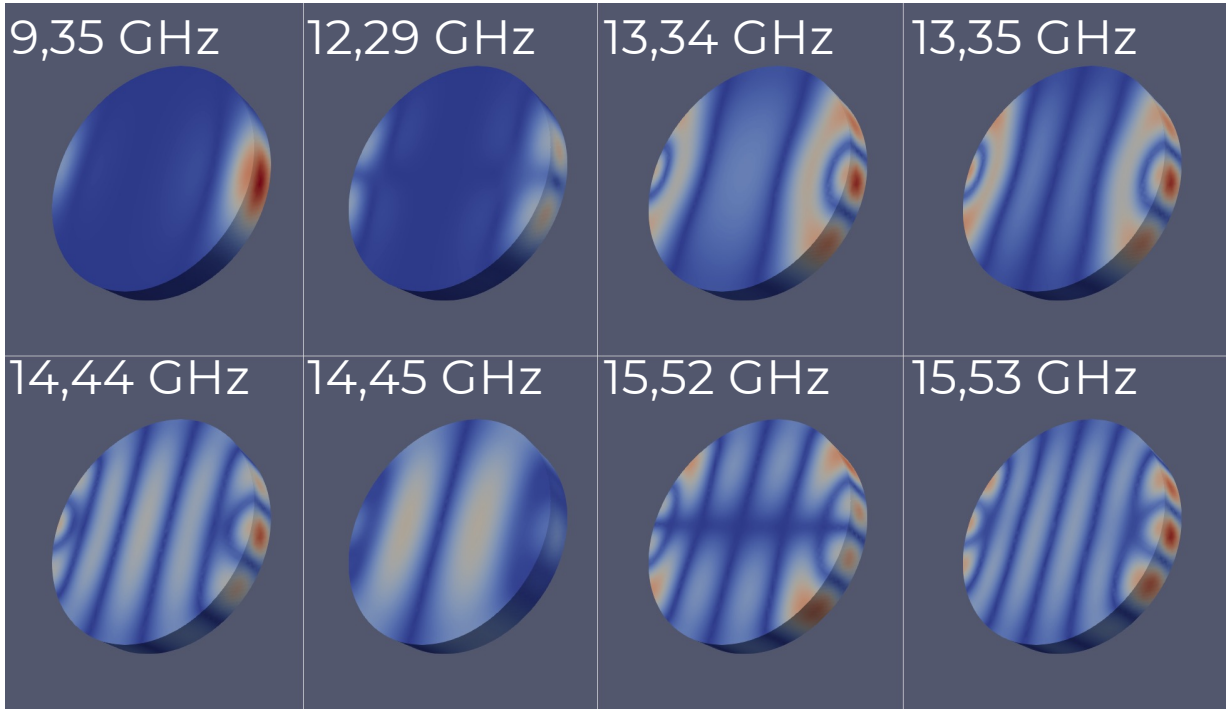
Linearized LLG equation with zero damping.
Oscillations around equilibrium state $\vec{m}_0$ in static external field

$$i\omega\delta\vec{m} = -\vec{m_0}\times\left(\delta\vec{h}_{\text{eff}} - h_0\delta\vec{m}\right)$$

$$\omega\boldsymbol{B_0}\delta\vec{m} = \boldsymbol{A_{0\perp}}\delta\vec{m}$$

- Generalized eigenvalue problem
- Matrix $\boldsymbol{A_{0\perp}}$ contains micromagnetic interactions
- Requires selection of oscillations compatible with $\vec{m}_0 \cdot \delta\vec{m} = 0$
- Implementation in GPU-accelerated FEM code

First eight eigenmodes in a Co nanodisk (r=100 nm, t=30nm, $\mu_0 H$=300mT)



Result yields eigenmodes and eigenfrequencies of the system.
No information about the stimulus required to excite these modes.

Linearized Magnetization Dynamics – Forced oscillations

Apply time-harmonic magnetic field:

$$\delta \boldsymbol{h}_{\mathrm{ext}}(\boldsymbol{x},t) = \mathrm{Re}\left\{\delta\hat{\boldsymbol{h}}_{\mathrm{ac}}(\boldsymbol{x})\exp(i\omega t)\right\}$$

$$\delta \boldsymbol{h}_{\mathrm{ext}} = \delta \boldsymbol{H}_{\mathrm{ext}}/M_s$$

Leads to set of linear equations:

$$-i\omega \boldsymbol{m}_0 \times \delta\hat{\boldsymbol{m}} = -\mathcal{P}_\perp\left(\delta\hat{\boldsymbol{h}}_{\mathrm{eff}} - h_0\delta\hat{\boldsymbol{m}}\right) - \mathcal{P}_\perp\delta\hat{\boldsymbol{h}}_{\mathrm{ac}} + i\omega\alpha\delta\hat{\boldsymbol{m}}$$

$$\mathcal{L}_0\delta\hat{\boldsymbol{m}} = \mathcal{P}_\perp\delta\hat{\boldsymbol{h}}_{\mathrm{ac}}$$

Linearized magnetic response $\delta\boldsymbol{m}$ can be calculated for any frequency and orientation of $\delta\boldsymbol{h}_{\mathrm{ext}}$

M. d'Aquino, R. Hertel
J. Appl. Phys. 133, 3, 033902 (2023)

Driven dynamics: Linear Response in Oscillating External Field

Linearized LLG in a weak oscillatory external field:

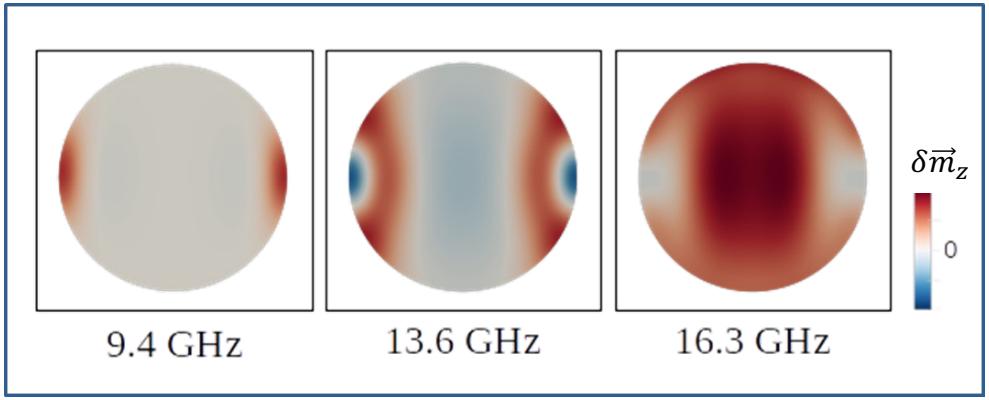
$$\delta\vec{h} = \delta\vec{h}_{\text{ext}} \cdot \exp(-i\omega t)$$

Aim: Calculate stationary, field-driven high-frequency dynamics.

- Linearized LLG leads to a linear system:

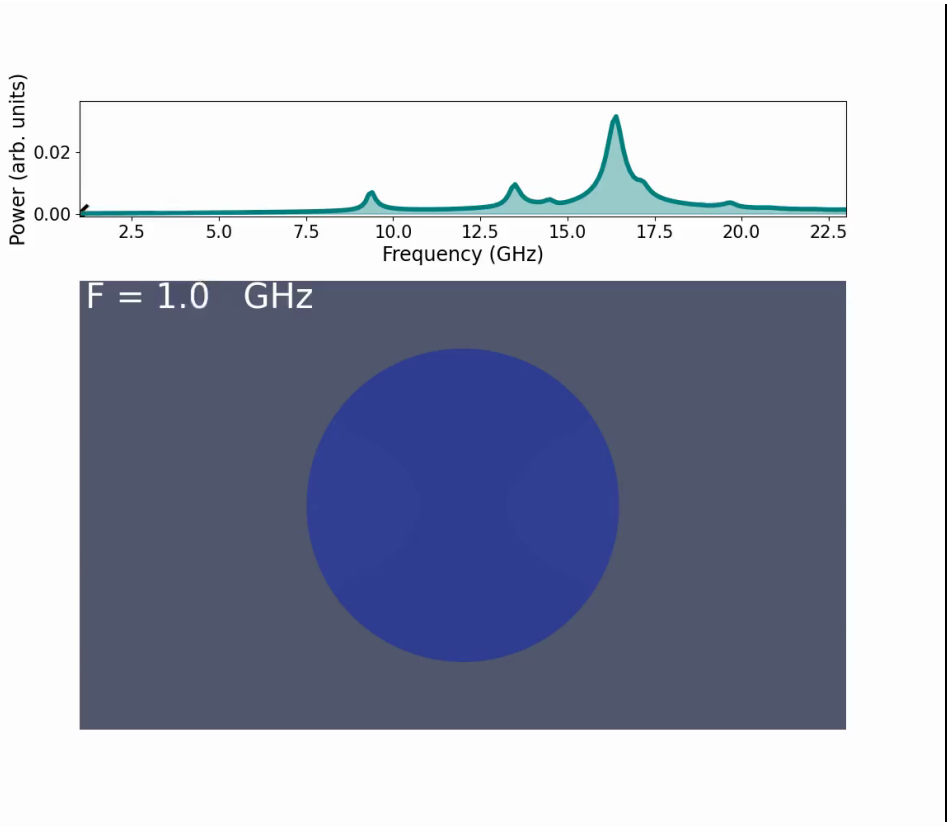
$$-i\omega\left(\alpha\delta\hat{\boldsymbol{m}} + \boldsymbol{m}_0 \times \delta\hat{\boldsymbol{m}}\right) = \mathcal{P}\cdot\left(h_0\delta\hat{\boldsymbol{m}} - \delta\hat{\boldsymbol{h}}_{\text{eff}} - \delta\hat{\boldsymbol{h}}_{\text{ext}}\right)$$

- Frequency ω, damping α, and $\delta\vec{h}_{\text{ext}}$ as input parameter
- Result gives oscillation profile $\delta\,\vec{m}$ at any frequency
- Direct calculation in the frequency domain, no LLG integration



Example:

Co nanodisk (r=100 nm, t=30nm, $\mu_0 H$=300mT, $\delta h = 0.5$ mT)



D. Marko et al., Phys. Rev. Appl. 20, 024059 (2023)

Driven dynamics – Semi-analytic approach

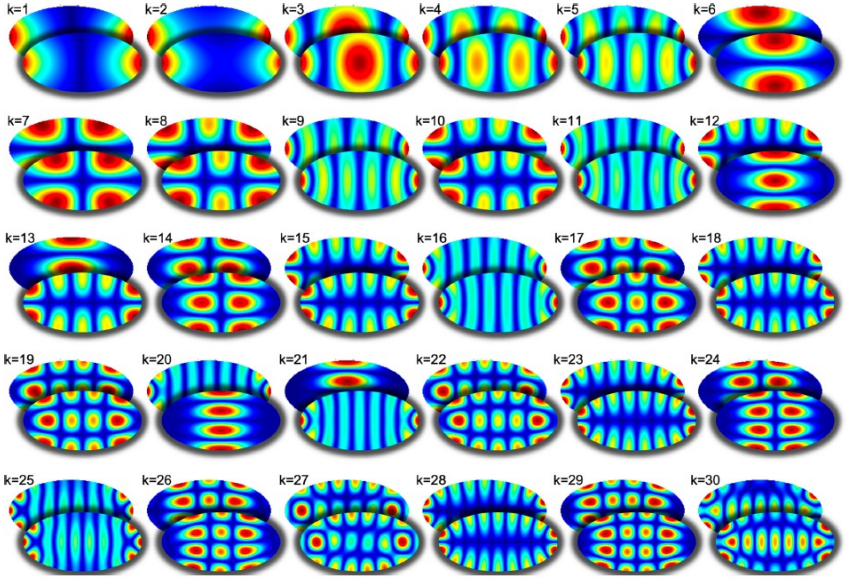
Eigenmodes as basis set of the dynamic magnetization

$$\underline{\delta\hat{m}} \approx \sum_{k=1}^{n} \frac{\omega_k}{\omega_k' - \omega}\, \underline{\varphi_k} \cdot \underline{\varphi_k^H} \cdot R^T \cdot P_{\boldsymbol{m}_0} \cdot \underline{\delta\hat{h}_{\mathrm{ac}}}$$

Frequency- and field-dependent magnetization dynamics represented as a superposition of eigenmodes

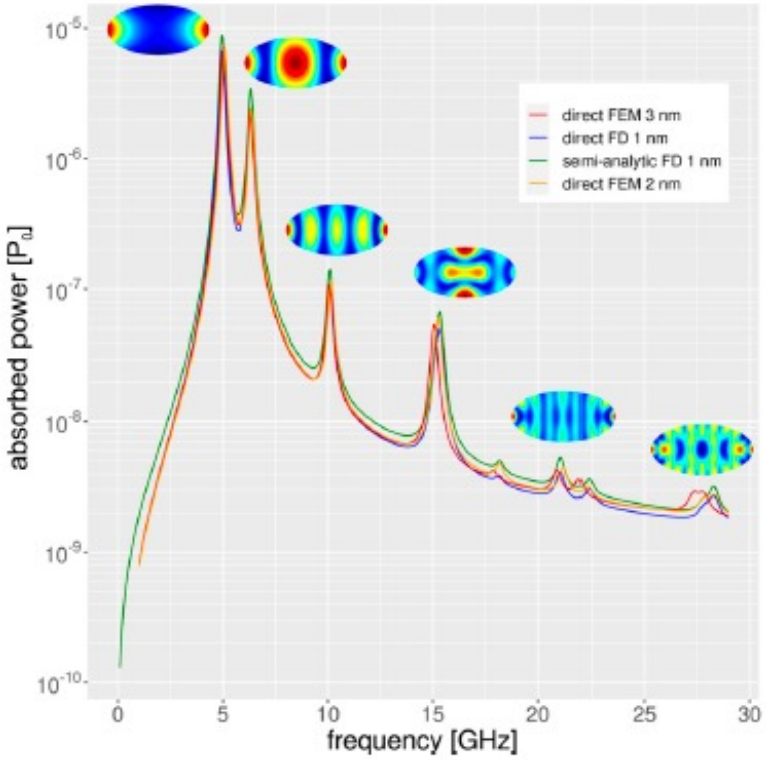
Analytic calculation of mode coefficients

Example: First 30 modes in a Py ellipse at zero field



Agreement between numerical schemes (FEM vs. FDM) and calculation methods (semi-analytical vs. direct)

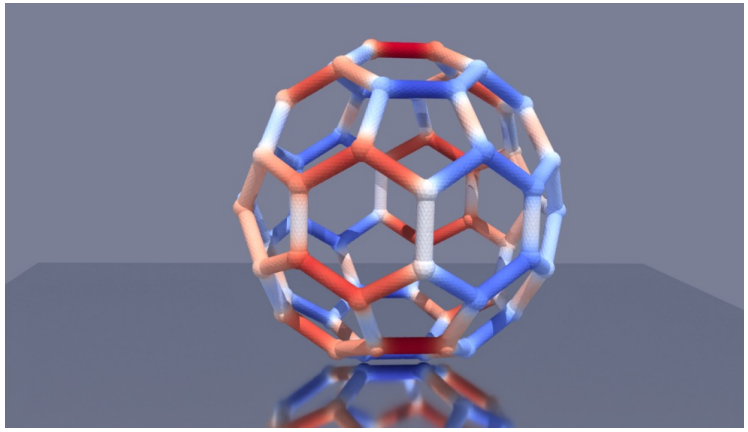
Absorption spectrum and oscillation patterns



Highly efficient method, particularly in the case of non-degenerate modes

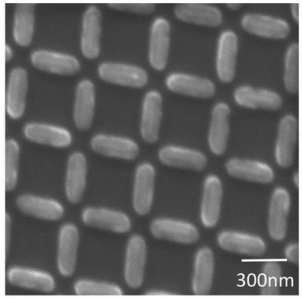
M. d'Aquino and R. Hertel
J. Appl. Phys. 133, 3, 033902 (2023)

Interconnected Nanowires

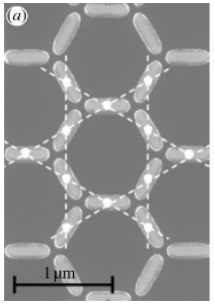


Artificial spin ice: From 2D to 3D

- Arrays of interacting nanomagnets
- Frustrated magnetization states and interactions
- Reconfigurable functionalities
- Potential applications in data storage, magnonics
- Recent advances: Three-dimensional artificial spin ice

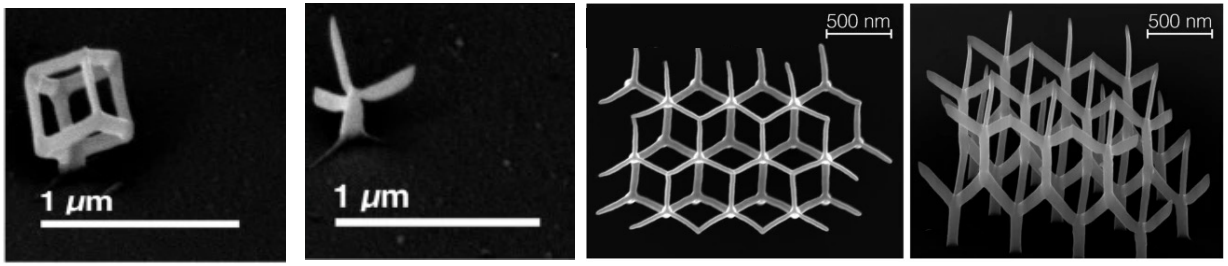


Square spin ice
JM Porro, New J. Phys., 15 55012(2013)

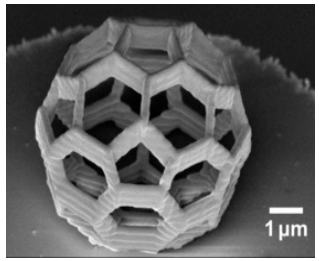


Kagome spin ice
RV Hügli,
Philos T R Soc. A,
370, 5767 (2012)

Three-dimensional architectures of interconnected magnetic nanowires



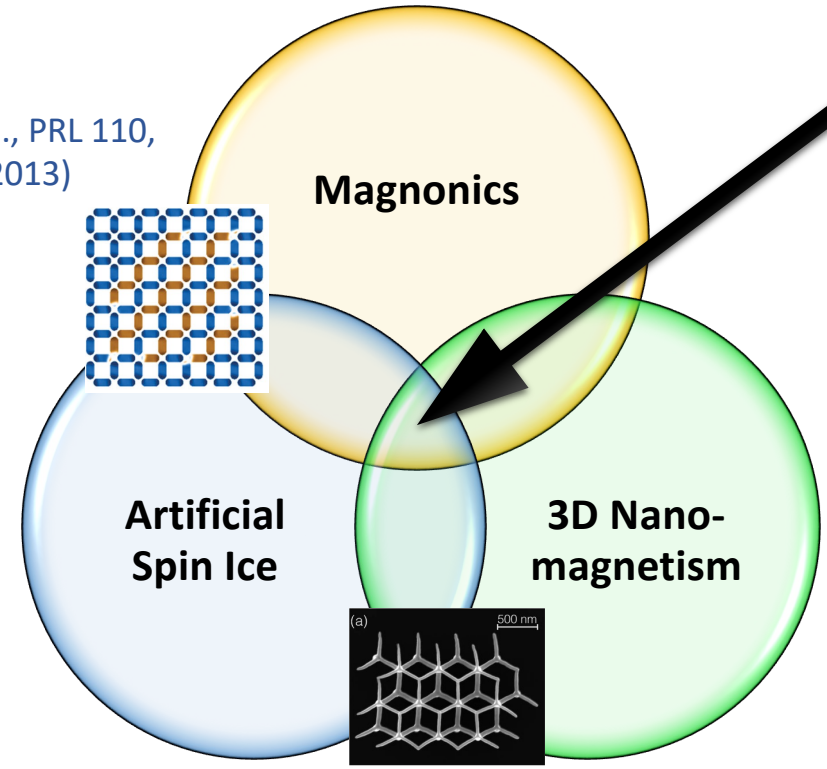
L. Keller et al., Sci Rep. 8, 6160 (2018)



C. Donnelly et al. Phys. Rev. Lett.
114, 115501 (2011)

Spin waves and high-frequency oscillations in complex magnetic nanostructures

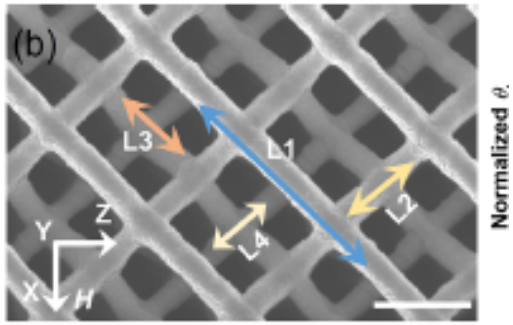
Gliga et al., PRL 110, 117205 (2013)



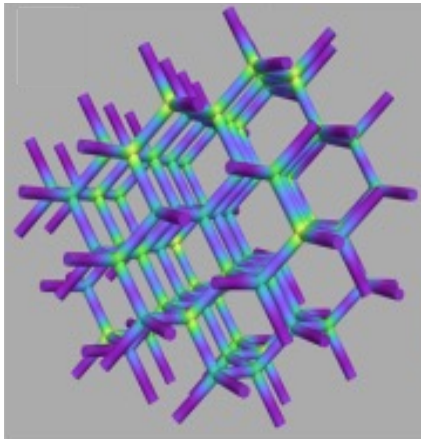
L. Keller et al., Sci Rep. 8, 6160 (2018)

Magnonics of 3D artificial spin ice systems: Interconnected nanowire arrays

- Switchable/programmable properties
- High-density 3D storage
- Signal propagation without Joule heating



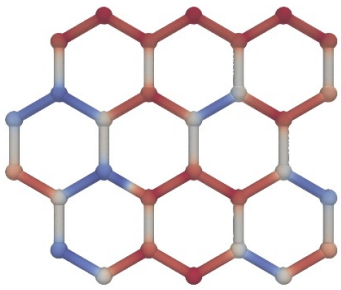
Sahoo et al. Nano Lett. 21, 4629 (2021)



R. Cheenikundil, PhD thesis Univ. Strasbourg (2021)

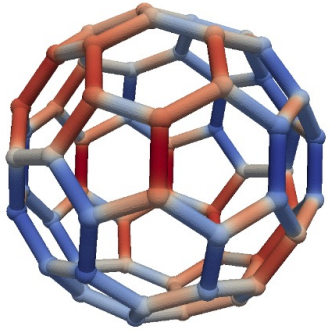
Three-dimensional ASI: Buckyball as model system

2D



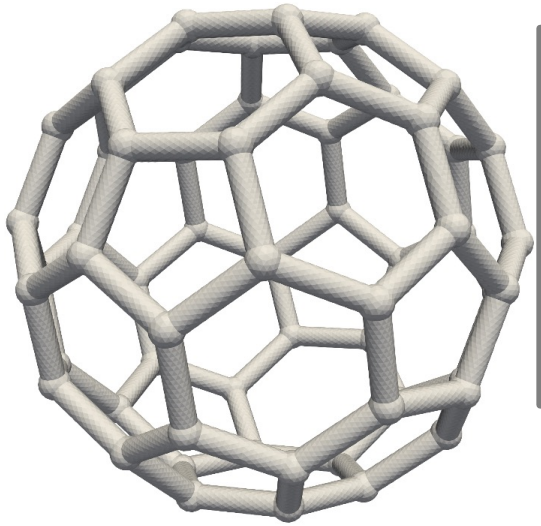
Hexagonal lattice

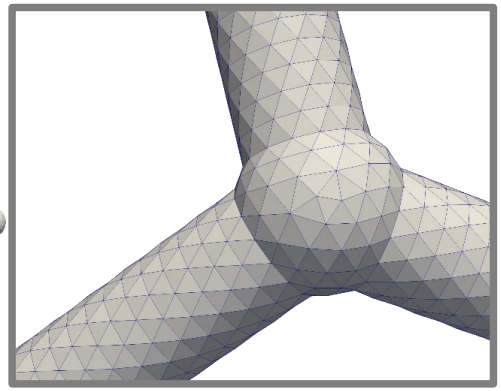
3D



Buckyball

- Buckyball: 3D counterpart of hexagonal lattice
- Differences between 2D and 3D?
- Simulation of static magnetic structure, hysteresis, high-frequency excitations





Finite element model

90 nanowires, 60 vertices

L : R : S = 25 : 3 : 4

Size : 130 nm - 1.3 µm

Number of elements : 60,000 – 1.9 Million

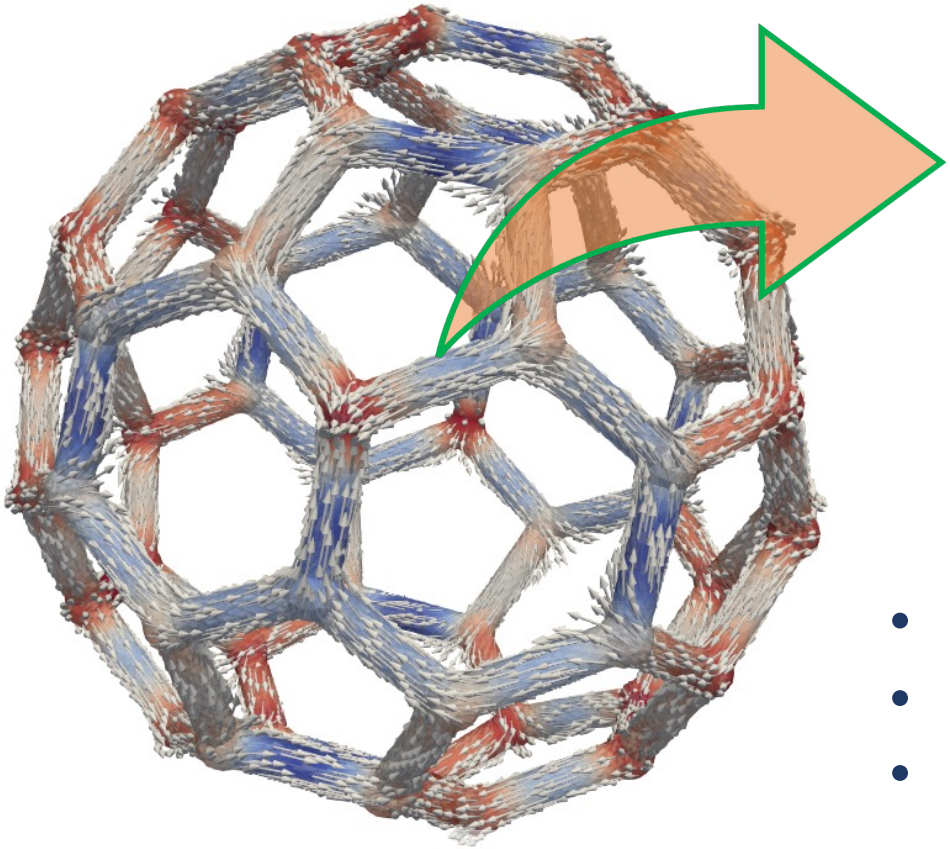
Material parameters: FEBID-Co

$\mu_0 M_s$ = 1.2 T

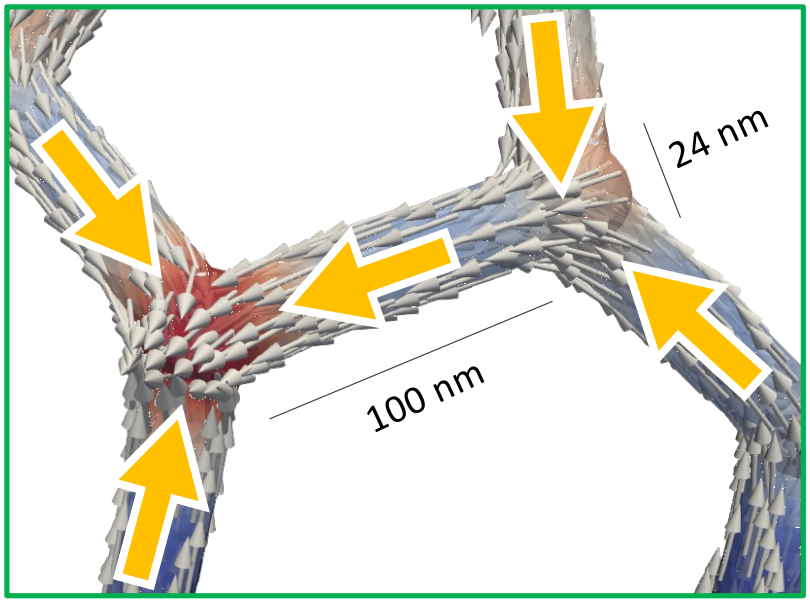
A = 1.5 × 10^{-11} J/m

zero crystalline anisotropy

Magnetic structure at the vertex points

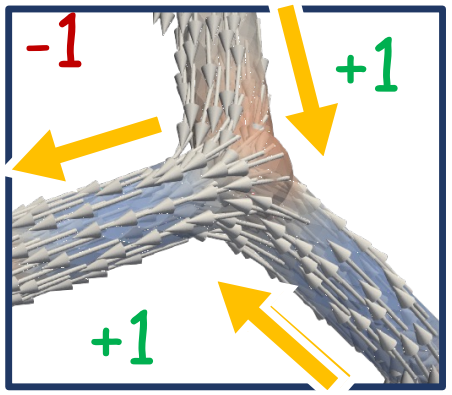


Relaxed magnetic structure at zero field

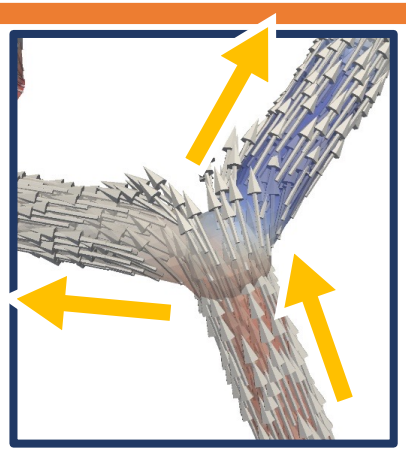


- Thin nanowires with axial magnetization
- Ising-like macroscopic dipoles
- Frustrated interaction at vertices

Micrpgnetic configurations at vertices

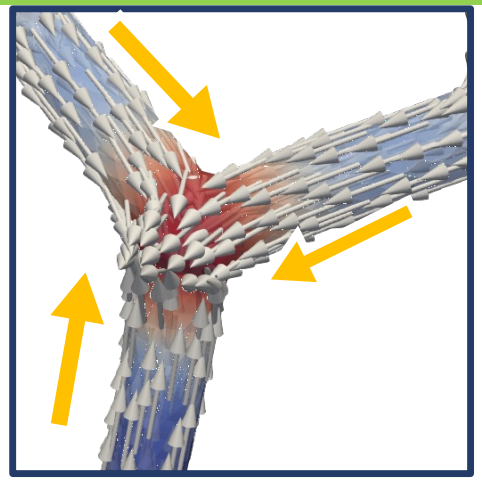


two-in/one-out
+1q charge

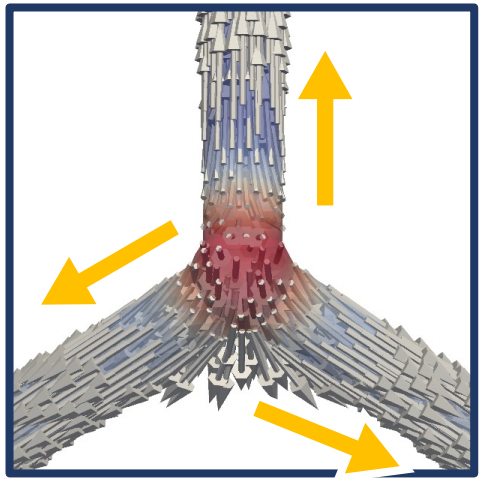


Ice rule obeying states
single vharges

one-in/two-out
-1q charge



three-in
+3q charge

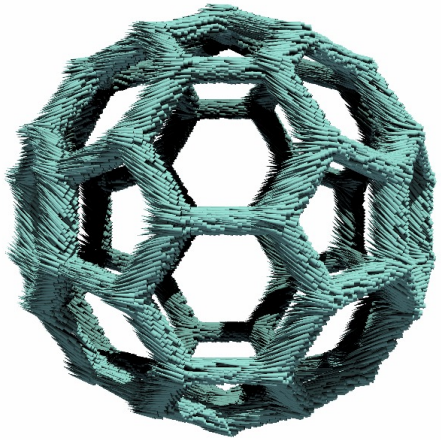


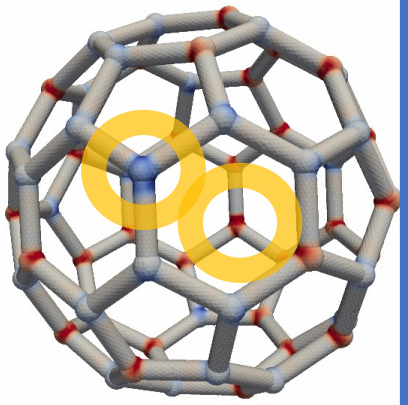
three-out:
-3q charge

Defect configurations
triple charges

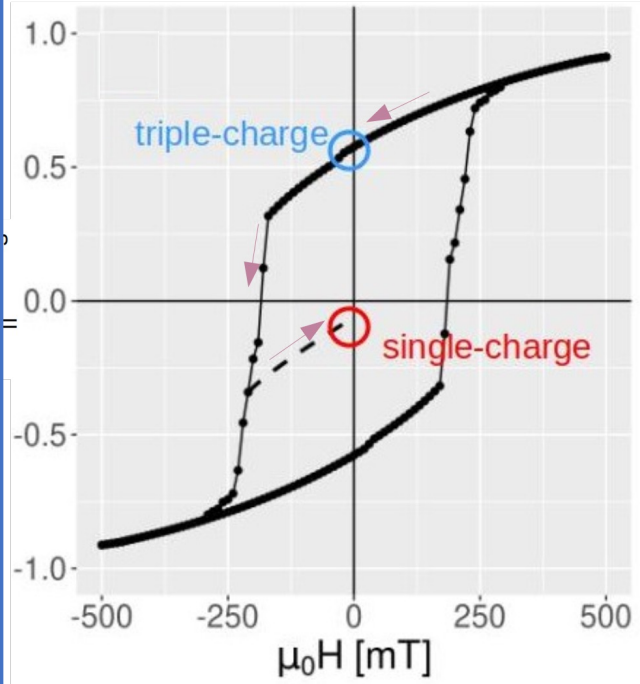
Formation and removal of triple-charge defects

Remanent state after saturation

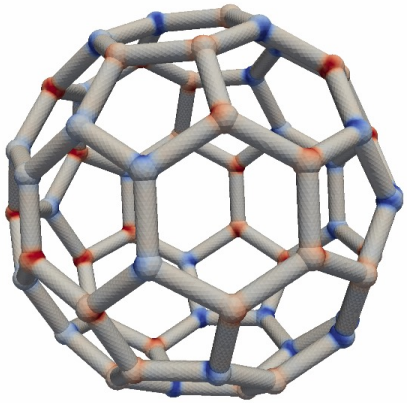




"Onion state" formed after saturation with two triple-charge vertices (+3q and -3q) on opposite sides



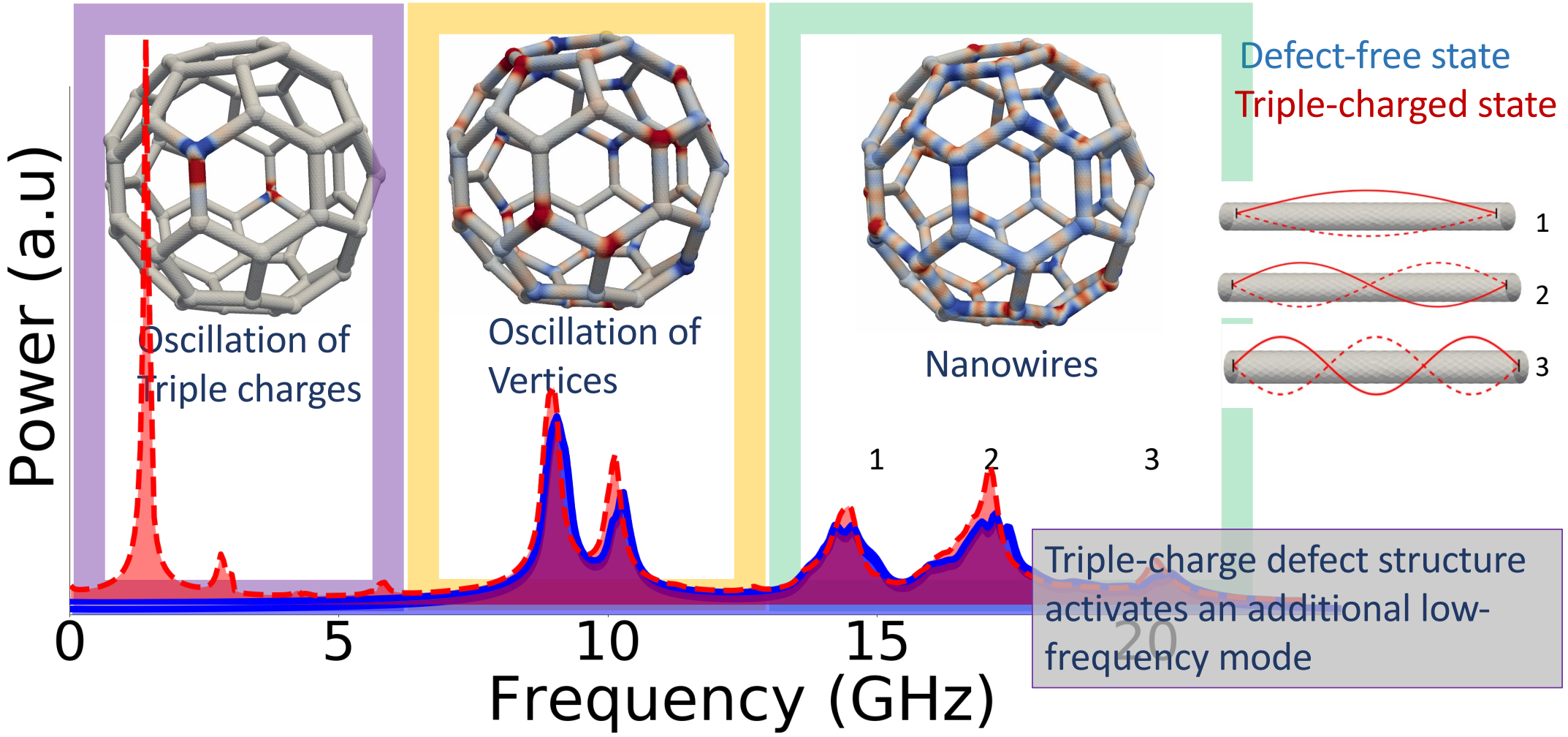
Zero-field state after minor loop



Defect-free state with single-charge configurations

R. Cheenikundil and R. Hertel , Appl. Phys. Lett. 118, 212403 (2021)

Switchable high-frequency properties



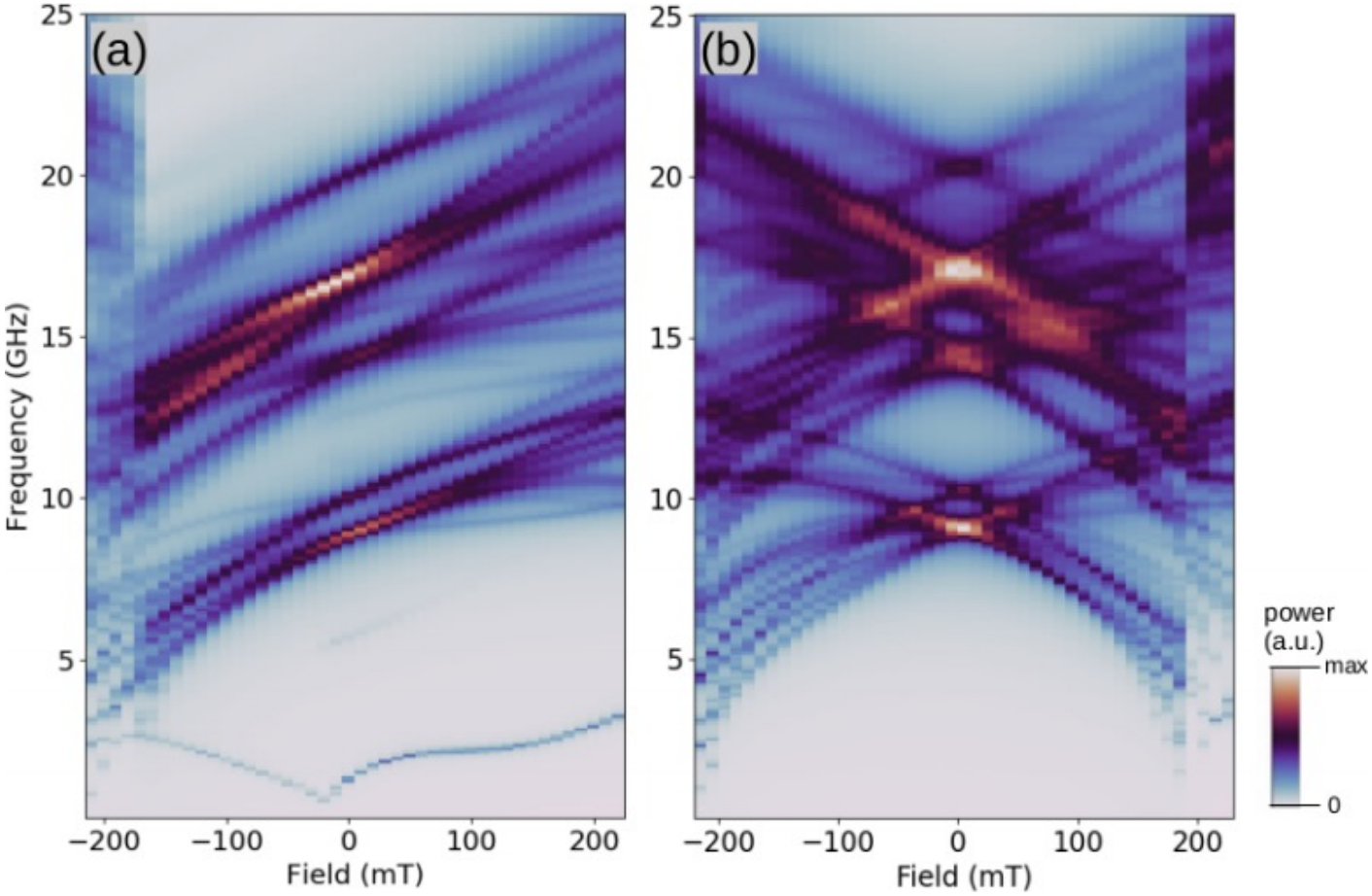
Triple-charge defect structure activates an additional low-frequency mode

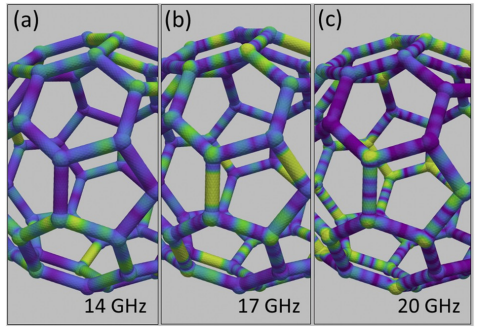
R. Cheenikundil et al., APL Mater. 10, 081106 (2022)

Magnetic buckyball: Field-dependence of resonance spectra

High-remanence state with triple-charge defects

Randomized state containing only defect-free vertices





Simulation with linear magnetic response solver

M. d'Aquino, R. Hertel
J. Appl. Phys. 133, 3, 033902 (2023)

Strongly different field dependence for the two configurations

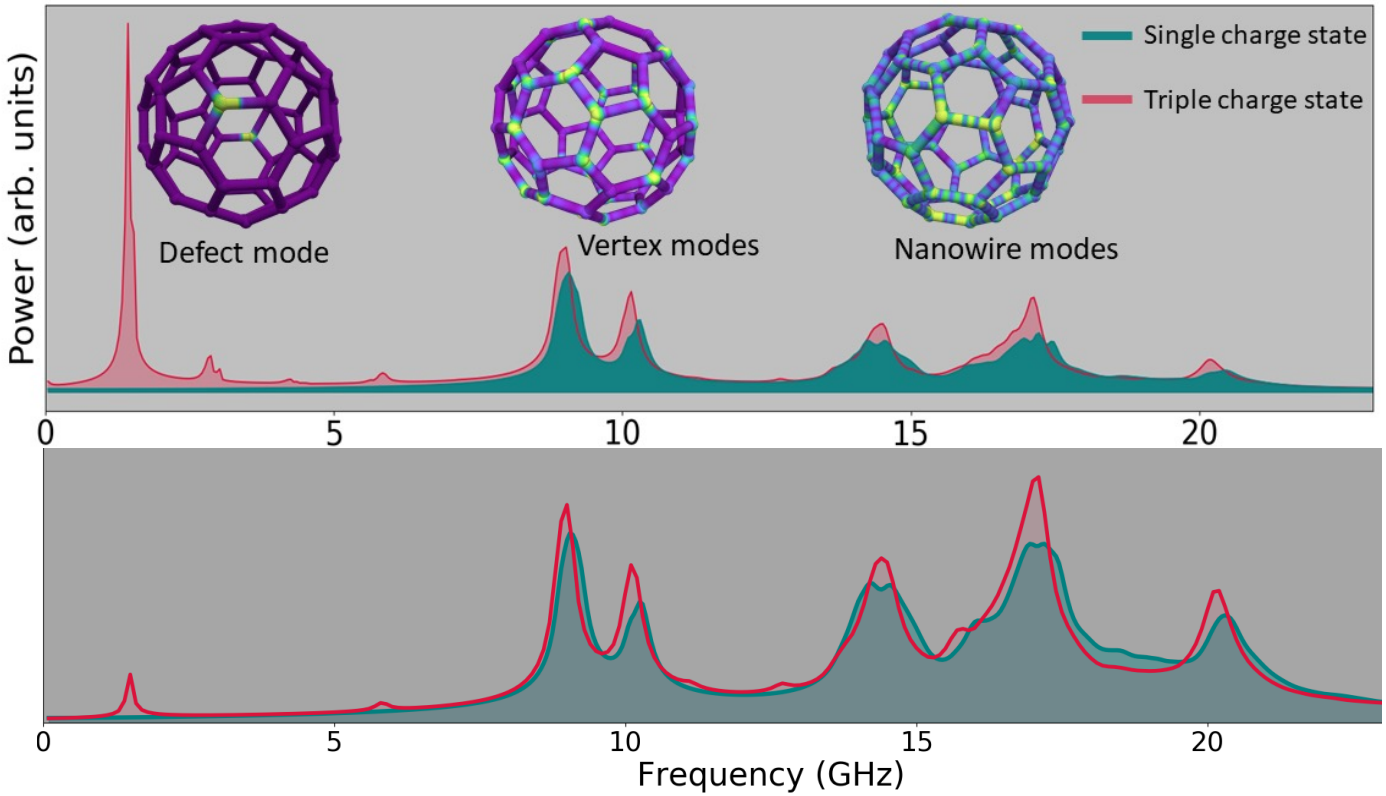
Switching processes at large fields lead to discontinuities in the spectrum

R. Cheenikundil et al.
APL Materials 10, 8, 081106 (2022)

Differences between ringdown and field-driven dynamics

Ringdown method, pulse excitation

Linearized dynamics in RF field

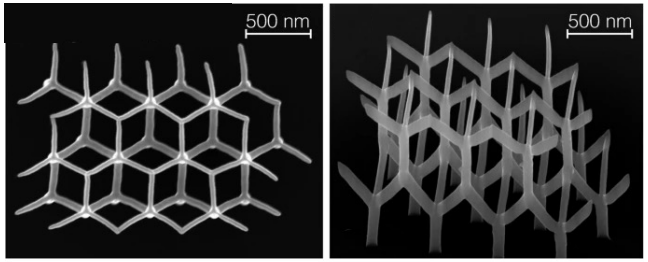


Same frequencies, same mode profiles.
Differences in relative peak heights

Reason for (significant) changes in peak heights:

- Different **excitation type** (continuous vs. single-pulse)
- **Lifetime of modes** has strong impact in ringdown method

Artificial Diamond-Type Lattice



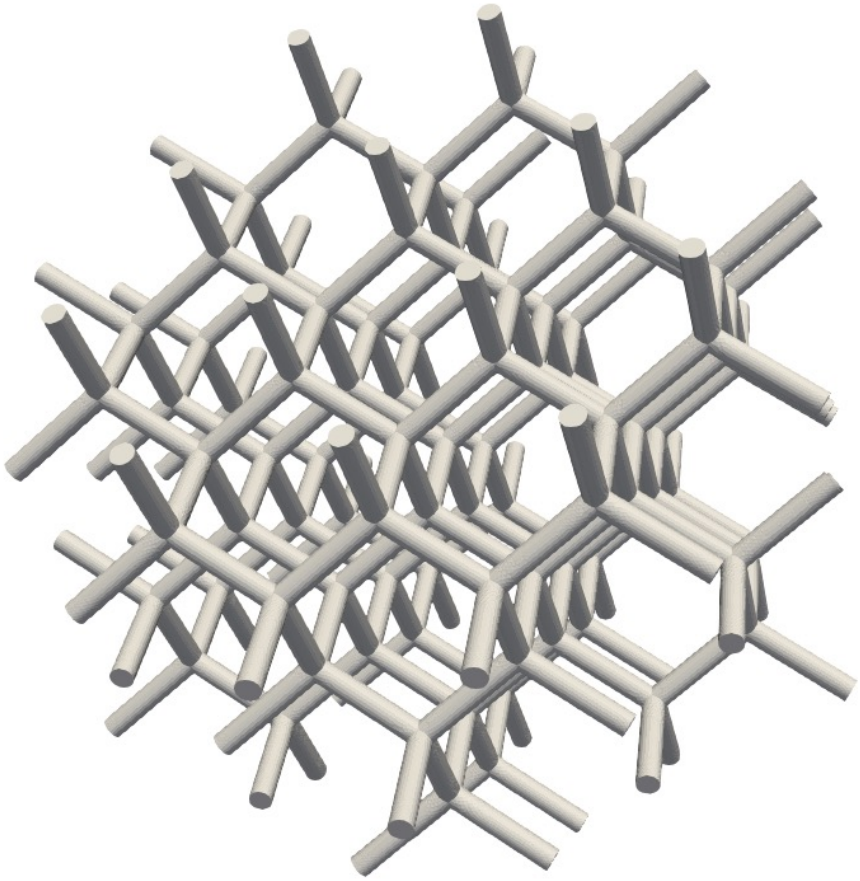
L. Keller et al., Sci Rep, 8, (2018)

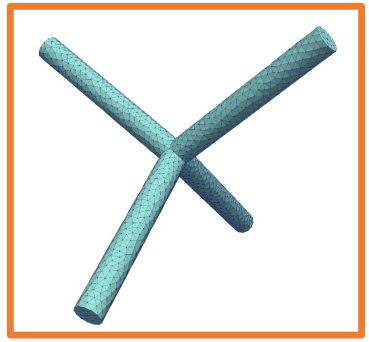
Geometry

- 3D interconnected nanowire array
- Vertices placed at positions corresponding to those of a diamond crystal
- Nanowires connect nearest neighbor vertices
- Wires with free ends at the surface

Model

- Wire diameter 14 nm, length 70 nm
- Material: FEBID-Co
- Size: approx. $450 \times 450 \times 450$ nm
- 202 nanowires and 83 vertex points
- FEM mesh with ≈800 000 elements

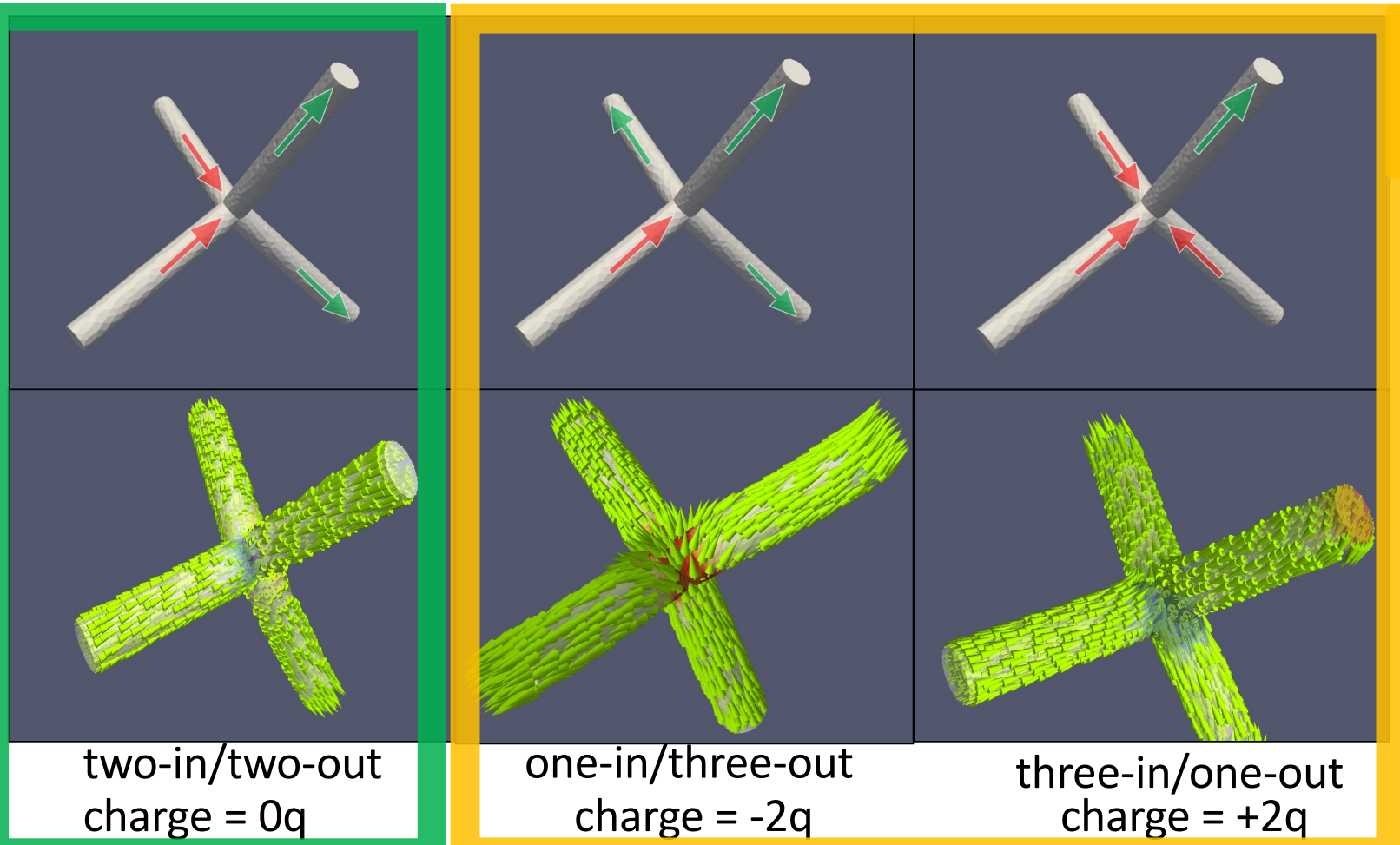




Vertex configurations in diamond-type array

Ice-rule obeying configuration

charged defect-type vertices



two-in/two-out
charge = 0q

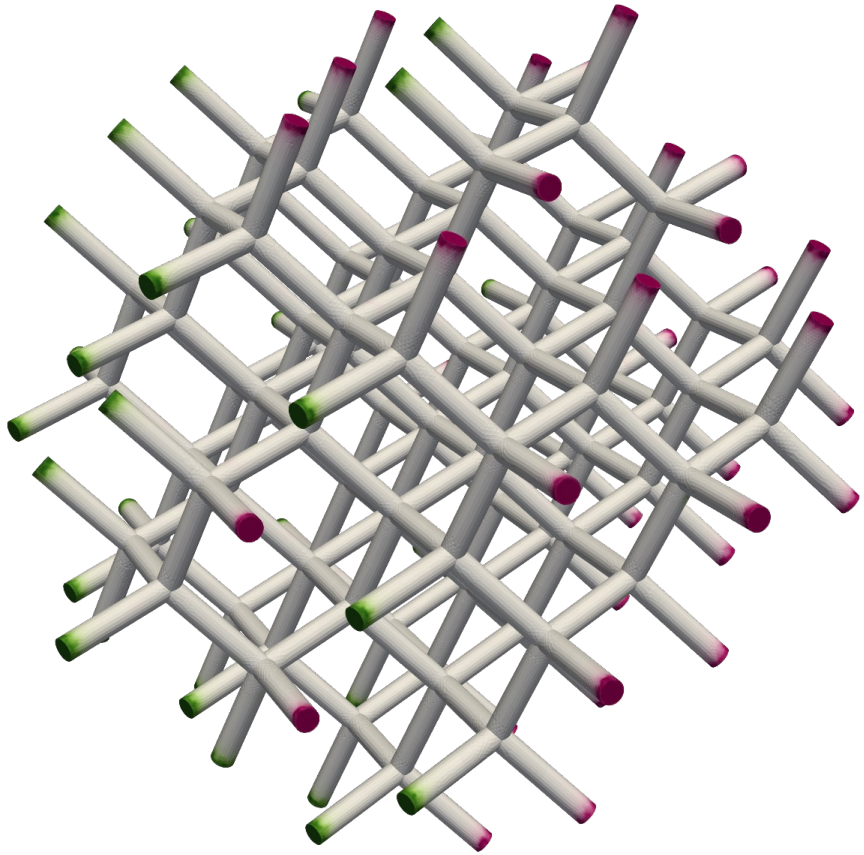
one-in/three-out
charge = -2q

three-in/one-out
charge = +2q

No distinction between type I and type II vertices known from square spin ice

Multiple zero-field magnetic configurations

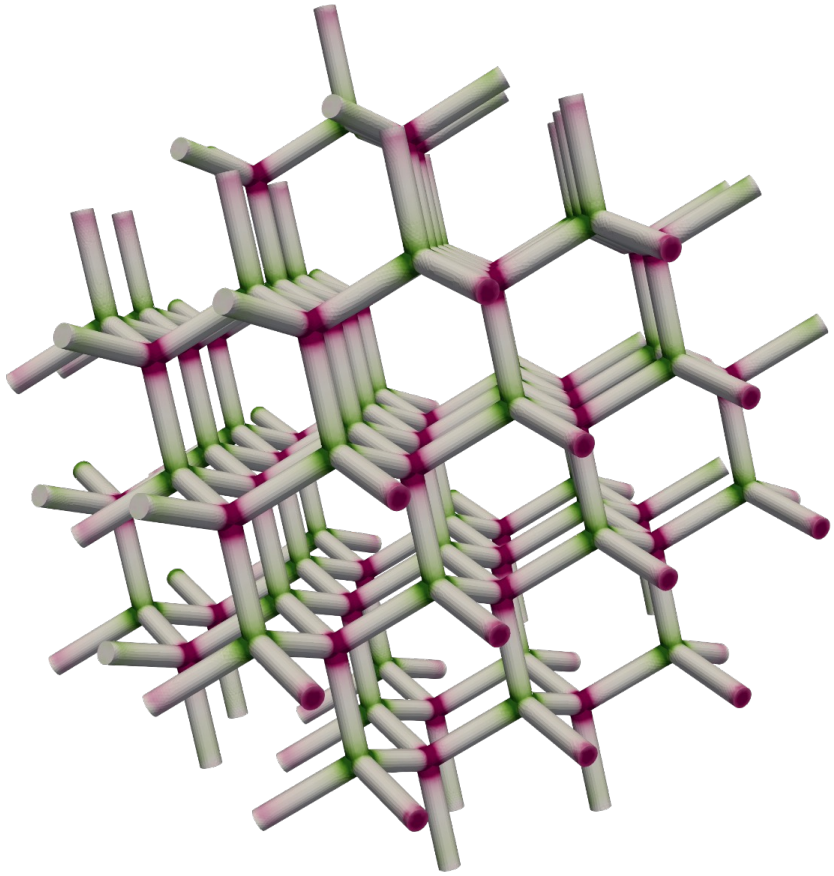
- Configuration at vertices depends on magnetic history
- Saturating the lattice along a diagonal direction yields defect-free state
- Saturating parallel to one set of wires: +2q/-2q state
- Relaxing from random initial state: disordered state



Only zero-charge vertices

Multiple zero-field magnetic configurations

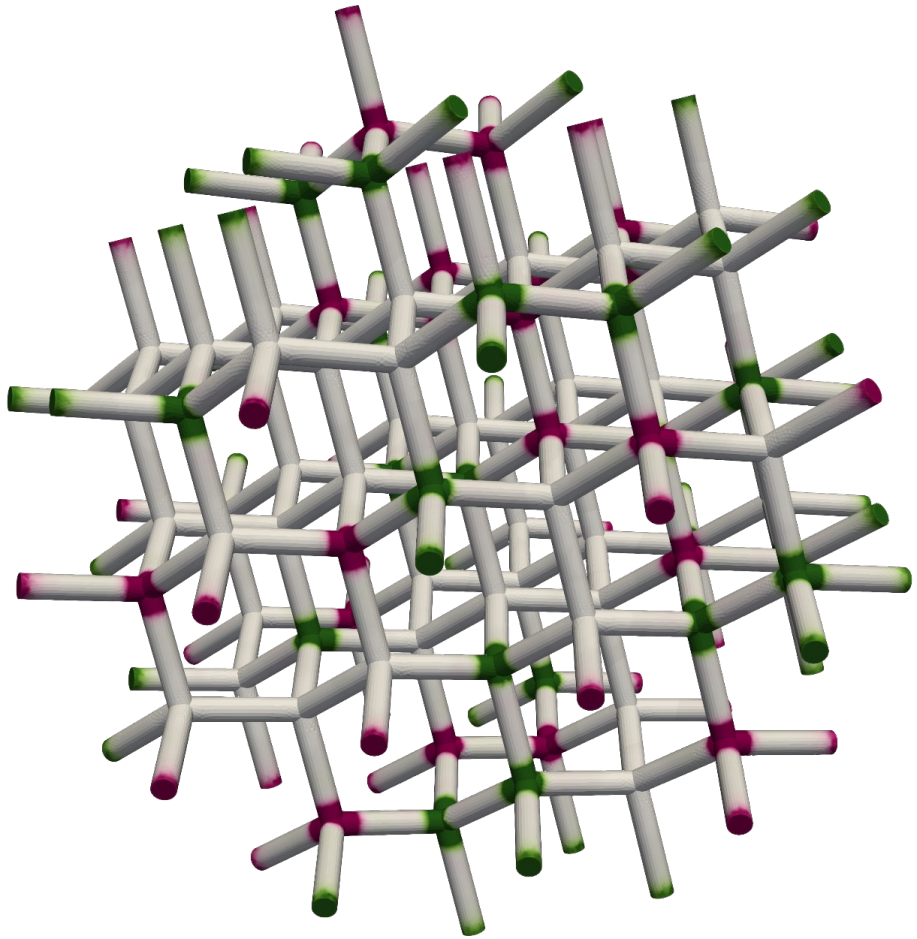
- Configuration at vertices depends on magnetic history
- Saturating the lattice along a diagonal direction yields defect-free state
- Saturating parallel to one set of wires: +2q/-2q state
- Relaxing from random initial state: disordered state



Alternating layers of +2q, -2q charges

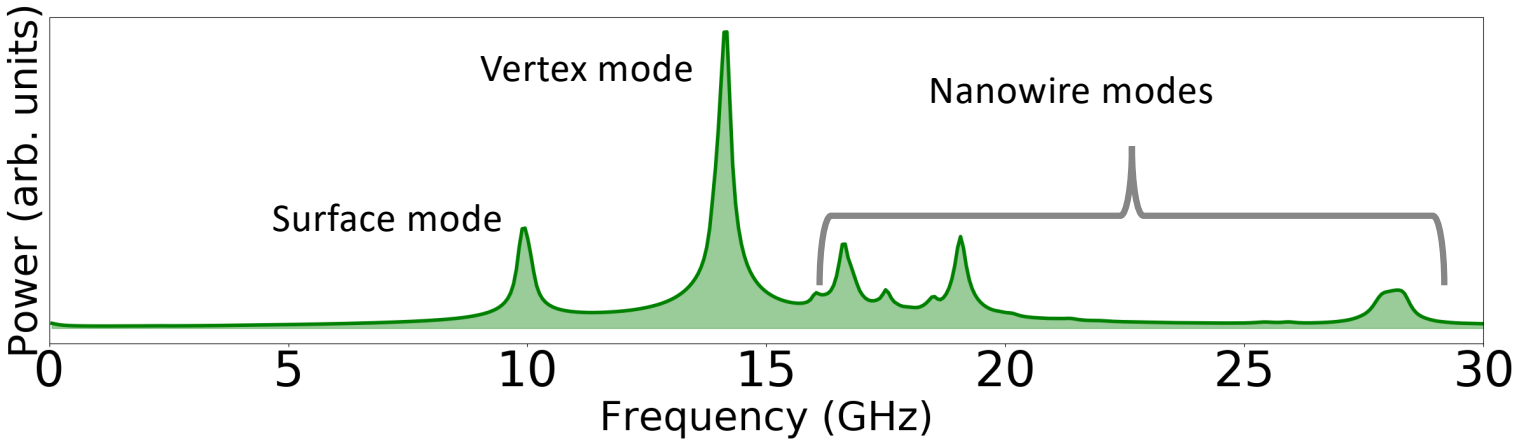
Multiple zero-field magnetic configurations

- Configuration at vertices depends on magnetic history
- Saturating the lattice along a diagonal direction yields defect-free state
- Saturating parallel to one set of wires: +2q/-2q state
- Relaxing from random initial state: disordered state

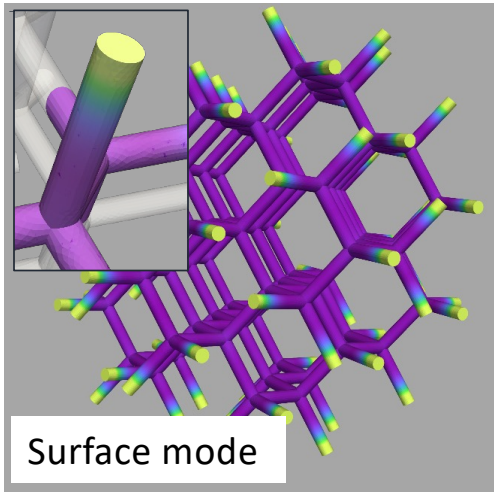


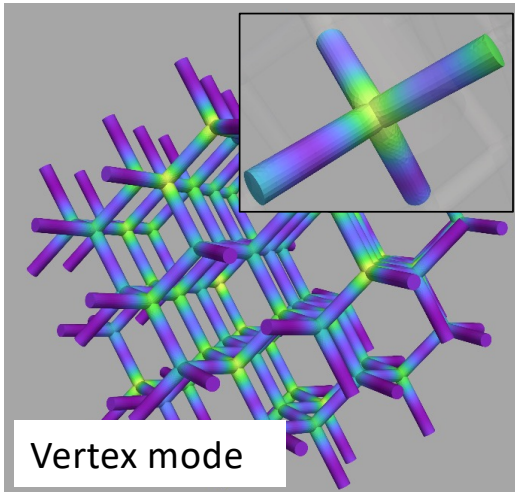
Random distribution of three types of vertex configurations

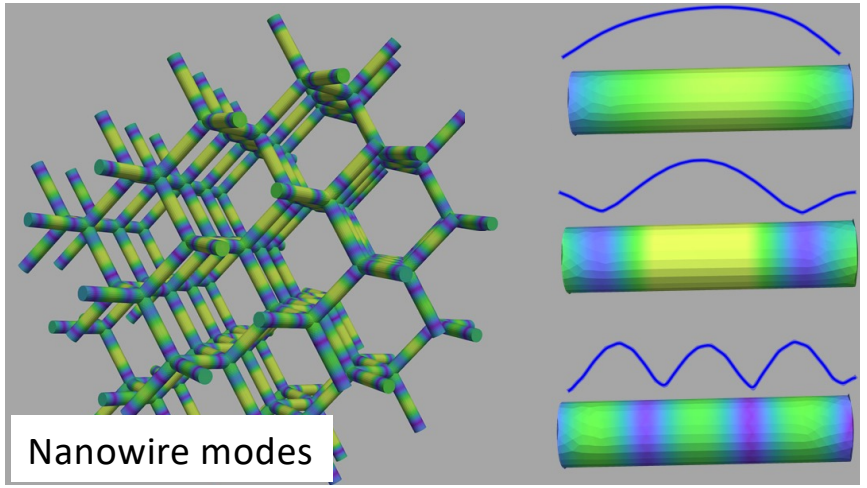
High-frequency spectrum of the defect-free state



Peaks are related to specific geometric features:
wires, intersection points, surface

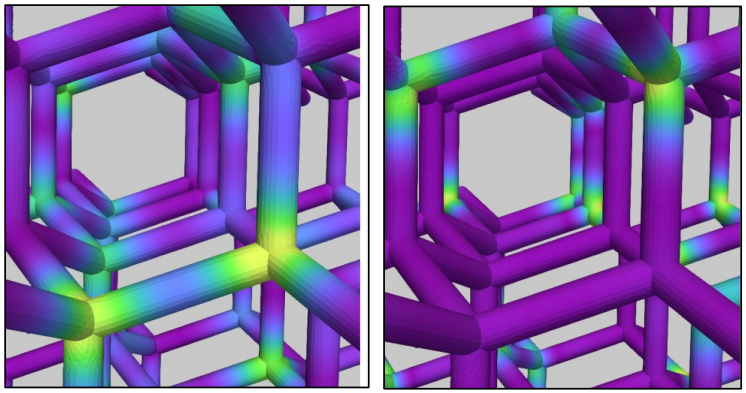






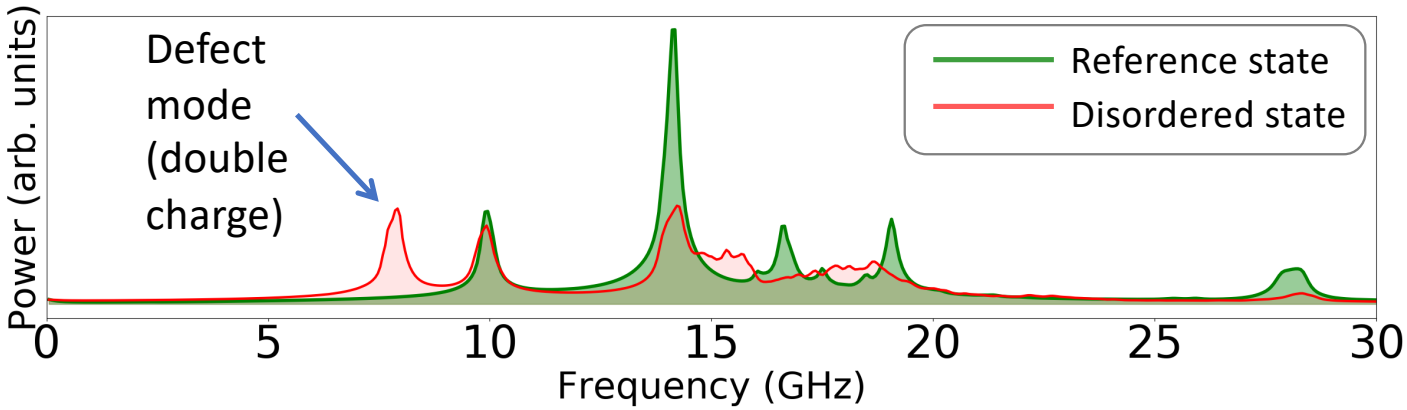
Cheenikundil, d'Aquino, Hertel, *npj Comp. Mater.* **11**, 297 (2025)

Disordered state: Impact of magnetic defect structures



Double charges

Zero charges



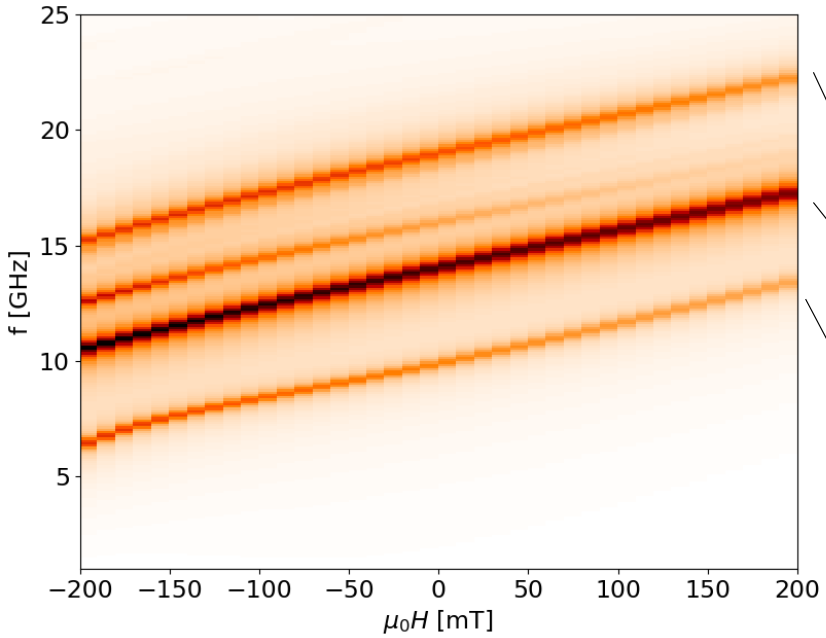
- Charged vertices oscillate at a lower frequency
- Disorder leads to significant broadening of wire modes
  - charged vertices generate local magnetic fields
  - changes in the micromagnetic configurations at the wire ends modify boundary conditions

Cheenikundil, d'Aquino, Hertel, *npj Comp. Mater.* **11**, 297 (2025)

Magnetic-field spectra of defect-free diamond-type lattice

Two different situations considered in the reference state:

Field applied **parallel** to the remanent magnetization

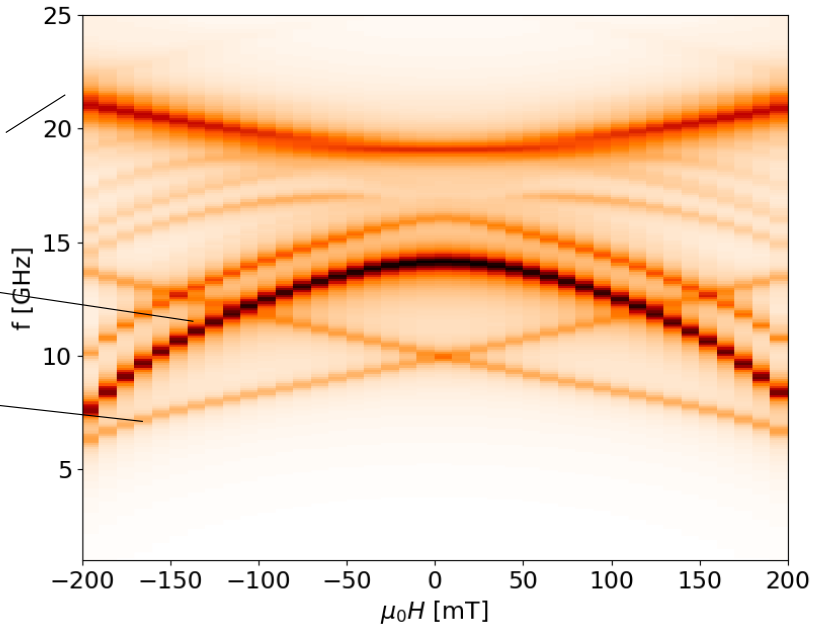


Nanowire modes

Vertex modes

Surface modes

Field **perpendicular** to the remanent magnetization



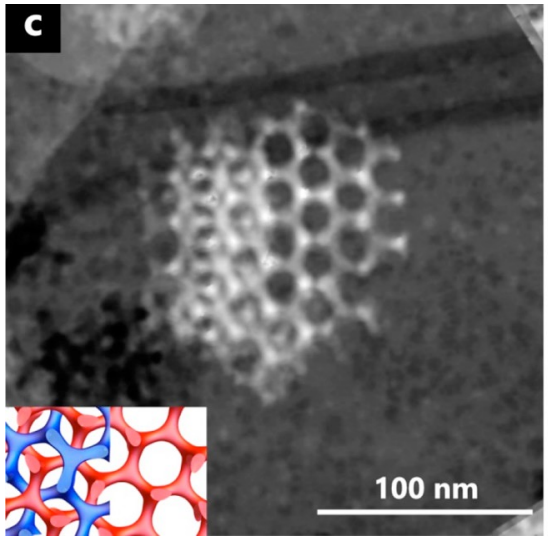
Anisotropic dynamic response:

- Almost linear variation of frequency with applied field strength (remanent direction)
- Splitting of modes when the static field is applied in a perpendicular direction

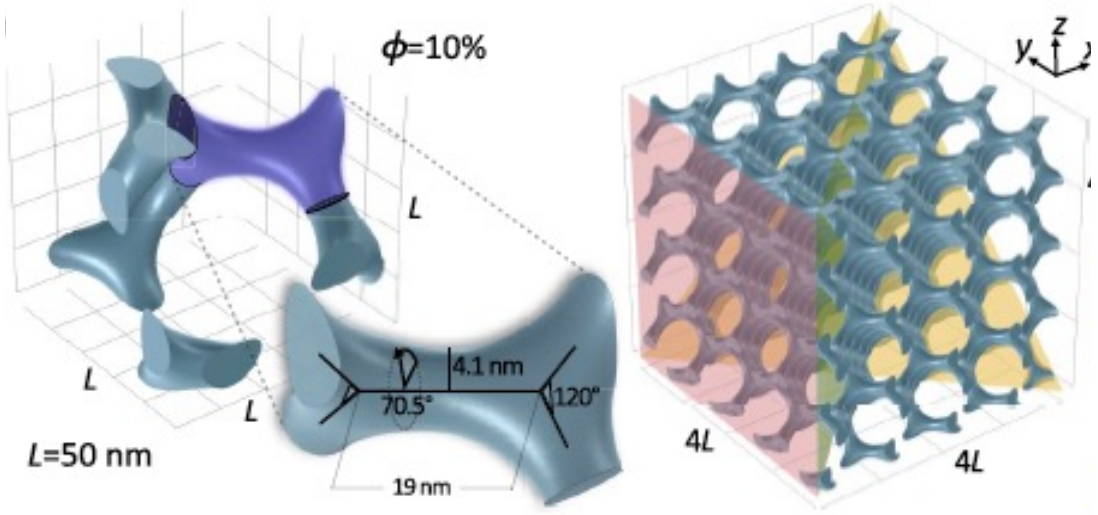
Cheenikundil et al., npj Comp. Mater. 11, 297 (2025)

Magnetic gyroid – Geometry and Finite-element model

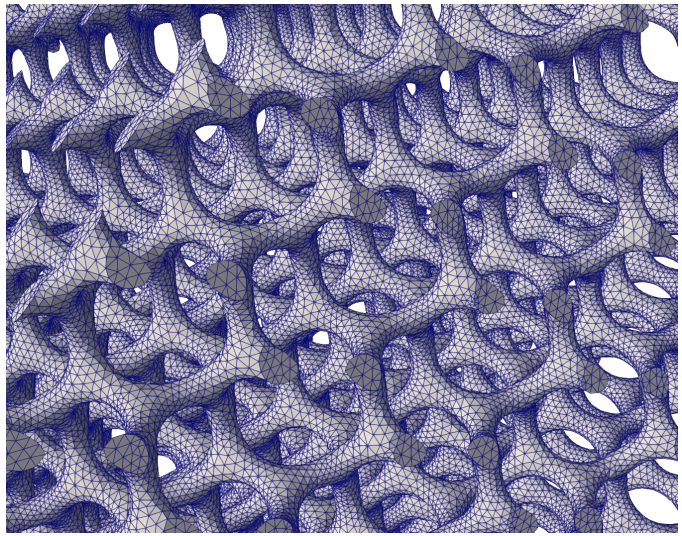
- Three-dimensional periodic chiral network
- Rounded, nanowire-like struts
- Vertices with three connections

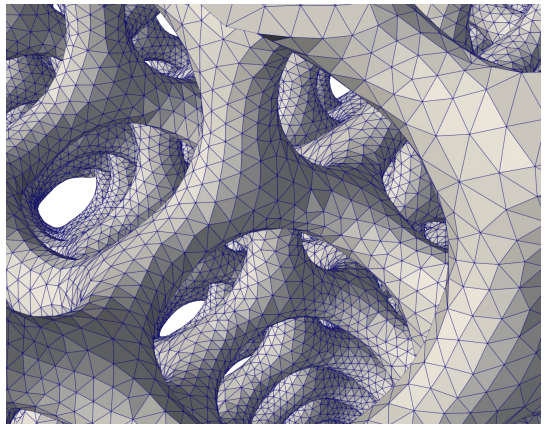


J. Llandro, et al.,
Nano Lett., 20, 3642 (2020)



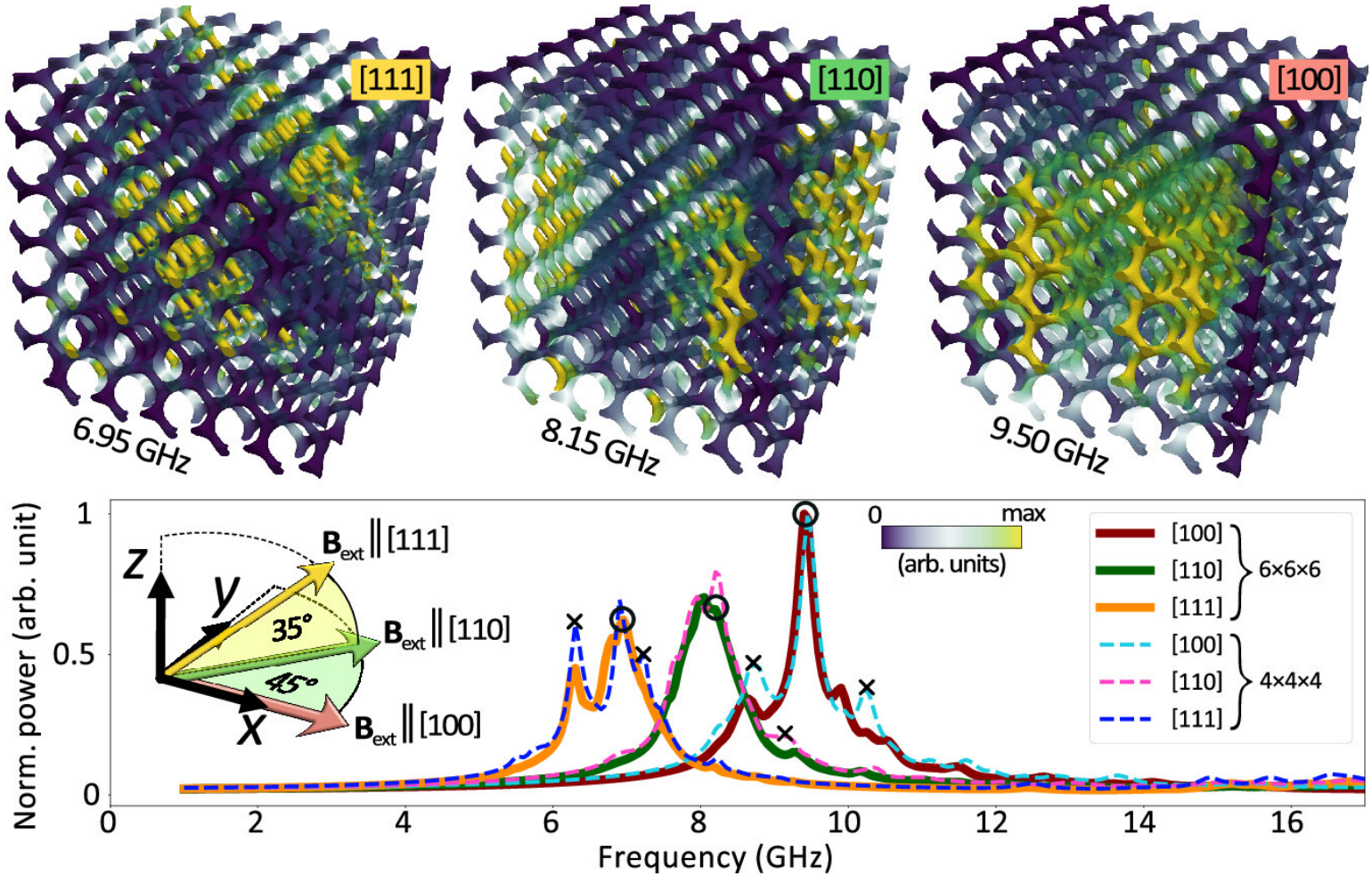
M. Golebiewski, et al.,
ACS Appl. Mater.
Interfaces 16, 22177 (2024)





FEM model of a gyroid with
6 x 6 x 6 unit cells

High-frequency oscillation: Dependency on the field orientation



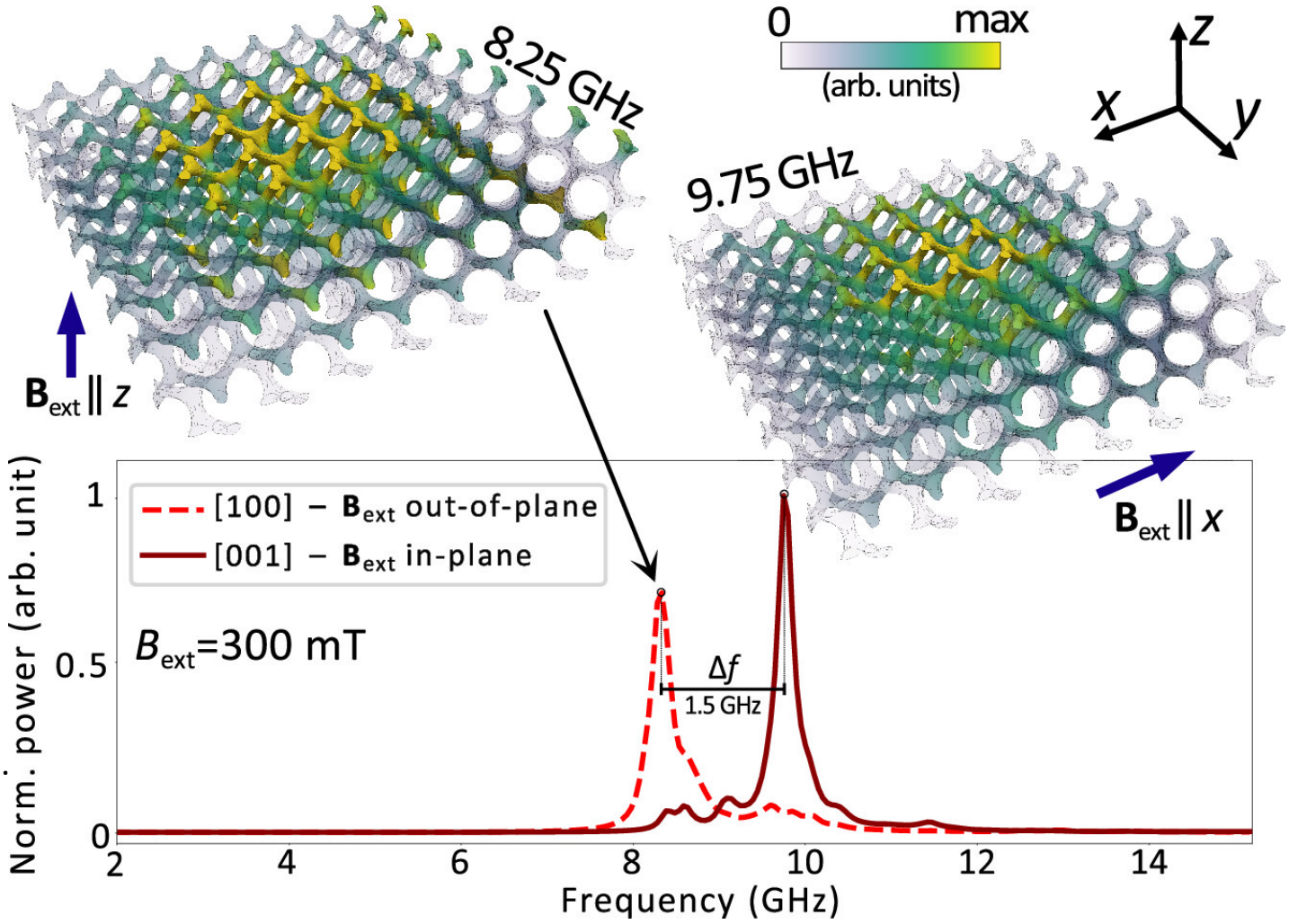
M. Golbeiewski, R. Hertel, M. d'Aquino et al.,
ACS Appl. Mater. Interfaces 16, 22177 (2024)

Macroscopic shape anisotropy

Flat gyroid sample:
8 x 8 x 2 unit cells

Flat gyroid geometry: frequency of main mode depends on the field orientation with respect to the surface normal.

Macroscopic shape anisotropy may explain frequency mismatch between experiment and simulation.



M. Golbeiewski, R. Hertel, M. d'Aquino et al.,
ACS Appl. Mater. Interfaces 16, 22177 (2024)